National Physical Laboratory

REPORT

NPL Report ENG 19

Determination of the Boltzmann constant: Acoustic models and corrections for Argon and Helium

Gavin Sutton

OCTOBER 2009

National Physical Laboratory, Hampton Road, Teddington, Middlesex, United Kingdom, TW11 0LW
Switchboard 020 8977 3222 NPL Helpline 020 8943 6880 Fax 020 8614 0446 E-mail enquiry@npl.co.uk www.npl.co.uk

DETERMINATION OF THE BOLTZMANN CONSTANT: ACOUSTIC MODELS AND CORRECTIONS FOR ARGON AND HELIUM

Gavin Sutton
Engineering Measurement

ABSTRACT

This document contains the relationships and *Labview* code used to calculate the thermo-viscous corrections to the resonance frequencies to terms in P^2 for argon, and to terms in P for helium. It also includes:

- The shell-coupling model of *Mehl* [1] for radial modes.
- The improved shell-coupling model of *Pitre* [13].
- The duct correction of *Mehl* [14].
- The transducer correction.
- The 2^{nd} order shape correction for a tri-axial ellipsoid.
- Correction to the triple point of water temperature.
- Calculation of the speed of sound.
- Least squares fitting procedures.

The location of the working Software suite and the back-up files is given in the Appendix.

ISSN 1754-2987

National Physical Laboratory
Hampton Road, Teddington, Middlesex, TW11 0LW

Approved on behalf of the Managing Director, NPL
by Martyn Sene, Director of Operations.

CONTENTS

1) INTRODUCTION

To second order in pressure, the speed of sound can be written as [2]:

$$U^2 = \frac{\gamma_0 RT}{M}\left(1 + A_2 P + A_3 P^2\right) \tag{1}$$

Where:

γ_0 is the ideal ratio of specific heats at constant pressure and constant volume.
R is the molar gas constant.
T is the temperature.
M is the molar mass of the gas.
P is the pressure.

and $$A_2 = \frac{\beta}{RT} \quad \text{and} \quad A_3 = \frac{\phi}{(RT)^2} = \frac{L - B\beta}{(RT)^2} \tag{2}$$

β and ϕ are known as the second and third acoustic virial coefficients respectively.

with: $$\beta = 2B + 2(\gamma_0 - 1)T\frac{dB}{dT} + \frac{(\gamma_0 - 1)^2}{\gamma_0}T^2\frac{d^2B}{dT^2} \tag{3}$$

and:

$$L = \left[B + (2\gamma_0 - 1)T\frac{dB}{dT} + (\gamma_0 - 1)T^2\frac{d^2B}{dT^2}\right]^2\left(\frac{\gamma_0 - 1}{\gamma_0}\right) + \left(\frac{1 + 2\gamma_0}{\gamma_0}\right)C + \left(\frac{\gamma_0^2 - 1}{\gamma_0}\right)T\frac{dC}{dT} + \frac{(\gamma_0 - 1)^2}{2\gamma_0}T^2\frac{d^2C}{dT^2} \tag{4}$$

B and C are the second and third (density) virial coefficients.

We see from Equation 1 that knowledge of the second and in the case of argon, the third virial coefficient is required to achieve the highest accuracy. Because of the fitting requirements on the virial coefficients, all parameters are valid over the temperature range 180 K < T < 380 K only. If a wider temperature range is required, the Labview code will need to be changed accordingly.

2) SECOND VIRIAL COEFFICIENT: B [cm^3mol^{-1}]

Helium

A fit was made to the most up to date data of *Hurley* and *Mehl* [3]. The fit is shown in Figure 1 and can be found in the excel file '*Determination of the second acoustic virial coefficient for He4.xls*'. The *LabView* VI is shown in Figure 2.

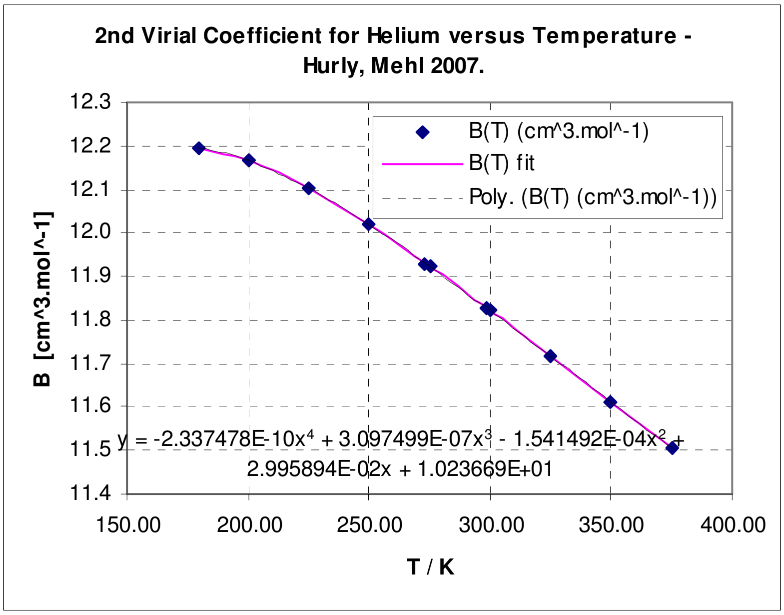

Figure 1 Fitting of the second virial coefficient, B, for helium.

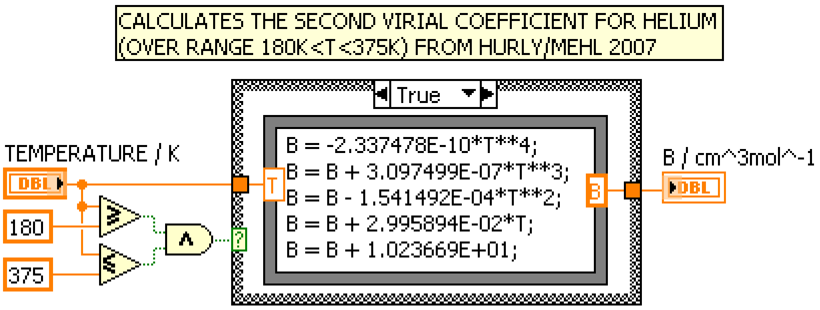

Figure 2 *Labview* code: **B_He_2007.vi**

Argon

A fit was made to the data provided by *REFPROP* [4], a program developed by the *National Institute of Standards and Technology* (*NIST*) for calculating the Thermophysical and transport properties of fluids to the highest accuracy. Figure's 3 and 4 show the fit and *LabView* VI respectively.

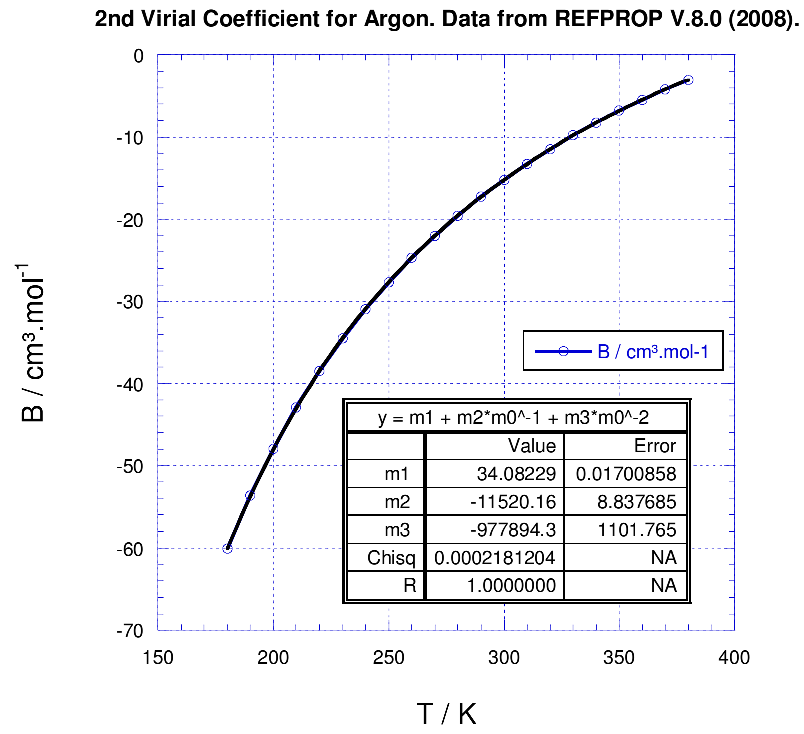

Figure 3 fitting of the second virial coefficient, B, for argon.

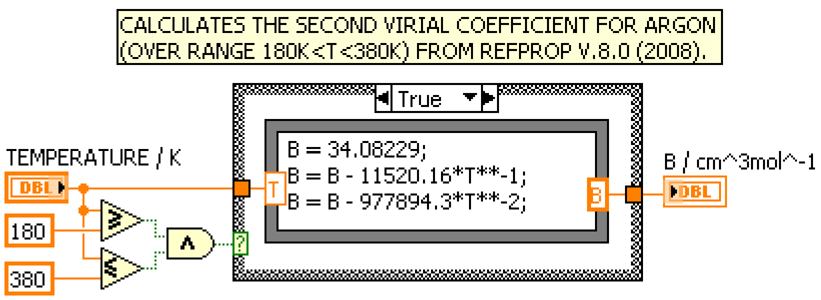

Figure 4 *LabView* code: **B_Ar_2007.vi**

3) FIRST DERIVATIVE OF SECOND VIRIAL COEFFICIENT: dB/dT [$cm^3mol^{-1}K^{-1}$]

Helium

A fit was made to the $T\dfrac{dB}{dT}$ data of *Hurley and Mehl* [3] and then the derivative extracted (this gave a better quality fit). The fit is shown in Figure 5 and can be found in the excel file '*Determination of the second acoustic virial coefficient for He4.xls*'. Figure 6 shows the *LabView* VI.

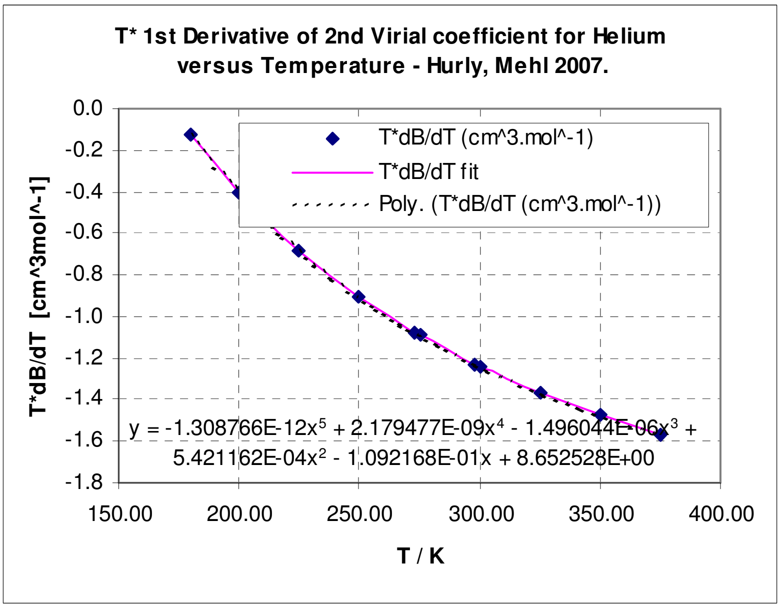

Figure 5 Fitting of $T\dfrac{dB}{dT}$ for helium.

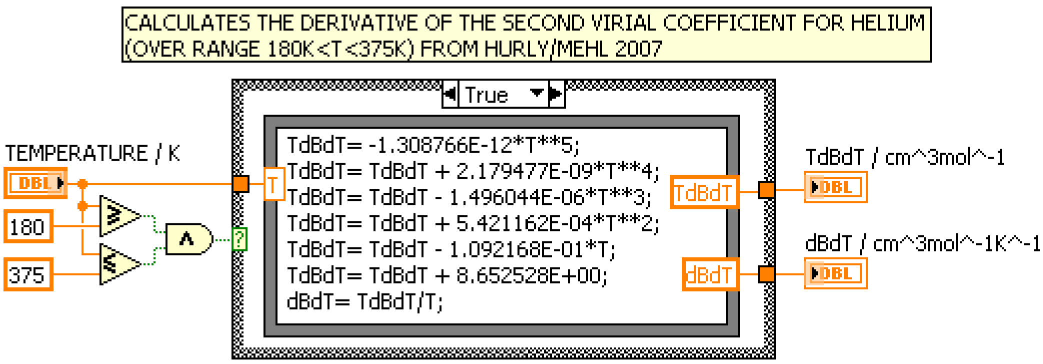

Figure 6 *LabView* code: **dBdT_He_2007.vi**

Argon

A fit was made to the $\frac{dB}{dT}$ data provided by *REFPROP* [4]. Figure's 7 and 8 show the fit and *LabView* VI respectively.

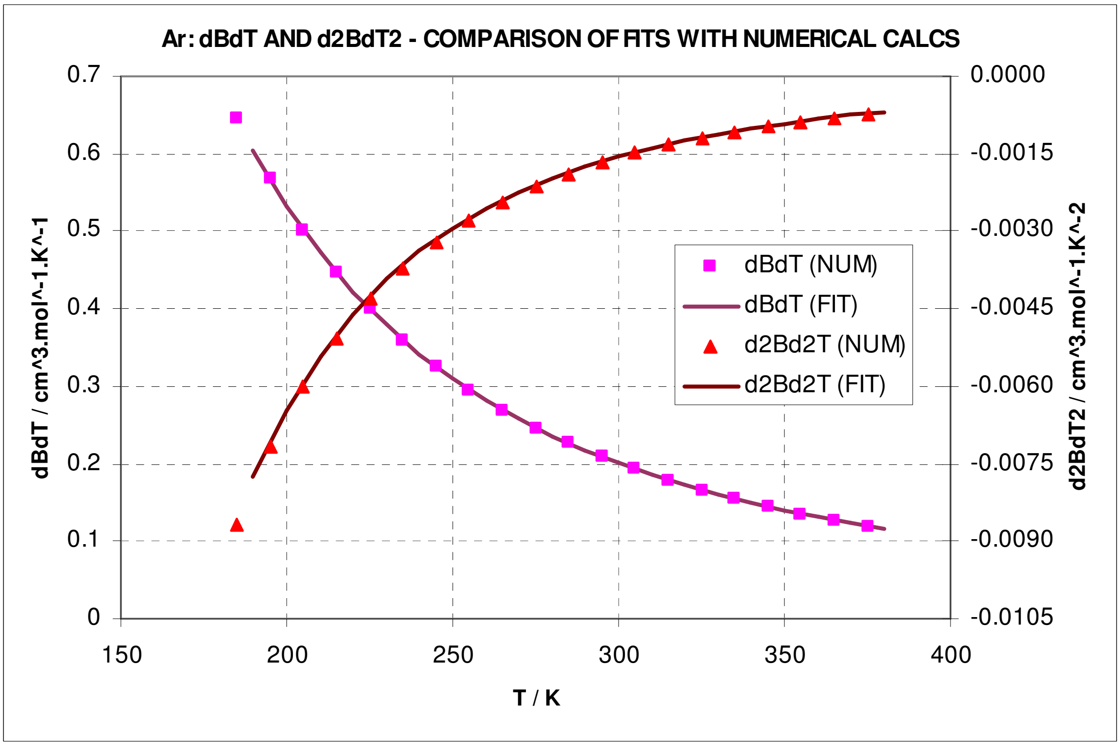

Figure 7 Fitting of $\frac{dB}{dT}$ and $\frac{d^2B}{dT^2}$ for argon.

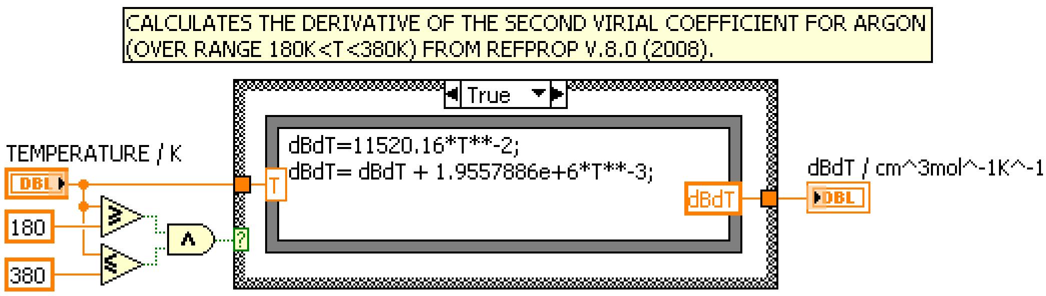

Figure 8 *LabView* code: **dBdT_Ar_2007.vi**

4) SECOND DERIVATIVE OF SECOND VIRIAL COEFFICIENT: d^2B/dT^2 [$cm^3mol^{-1}K^{-2}$]

Helium

A fit was made to the $T^2 \dfrac{d^2B}{dT^2}$ data of *Hurley* and *Mehl* [3] and then the second derivative extracted (this gave a better quality fit). The fit is shown in Figure 9 and can be found in the excel file '*Determination of the second acoustic virial coefficient for He4.xls*'. Figure 10 shows the *LabView* VI.

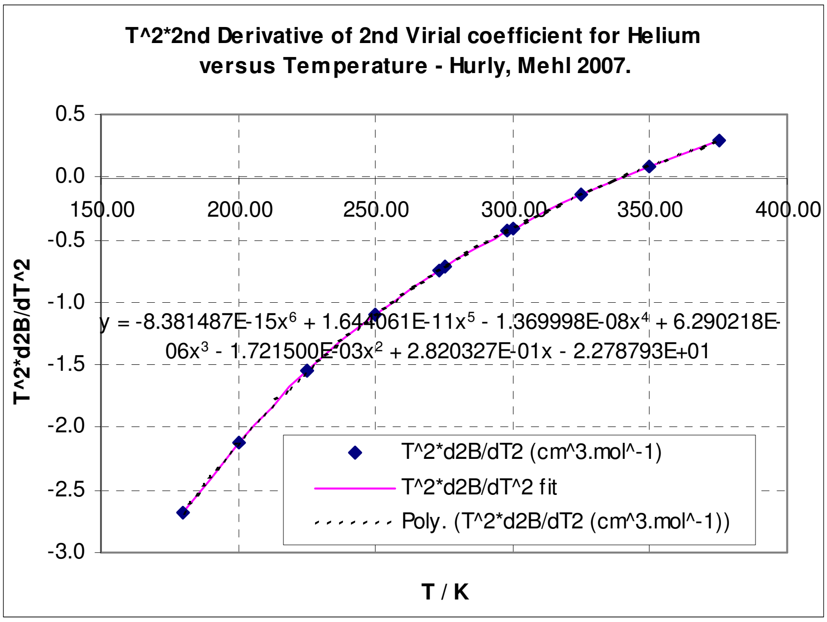

Figure 9 Fitting of $T^2 \dfrac{d^2B}{dT^2}$ for helium.

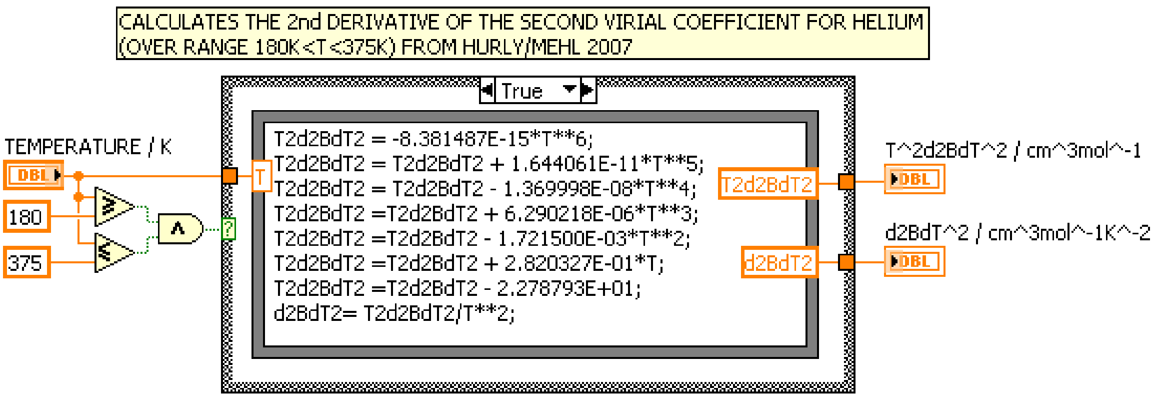

Figure 10 *LabView* code: **d2BdT2_He_2007.vi**

Argon

A fit was made to the $\frac{d^2B}{dT^2}$ data provided by *REFPROP* [4]. Figure's 7 and 11 show the fit and *LabView* VI respectively.

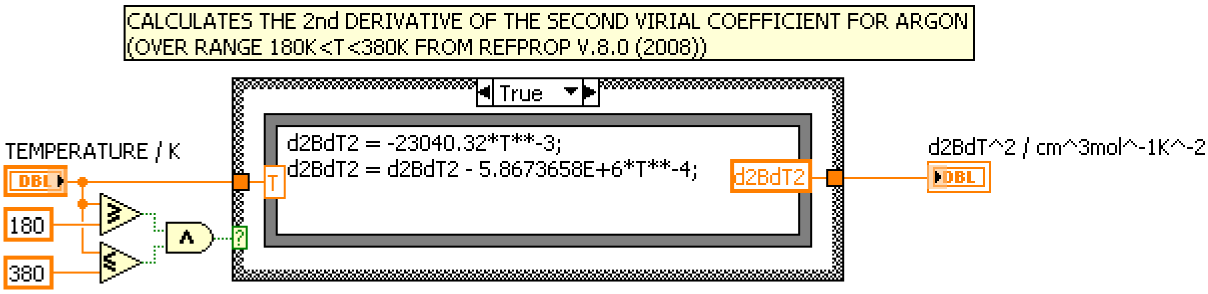

Figure 11 *LabView* code: **d2BdT2_Ar_2007.vi**

5) THIRD VIRIAL COEFFICIENT: C [cm^6mol^{-2}]

Helium

The third virial coefficient was not calculated for helium.

Argon

A fit was made to the data provided by *REFPROP* [4]. Figure's 12 and 13 show the fit and *LabView* VI respectively.

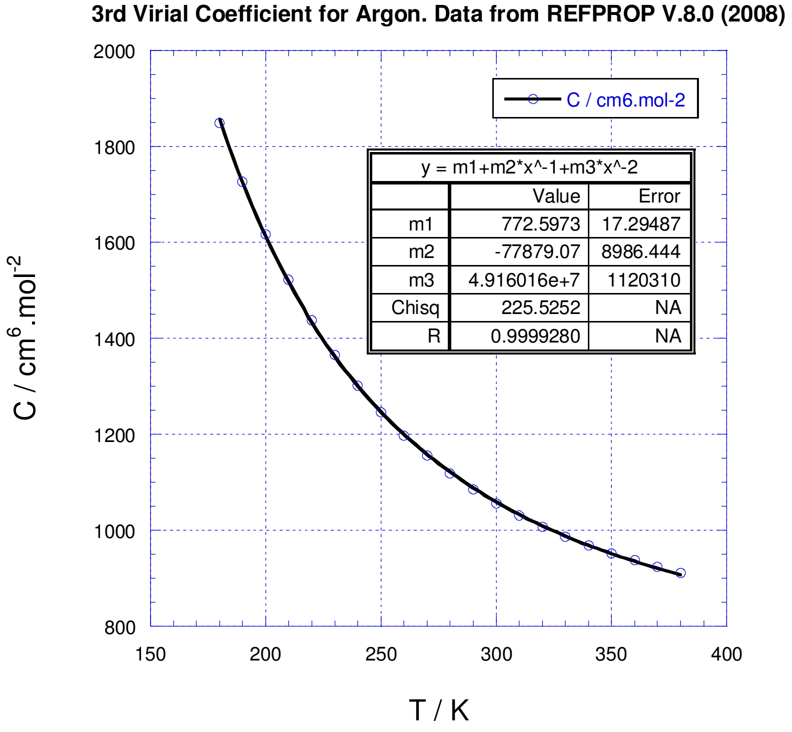

Figure 12 fitting of the third virial coefficient, C, for argon.

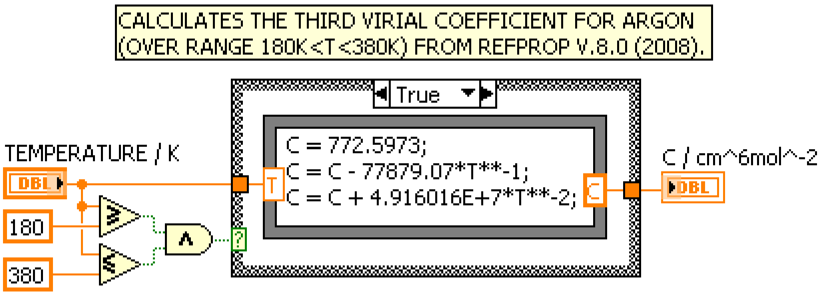

Figure 13 *LabView* code: **C_Ar_2007.vi**

6) FIRST DERIVATIVE OF THIRD VIRIAL COEFFICIENT: dC/dT [$cm^6mol^{-2}K^{-1}$]

Helium

The first derivative of the third virial coefficient was not calculated for helium.

Argon

A fit was made to the data provided by *REFPROP* [4]. Figure's 14 and 15 show the fit and *LabView* VI respectively.

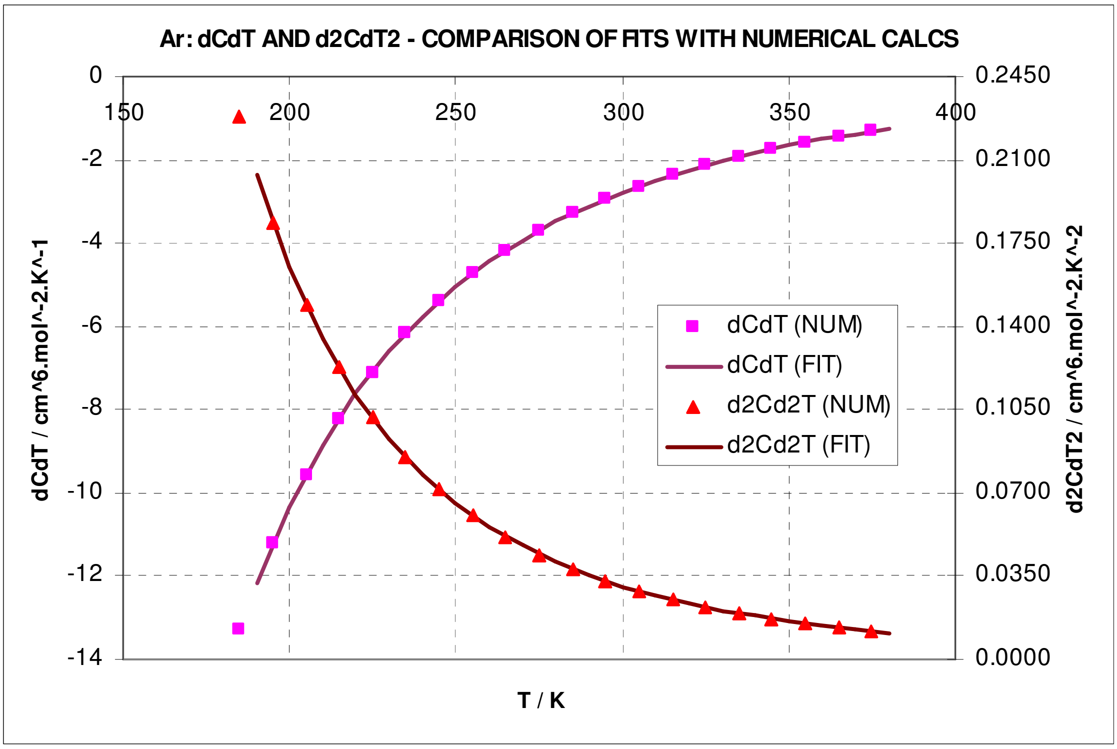

Figure 14 Fitting of $\frac{dC}{dT}$ and $\frac{d^2C}{dT^2}$ for argon.

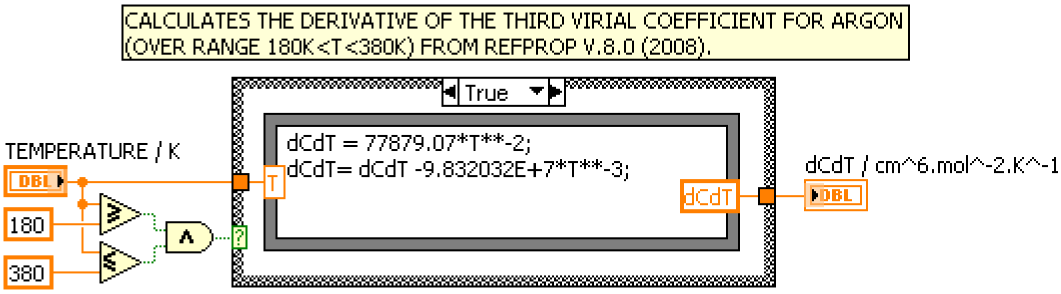

Figure 15 *LabView* code: **dCdT_Ar_2007.vi**

7) SECOND DERIVATIVE OF THIRD VIRIAL COEFFICIENT: d^2C/dT^2 [$cm^6 mol^{-2} K^{-2}$]

Helium

The second derivative of the third virial coefficient was not calculated for helium.

Argon

A fit was made to the data provided by *REFPROP* [4]. Figure's 14 and 16 show the fit and *LabView* VI respectively.

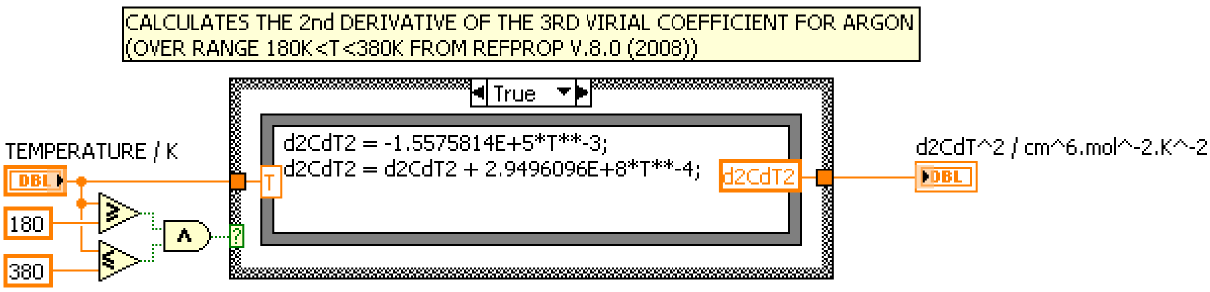

Figure 16 *LabView* code: **d2CdT2_Ar_2007.vi**

8) SECOND ACOUSTIC VIRIAL COEFFICIENT: $\beta\,[\mathrm{cm^3mol^{-1}}]$

The second acoustic virial coefficient is defined in terms of the second (density) virial coefficient and its derivatives as follows:

$$\beta = 2B + 2(\gamma_0 - 1)T\frac{dB}{dT} + \frac{(\gamma_0 - 1)^2}{\gamma_0}T^2\frac{d^2B}{dT^2} \tag{5}$$

Helium

Figure 17 shows how β varies with temperature for helium and Figure 18 shows the *LabView* VI.

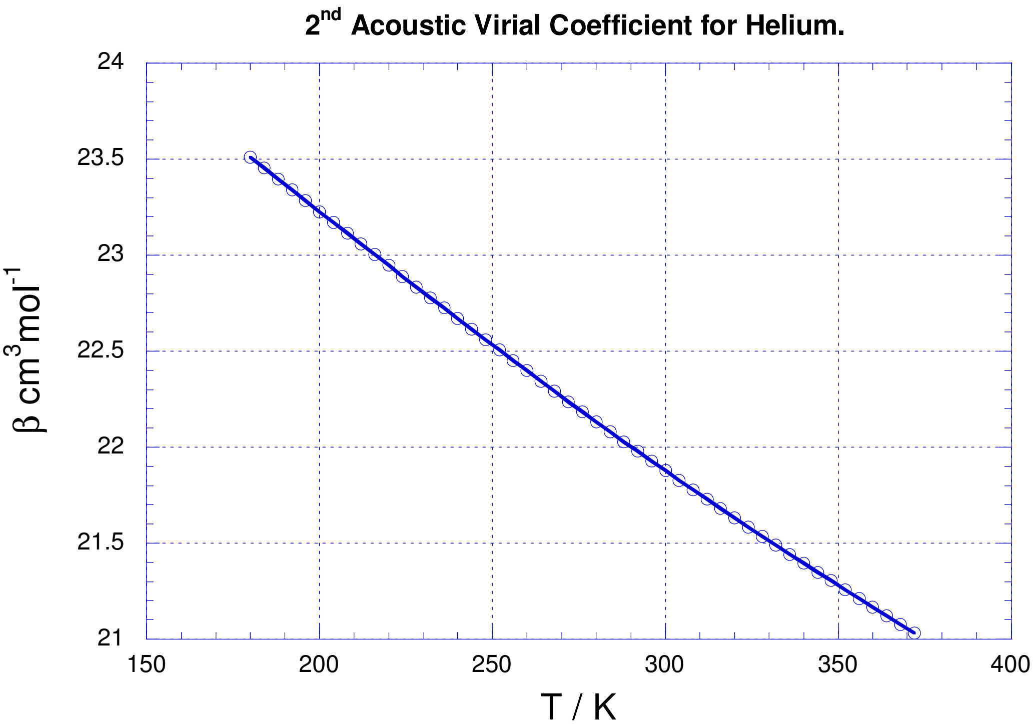

Figure 17 Second acoustic virial coefficient, β, for helium.

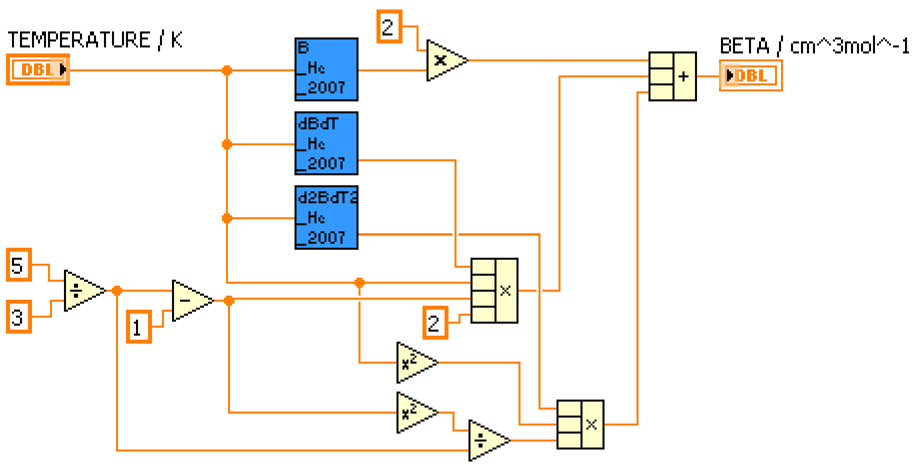

Figure 18 *LabView* code: **BETA_He_2007.vi**

Argon

Figure 19 shows how β varies with temperature for argon and Figure 20 shows the *LabView* VI.

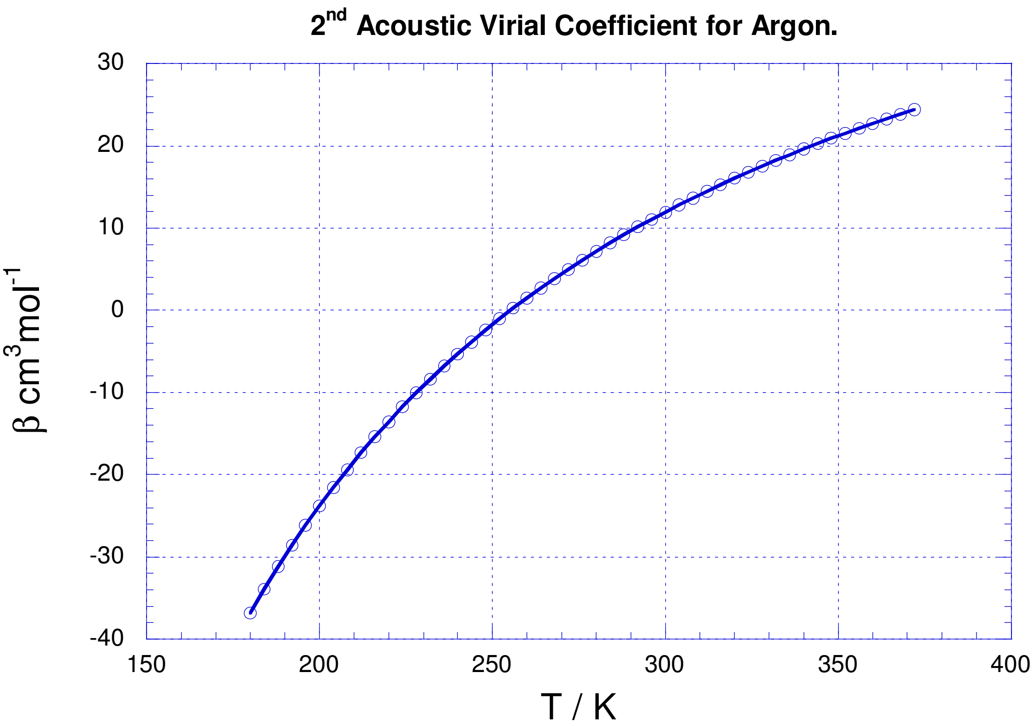

Figure 19 Second acoustic virial coefficient, β, for argon.

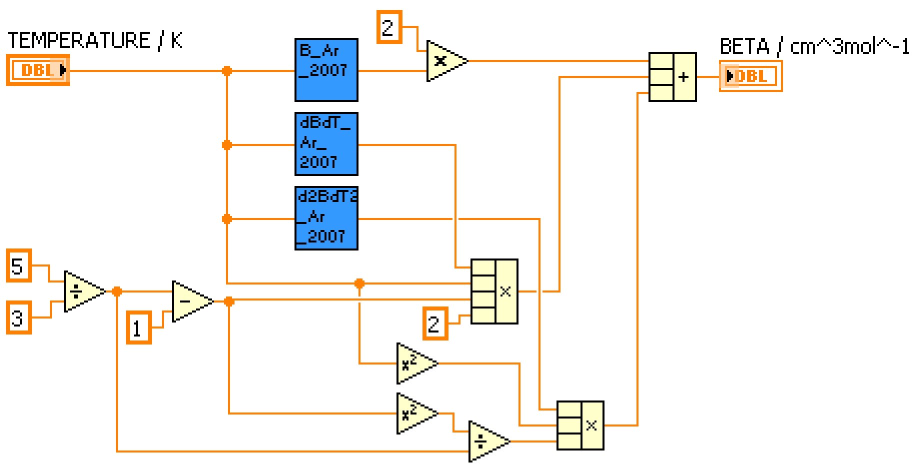

Figure 20 *LabView* code: **BETA_Ar_2007.vi**

9) THIRD ACOUSTIC VIRIAL COEFFICIENT: ϕ [cm^{6}mol^{-2}]

The third acoustic virial coefficient is defined in terms of the second and third (density) virial coefficient and their derivatives and the second acoustic virial coefficient as follows:

$$\phi = L - B\beta \tag{6}$$

Where β is defined in Equation 5 and L is given by:

$$L = \left[B + (2\gamma_0 - 1)T\frac{dB}{dT} + (\gamma_0 - 1)T^2\frac{d^2B}{dT^2}\right]^2\left(\frac{\gamma_0 - 1}{\gamma_0}\right) + \left(\frac{1+2\gamma_0}{\gamma_0}\right)C + \left(\frac{\gamma_0^2 - 1}{\gamma_0}\right)T\frac{dC}{dT} + \frac{(\gamma_0 - 1)^2}{2\gamma_0}T^2\frac{d^2C}{dT^2} \tag{7}$$

Helium

The third acoustic virial coefficient, ϕ, was not calculated for helium.

Argon

The third acoustic virial coefficient for argon is shown in figure 21. The *LabView* code is shown in Figure 22 and it is worth noting that the VI is called **DELTA_Ar_2007.vi** and not **Phi……..**

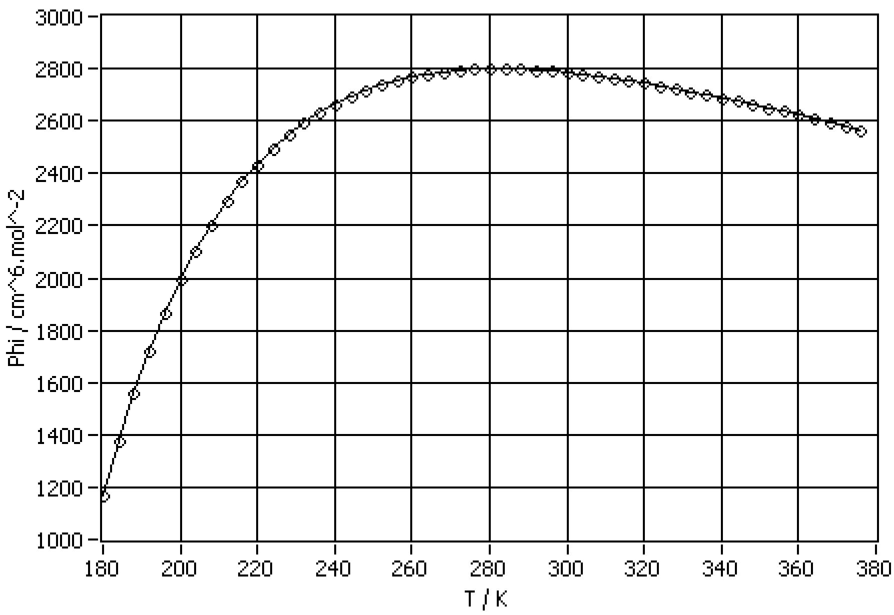

Figure 21 Third acoustic virial coefficient, ϕ, for argon.

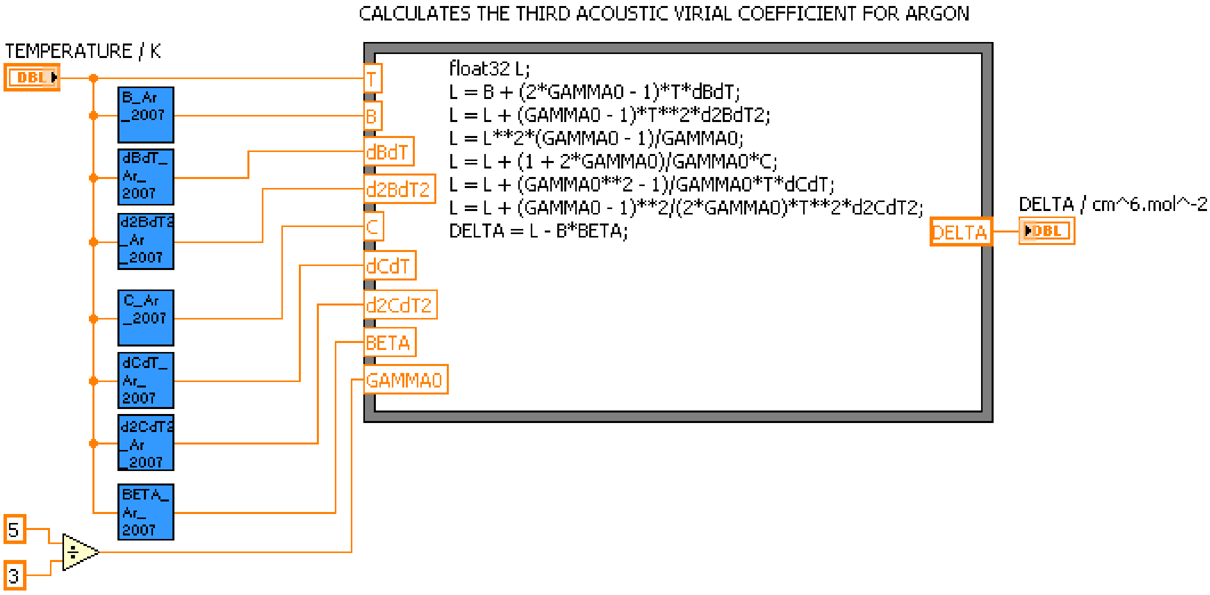

Figure 22 *LabView* code: **DELTA_Ar_2007.vi**

10) SPEED OF SOUND: U [ms^{-1}]

To second order in pressure the speed of sound of a real gas can be written as:

$$U = \left[\frac{\gamma_0 RT}{M} \left(1 + \frac{\beta}{RT} P + \frac{\phi}{(RT)^2} P^2 \right) \right]^{\frac{1}{2}} \tag{8}$$

Where β and ϕ are the second and third acoustic virial coefficients.

Helium

This VI calculates the speed of sound in helium to first order in pressure (i.e. $\phi = 0$). This is shown in Figure 23 for a temperature of 273.16 K. Figure 24 shows the *LabView* VI.

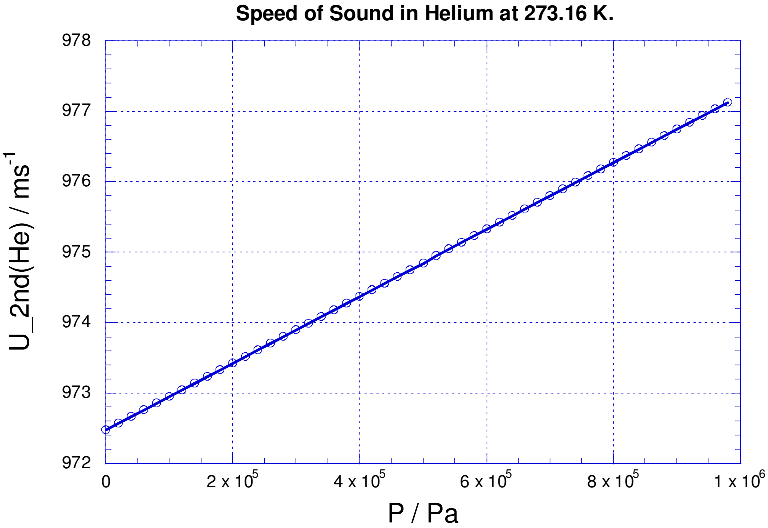

Figure 23 The speed of sound in helium at 273.16 K, to first order in pressure.

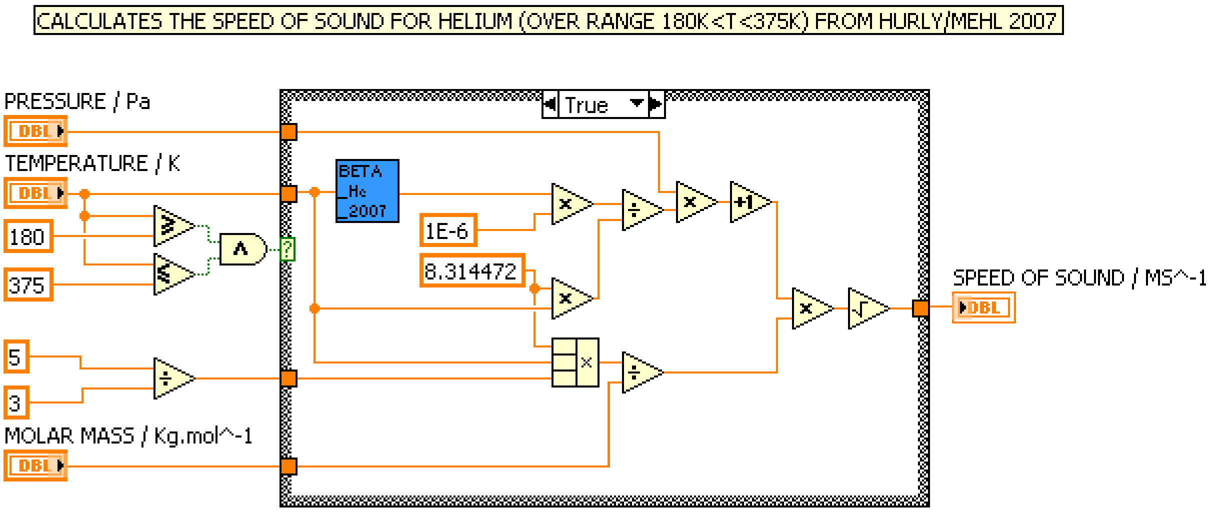

Figure 24 *LabView* code: **U_2ND_He_2007.vi**

Argon

This VI calculates the speed of sound in argon to <u>second</u> order in pressure. This is shown in Figure 25 for a temperature of 273.16 K. Figure 26 shows the *LabView* VI.

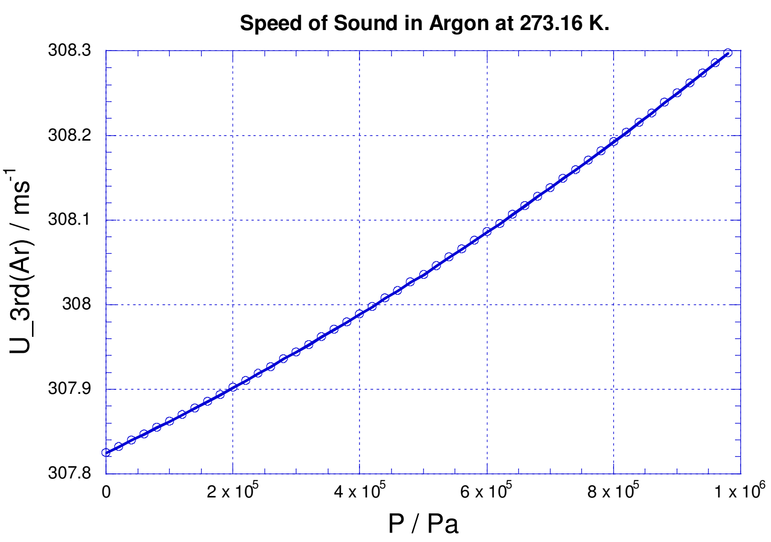

Figure 25 The speed of sound in argon at 273.16 K, to second order in pressure.

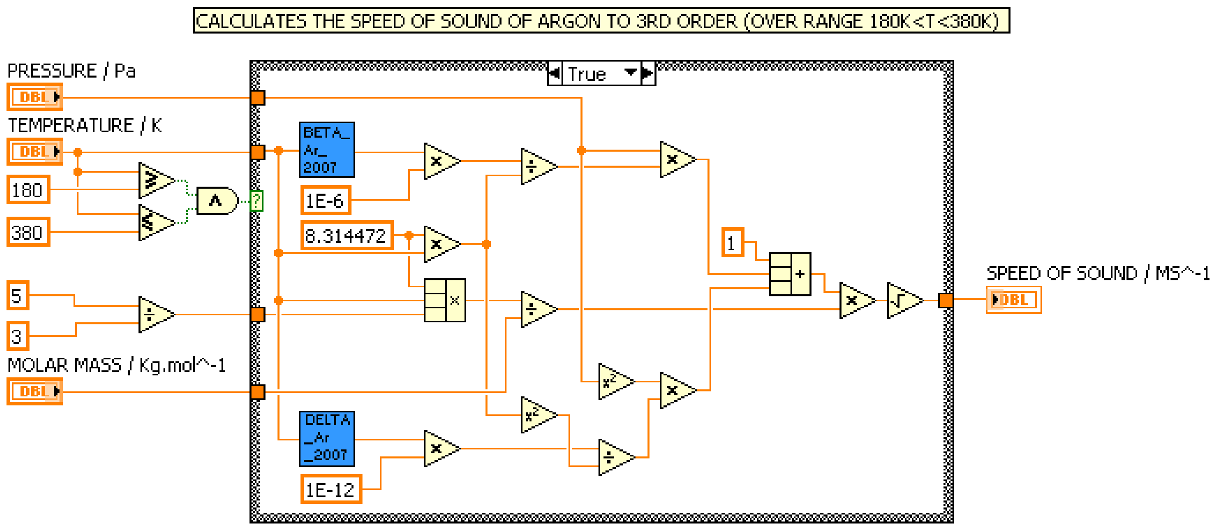

Figure 26 *LabView* code: **U_3ND_Ar_2007.vi**

11) EIGENVALUE OF THE (*n*,s) MODE FOR AN IDEAL SPHERE: Z(*n*,s)

The acoustic eigenvalue for a perfect sphere, *z(n,s)*, is given by the s^{th} zero of the derivative of the Spherical Bessel Function of order *n*. It is used to determine the ideal resonance frequencies. Figure 27 shows the eigenvalues up to order 19 and seventh zero. Where a zero appears, the *LabView* code was unable to generate the value to sufficient accuracy (0.01 PPM). Figure 28 shows the *Labview* VI.

s=1	s=2	s=3	s=4	s=5	s=6	s=7	
0	4.49340945	7.72525184	10.90412166	14.06619391	17.22075527	20.37130296	n=0
2.08157598	5.94036999	9.20584014	12.40444502	15.57923641	18.74264558	21.89969648	n=1
3.34209365	7.2899323	10.61385504	13.84611188	17.04290219	20.22185656	0	n=2
4.51409965	8.58375495	11.97273003	15.24428833	18.4679981	21.66658649	0	n=3
5.64670362	9.84044604	13.29556386	16.6093459	19.86242396	0	0	n=4
6.75645633	11.07020687	14.59055196	17.94686995	21.23106823	0	0	n=5
7.85107768	12.27933398	15.86322182	19.26270994	0	0	0	n=6
8.93483887	13.47203035	17.11750573	20.55942813	0	0	0	n=7
10.01037074	14.65126281	18.35631834	21.84001207	0	0	0	n=8
11.07941839	15.81921549	19.58188902	0	0	0	0	n=9
12.1432041	16.97754998	20.79596723	0	0	0	0	n=10
13.20262039	18.1275641	21.99995508	0	0	0	0	n=11
14.25834081	19.27029374	0	0	0	0	0	n=12
15.31088738	20.40658084	0	0	0	0	0	n=13
16.36067374	21.53712032	0	0	0	0	0	n=14
17.4080338	0	0	0	0	0	0	n=15
18.45324137	0	0	0	0	0	0	n=16
19.4965241	0	0	0	0	0	0	n=17
20.5380735	0	0	0	0	0	0	n=18
21.57805241	0	0	0	0	0	0	n=19

Figure 27 The acoustic Eigenvalues for a perfect sphere (*n* = 0 are the radial modes).

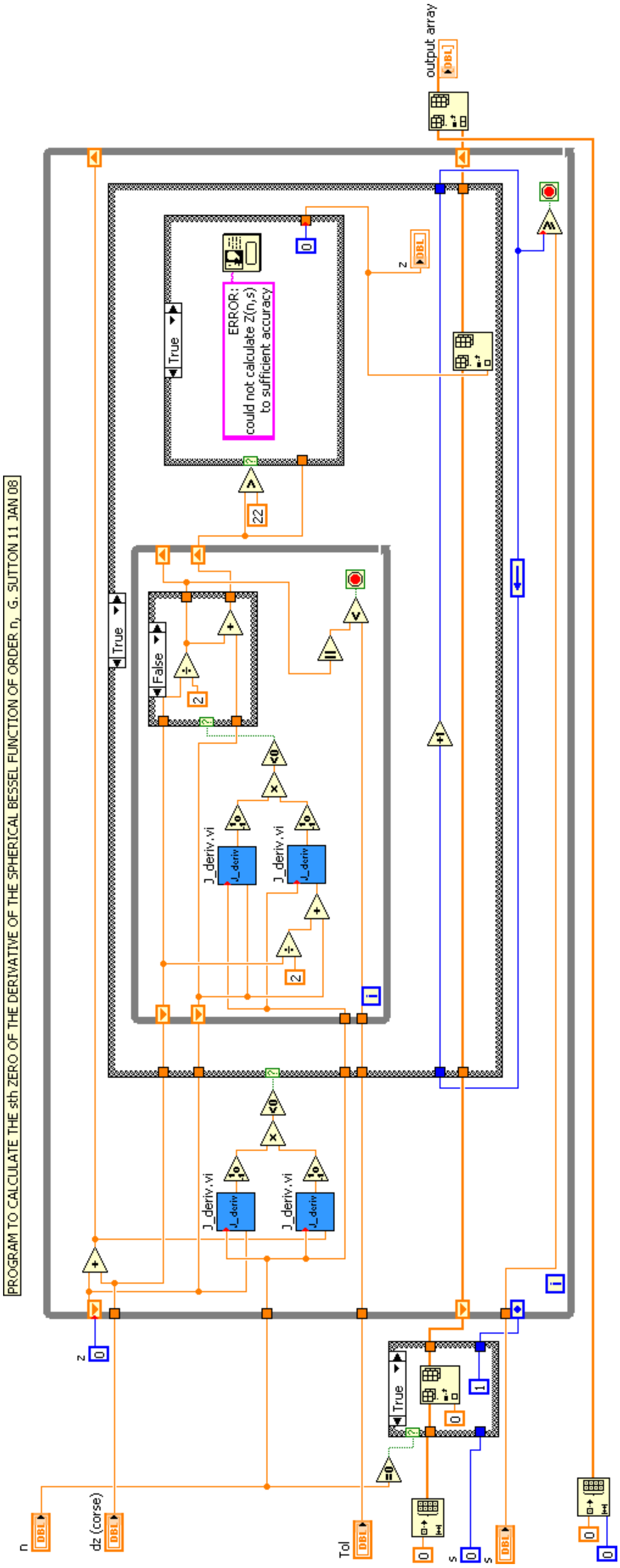

Figure 28 *LabView* code: **CALC_Z.vi**

12) RESONANCE FREQUENCIES FOR IDEAL SPHERE: F(n,m) [Hz]

The resonance frequencies of an ideal sphere are given by:

$$F(n,s) = \frac{z(n,s)}{2\pi a} U \tag{9}$$

Where: U is the speed of sound.
a is the radius.
$z(n,s)$ is the eigenvalue of the mode.
n is the mode order ($n = 0$ for radial modes).
s is the s[th] solution.

Helium

Figure 29 shows the VI for helium.

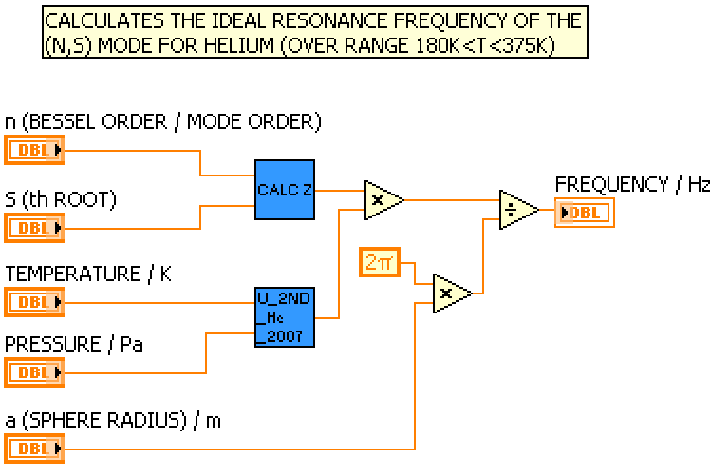

Figure 29 *LabView* code: **CALC_FREQ_He_2007.vi**

Argon

Figure 30 shows the VI for argon.

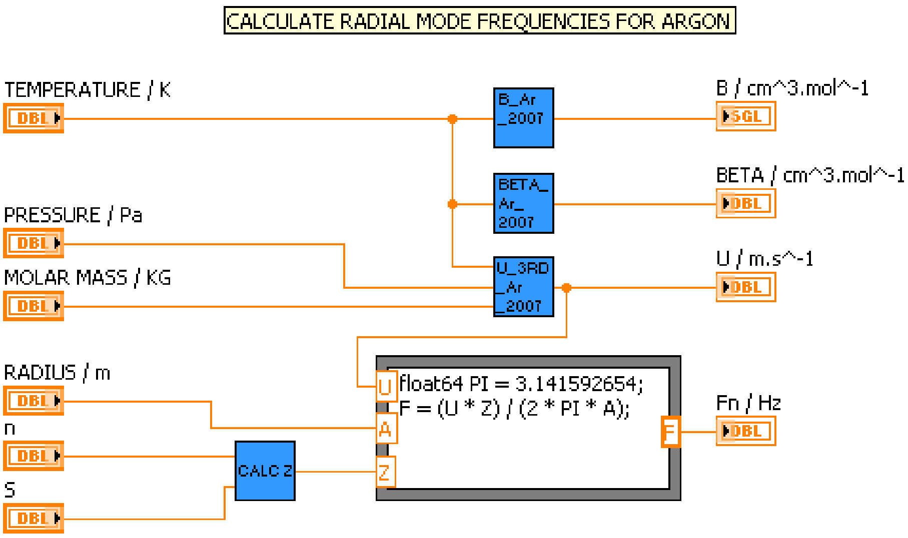

Figure 30 LabView code: **Calc_freq_Ar_2007.vi**

13) DENSITY OF GAS: ρ [kgm^{-3}]

Helium

For helium, the quadratic solution [5] correct to first order in pressure was used:

$$\rho = \frac{-RT + \left((RT)^2 + 4RTPB\right)^{\frac{1}{2}}}{2RTB} M \tag{10}$$

Figure 31 shows a plot of this for a temperature of 273.16 K. Figure 32 shows the VI.

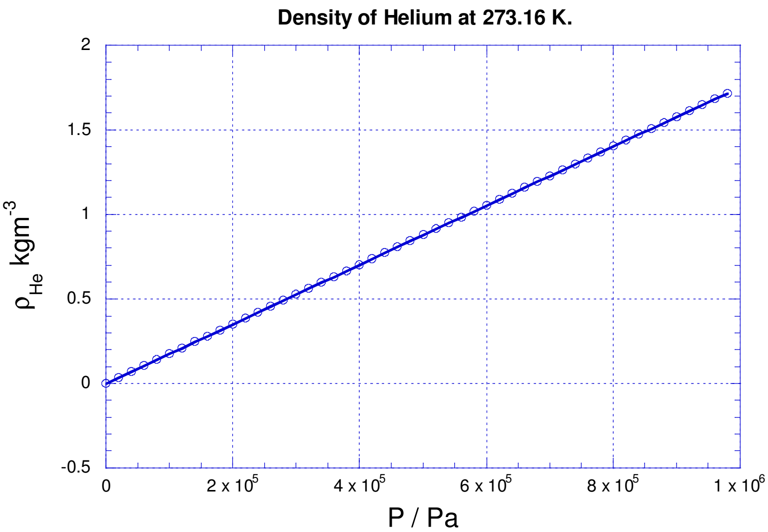

Figure 31 Density of helium at 273.16 K.

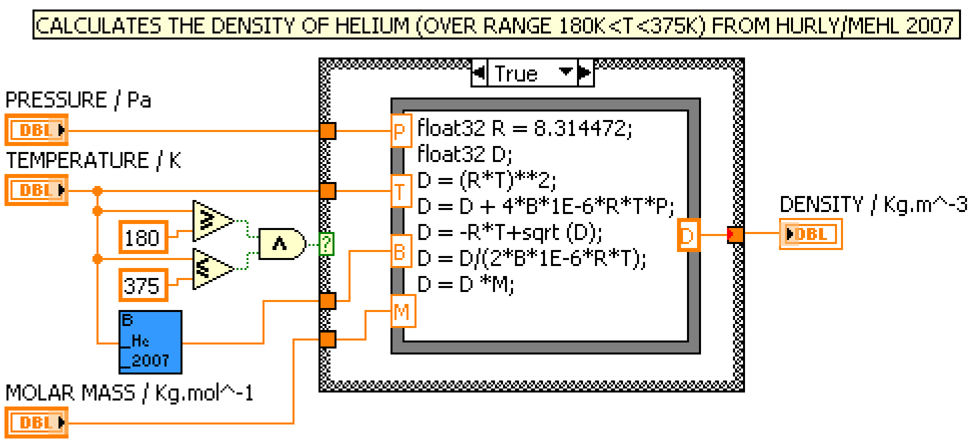

Figure 32 *LabView* code: **DEN_He_2007.vi**

Argon

For argon, the density was calculated to second order in pressure by using the 'pressure' virial expansion for a gas:

$$\frac{PV}{RT} = 1 + \frac{B}{RT}P + \frac{C - B^2}{(RT)^2}P^2 \tag{11}$$

Rearranging Equation 11, we obtain the molar volume:

$$V = \frac{RT}{P} + B + \frac{C - B^2}{RT}P \tag{12}$$

The mass density is then found by:

$$\rho = \frac{M}{V} \tag{13}$$

Figure 33 shows a plot of this for a temperature of 273.16 K. Figure 34 shows the VI.

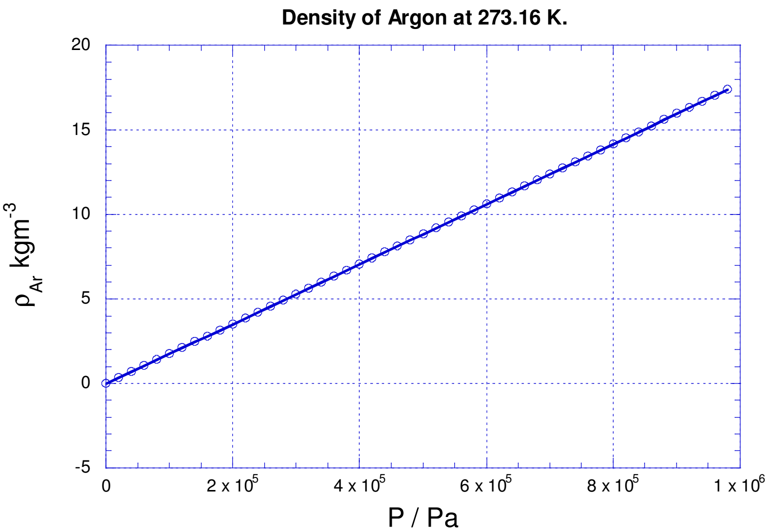

Figure 33 Density of Argon at 273.16 K.

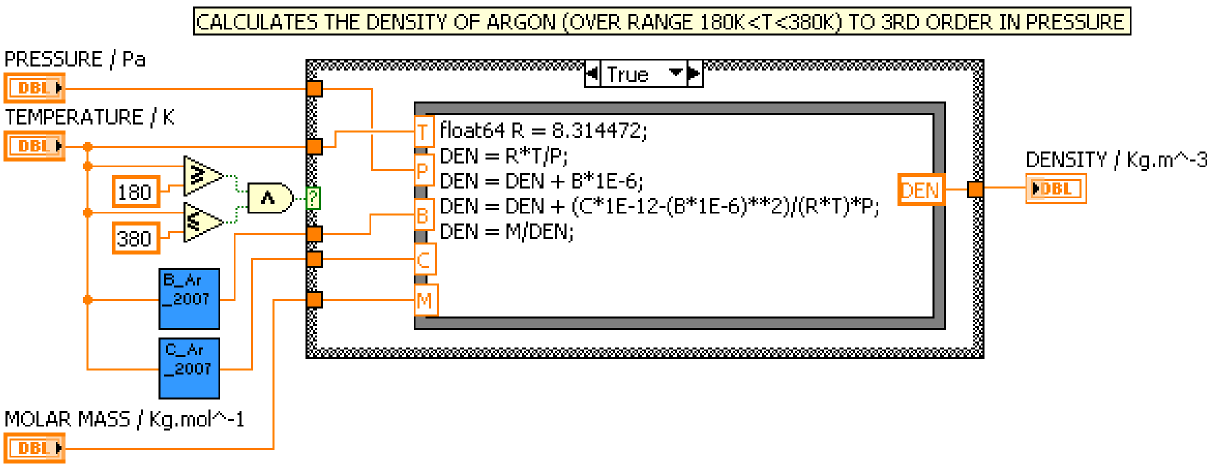

Figure 34 *LabView* code: **DEN_Ar_2007.vi**

14) HEAT CAPACITY AT CONSTANT PRESSURE: C_p [JkgK^{-1}]

Helium

For helium, the constant pressure heat capacity is found to first order in pressure using the relationship [6]:

$$C_p = \frac{5}{2}R - TP\frac{d^2B}{dT^2} \tag{14}$$

Figure 35 shows $C_p(He)$ at 1 atmosphere and Figure 36 shows the *LabView* VI.

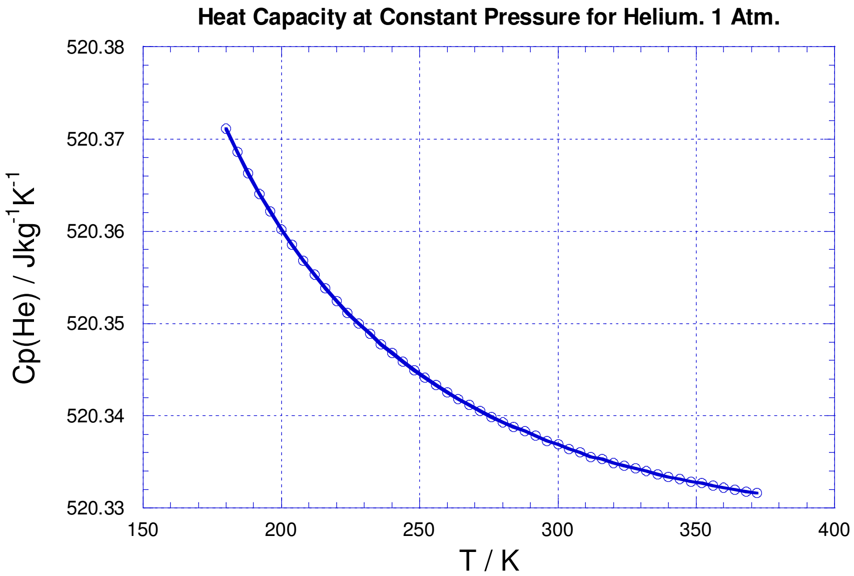

Figure 35 $C_p(He)$ at 1 atm.

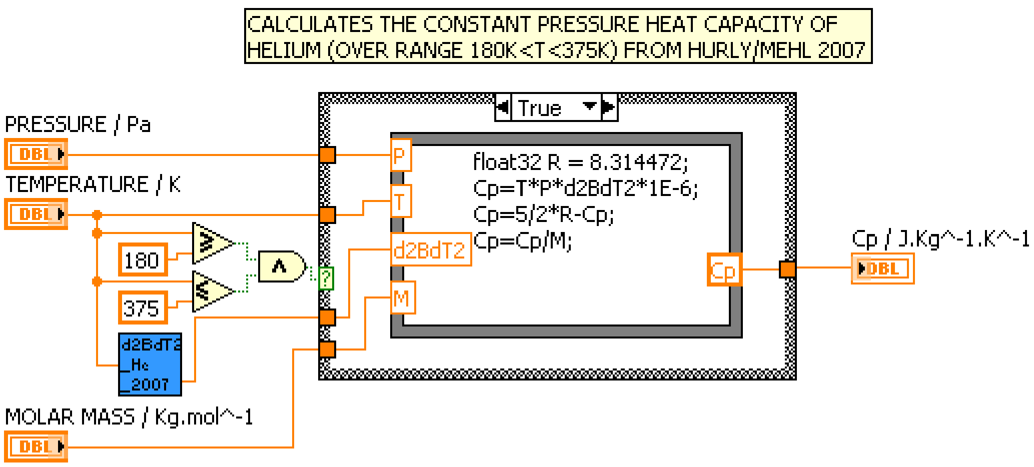

Figure 36 *LabView* code: **Cp_He_2007.vi**

Argon

For Argon, the constant pressure heat capacity is found to second order in pressure using the relationship [7]:

$$C_p = \frac{5}{2}R - R\left[\frac{T^2}{V}\frac{d^2B}{dT^2} - \frac{X}{V^2}\right] \tag{15}$$

Where:

$$X = \left[\left(B - T\frac{dB}{dT}\right)^2 - C + T\frac{dC}{dT} - \frac{T^2}{2}\frac{d^2C}{dT^2}\right] \tag{16}$$

and V is the molar volume given in Equation 12.

Figure 37 shows $C_p(Ar)$ at 1 atmosphere and Figure 38 shows the *LabView* VI.

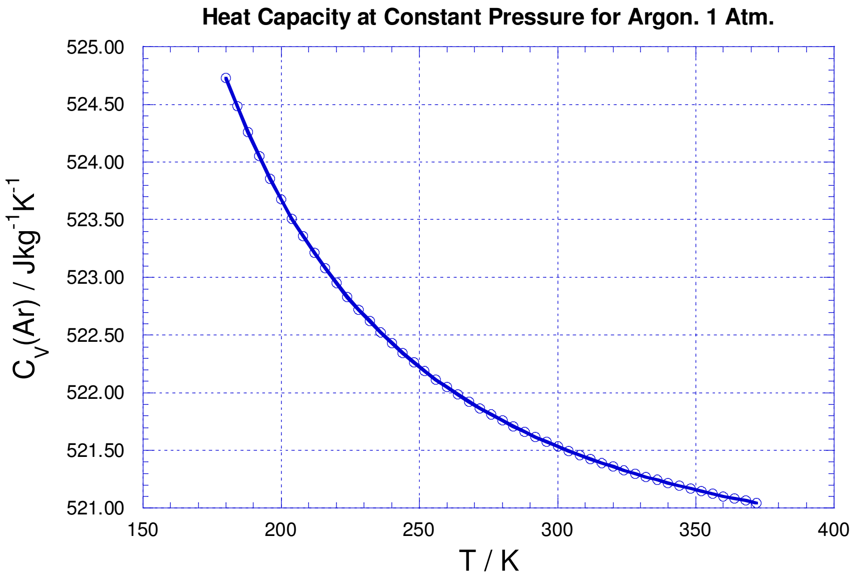

Figure 37 $C_p(Ar)$ at 1 atm.

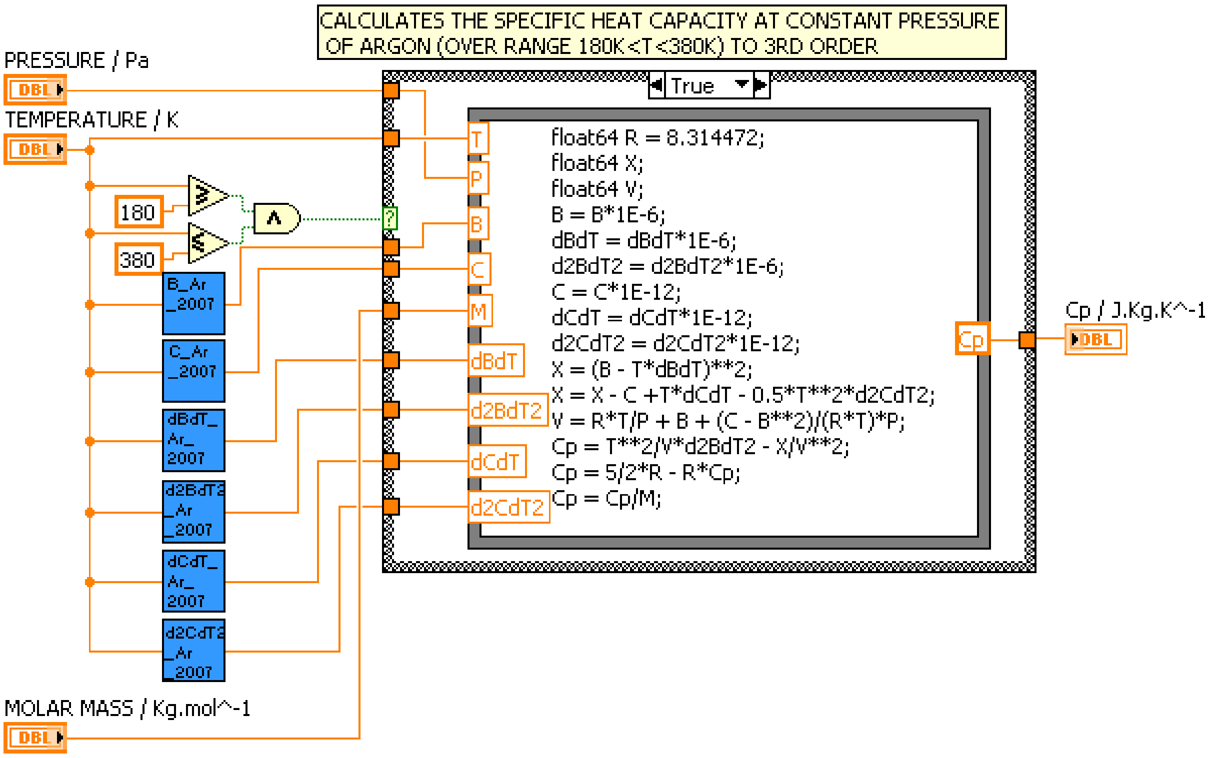

Figure 38 *LabView* code: **Cp_Ar_2007.vi**

15) HEAT CAPACITY AT CONSTANT VOLUME: C_V [JkgK^{-1}]

Helium

Not calculated.

Argon

The constant volume heat capacity was calculated [7] for argon to provide a simpler route to obtaining the ratio of heat capacities $\gamma = C_P / C_V$:

$$C_V = \frac{3}{2}R - R\left[\frac{2T}{V}\frac{dB}{dT} + \frac{T^2}{V}\frac{d^2B}{dT^2} + \frac{T}{V^2}\frac{dC}{dT} + \frac{T^2}{2V^2}\frac{d^2C}{dT^2}\right] \qquad (17)$$

Where V is the molar volume given in Equation 12.

Figure 39 shows the constant volume heat capacity of argon at 1 atm. And Figure 40 shows the *LabView* VI.

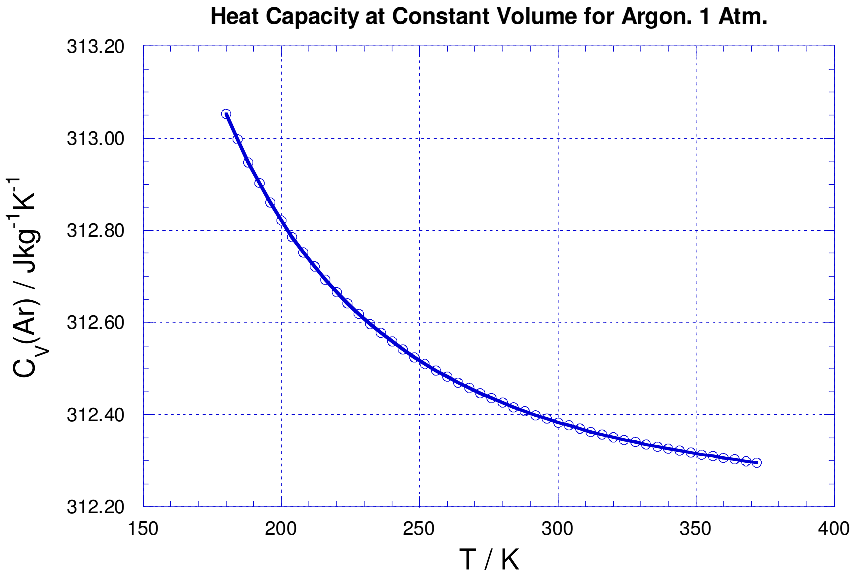

Figure 39 $C_V(Ar)$ at 1 atm.

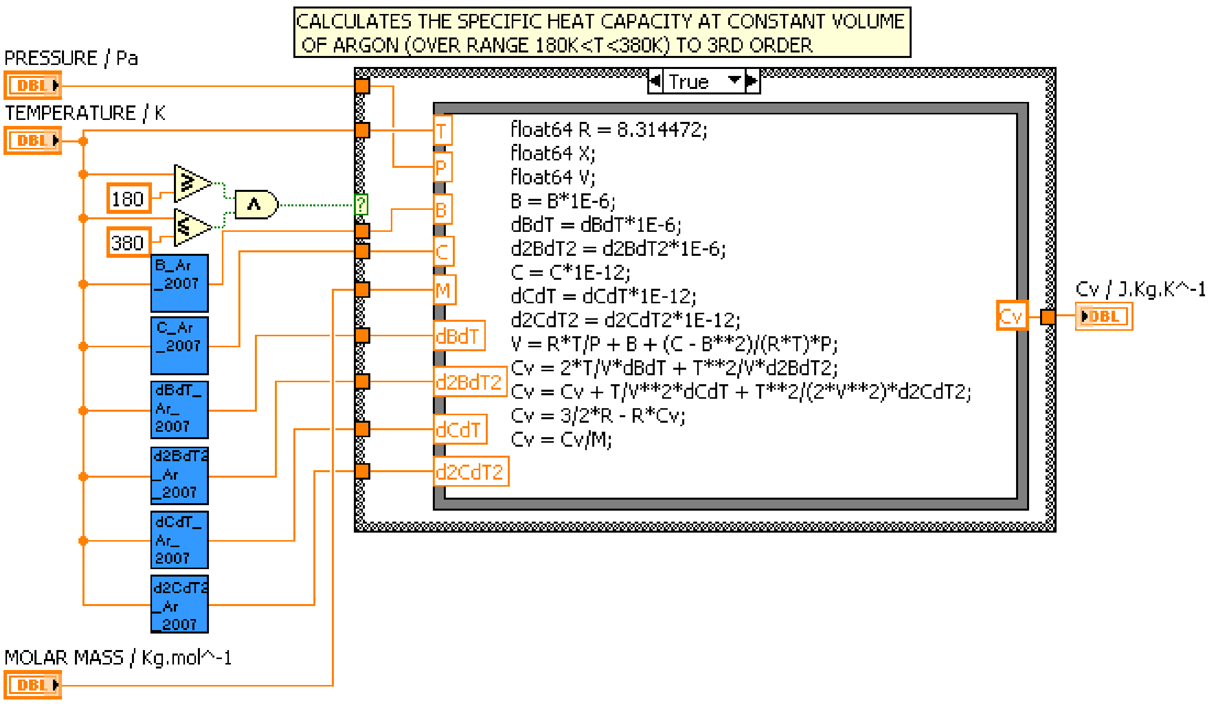

Figure 40 *LabView* code: **Cv_Ar_2007.vi**

16) RATIO OF HEAT CAPACITIES: γ

Helium

For helium, we use the expression of *Moldover* [6]:

$$\gamma = \frac{5}{3}\left[1 + 2(\gamma - 1)\frac{dB}{dT}\frac{P}{R} + (\gamma - 1)^2 T \frac{d^2B}{dT^2}\frac{P}{R}\right] \tag{18}$$

This can be solved quadratically to give γ.

Figure 41 shows γ for helium at 1 atm. and Figure 42 shows the *LabView* VI.

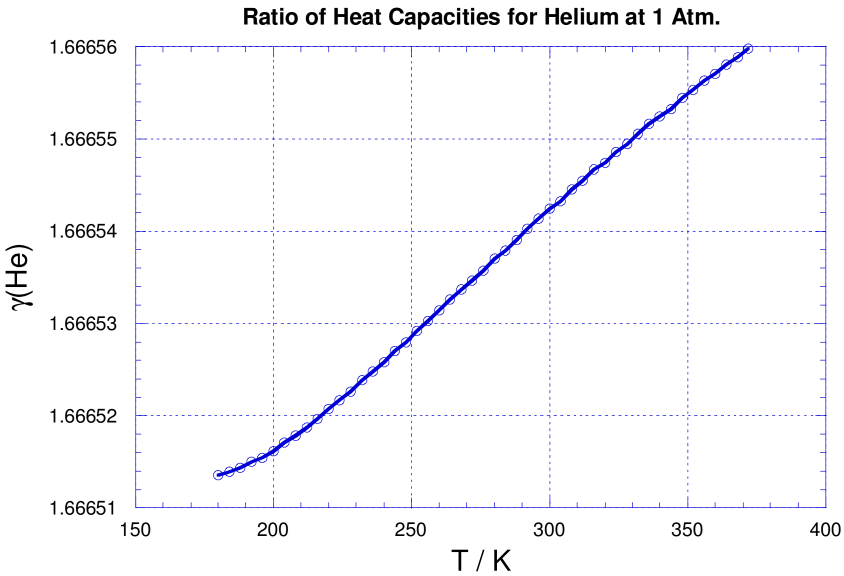

Figure 41 γ for helium at 1 atm.

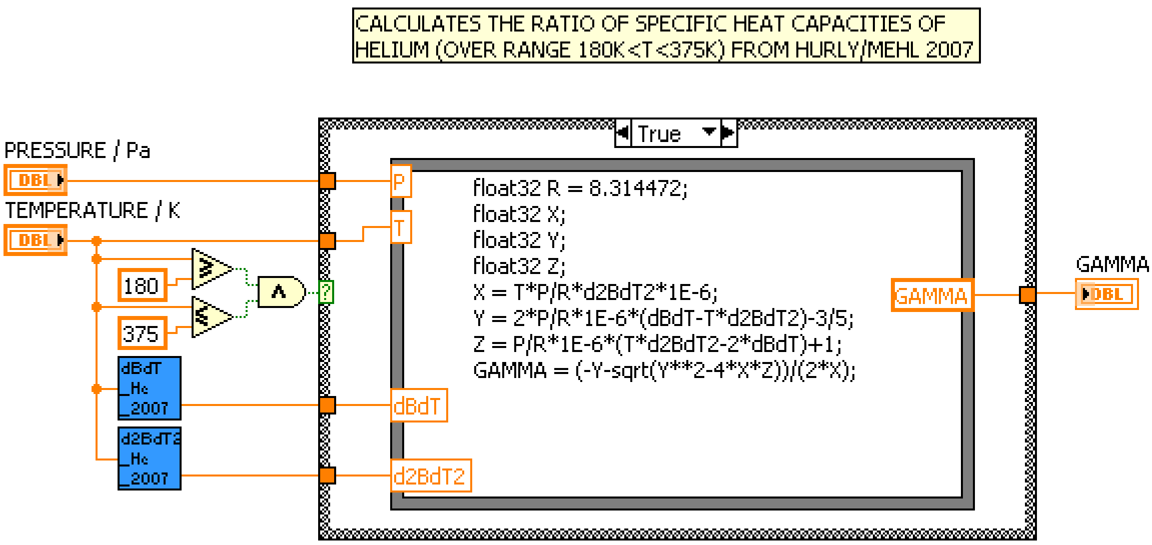

Figure 42 *LabView* code: **GAMMA_He_2007.vi**

Argon

For argon, we simply use the ratio of C_P/C_V . Figure 43 shows γ for argon at 1 atm. and Figure 44 shows the *LabView* VI.

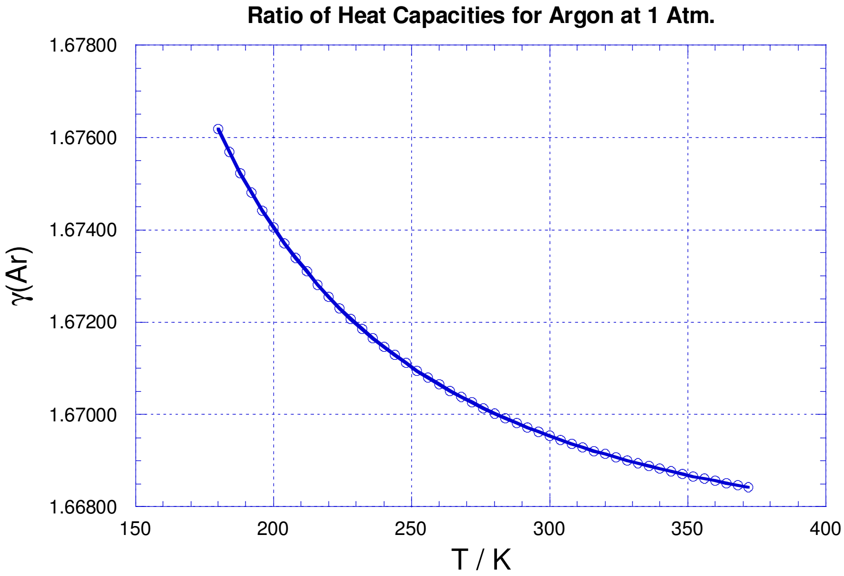

Figure 43 γ for argon at 1 atm.

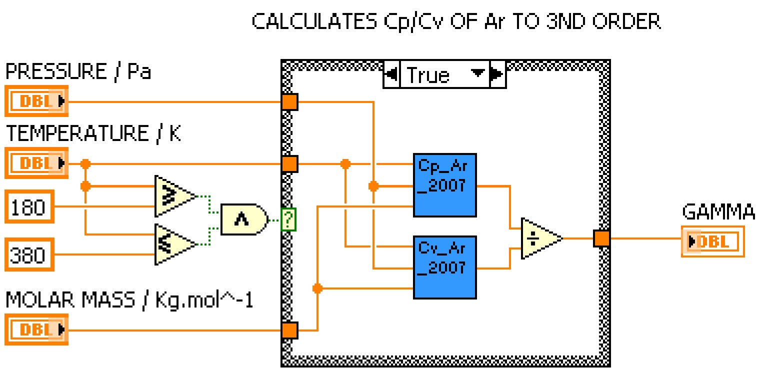

Figure 44 *LabView* code: **GAMMA_Ar_2007.vi**

17) THERMAL CONDUCTIVITY: λ [WM^{-1}K^{-1}]

Helium

The thermal conductivity of helium was calculated by fitting the data of Mehl [3]:

$$\lambda = 3.287864\times10^{-10}T^3 - 4.617073\times10^{-7}T^2 + 5.419125\times10^{-4}T + 2.575358\times10^{-2} + 292.7\times10^{-6}\rho \tag{19}$$

Where ρ is the density given in §12.

Figure 45 shows the fit and Figure 46 shows the *LabView* VI.

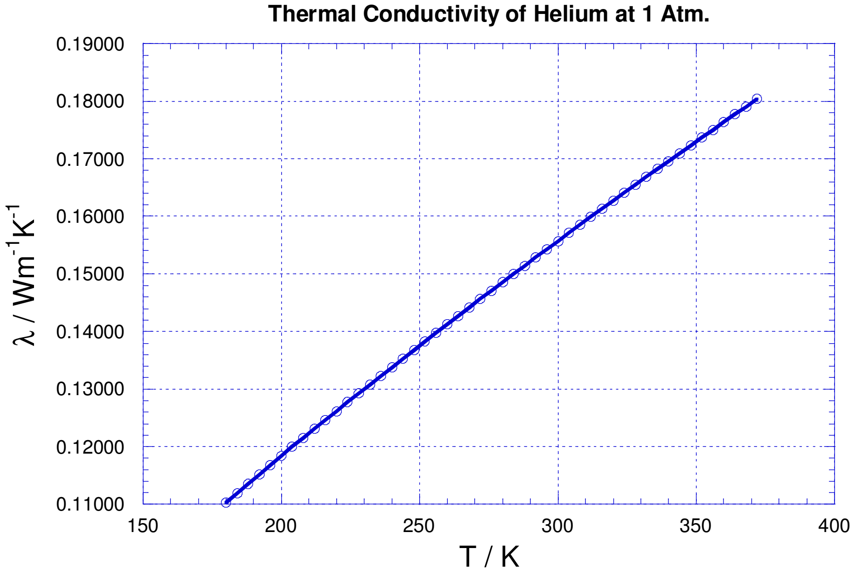

Figure 45 Thermal conductivity of helium at 1 atm.

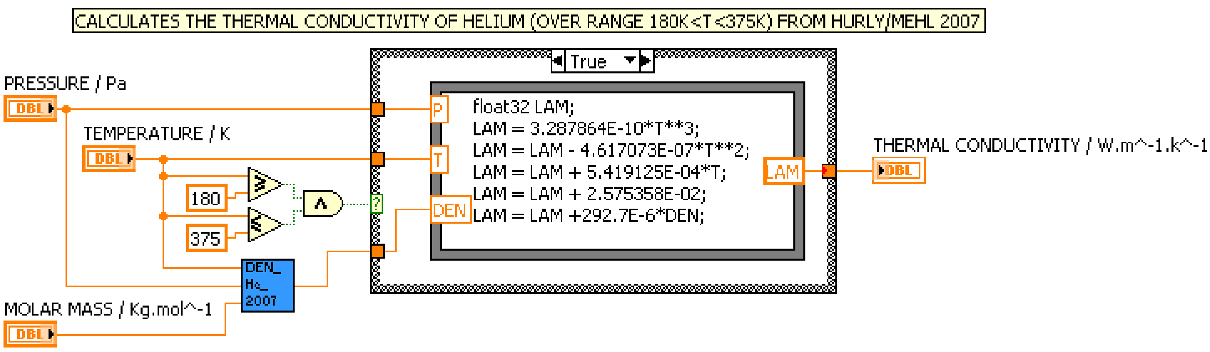

Figure 46 *LabView* code: **TH_CON_He_2007.vi**

Argon

The thermal conductivity of argon was calculated by using the fit of *Moldover* [8]:

$$\lambda = 6.4622\times10^{-5}T - 7.7489\times10^{-11}T^3 + 5.4288\times10^{-14}T^4 + 2.16\times10^{-5}\rho \qquad (20)$$

Where ρ is the density given in §12.

Figure 47 shows the fit and Figure 48 shows the *LabView* VI.

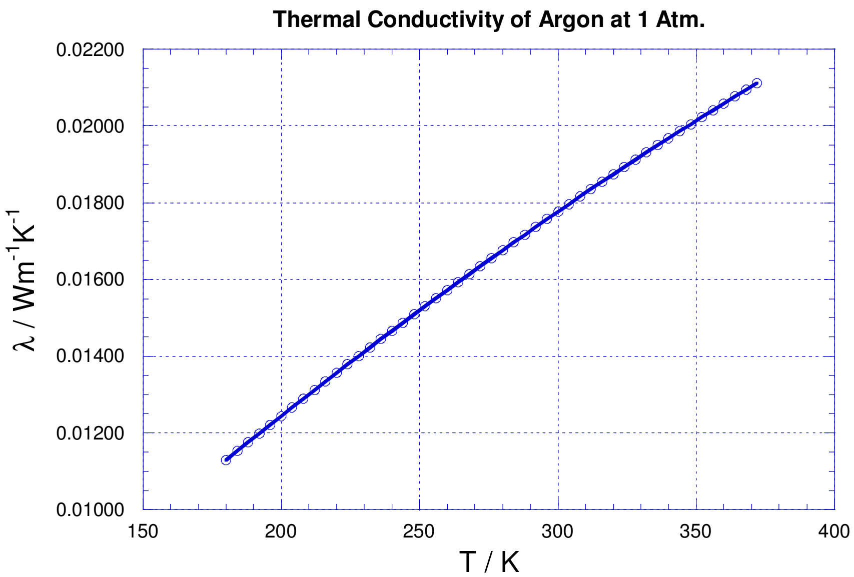

Figure 47 Thermal conductivity of argon at 1 atm.

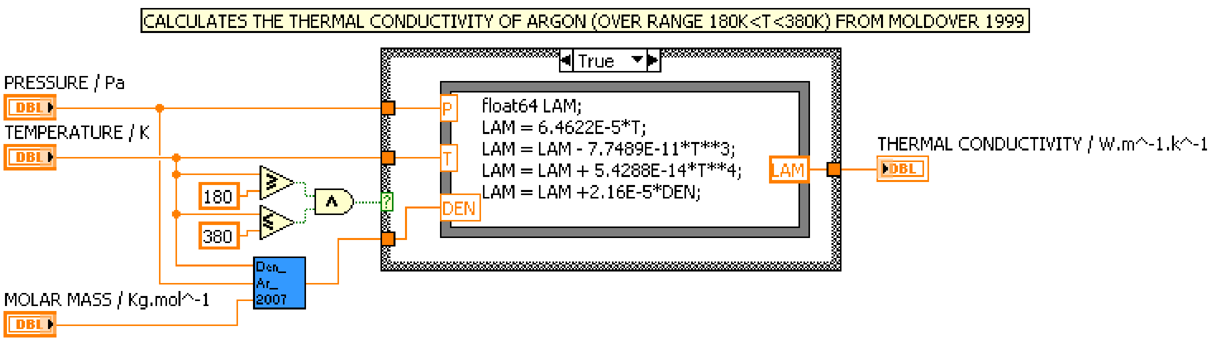

Figure 48 *LabView* code: **TH_CON_Ar_2007.vi**

18) VISCOSITY: η [PaS]

Helium

The viscosity of helium versus temperature is taken from *Mehl* [3] and a density term is added [9] to account for changes with pressure. Figure 49 shows this for a pressure of 1 atm. Figure 50 shows the *LabView* VI.

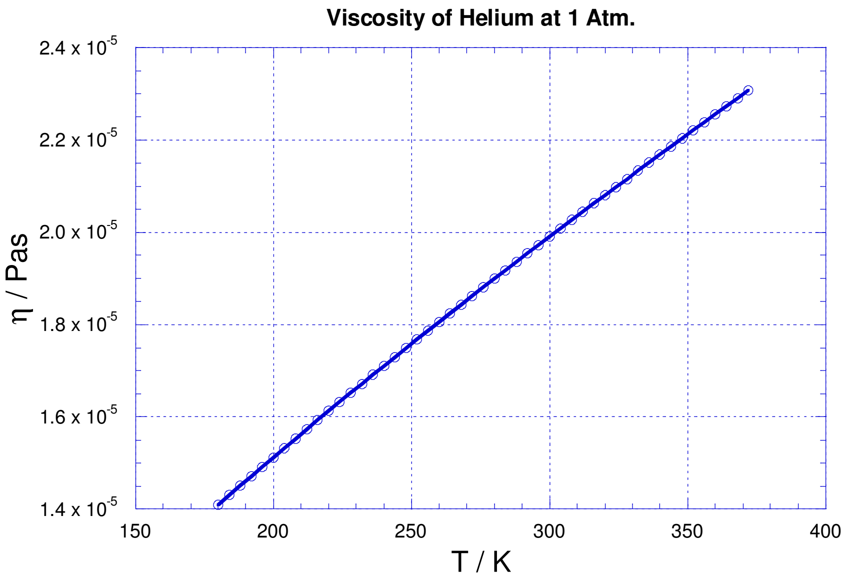

Figure 49 Viscosity of helium at 1 atm.

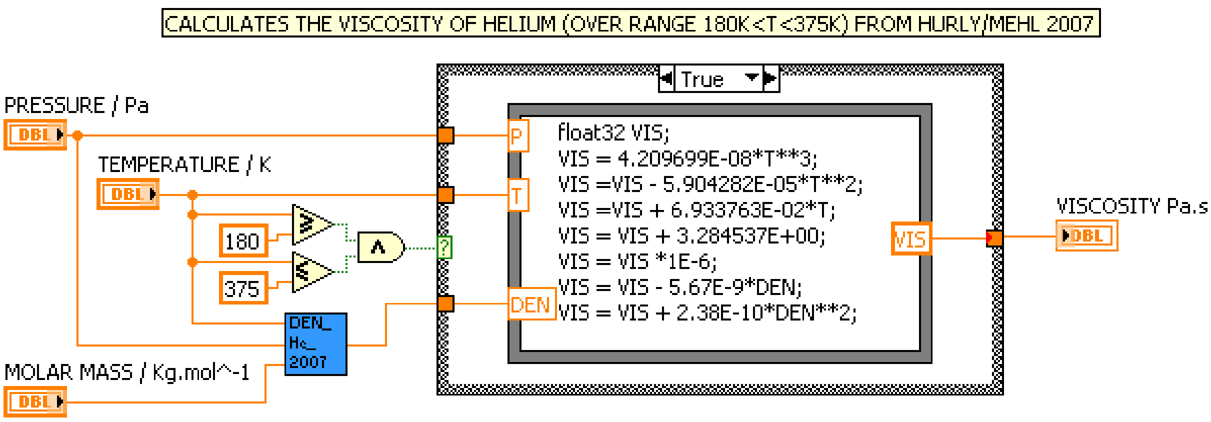

Figure 50 *LabView* code: **VISC_He_2007.vi**

Argon

The viscosity of argon is calculated using the relationship of *Benedetto* [5]:

$$\eta = 8.2822\times10^{-8} T - 1.0088\times10^{-13} T^3 + 7.1206\times10^{-17} T^4 + 11.10\times10^{-9} \rho \qquad (21)$$

Where ρ is the density given in §12.

This is shown in Figure 51. The *LabView* VI is shown in Figure 52.

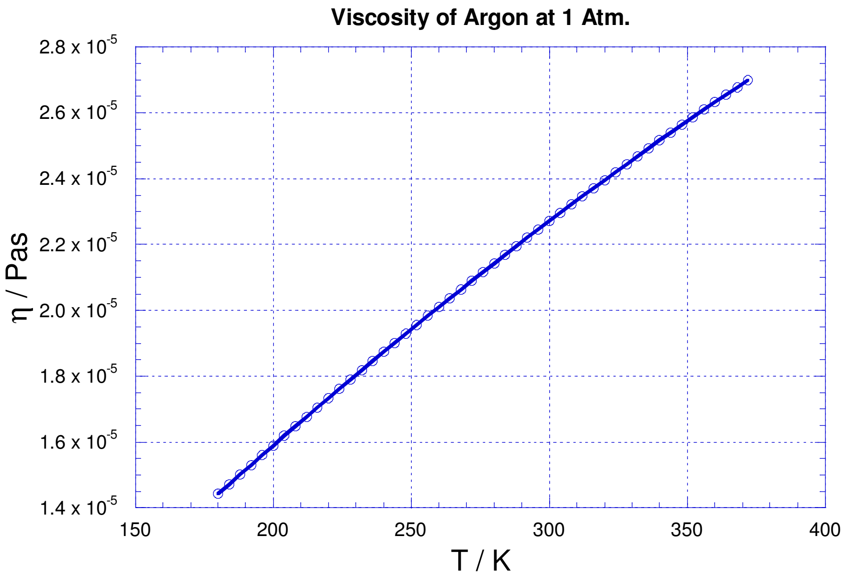

Figure 51 Viscosity of argon at 1 atm.

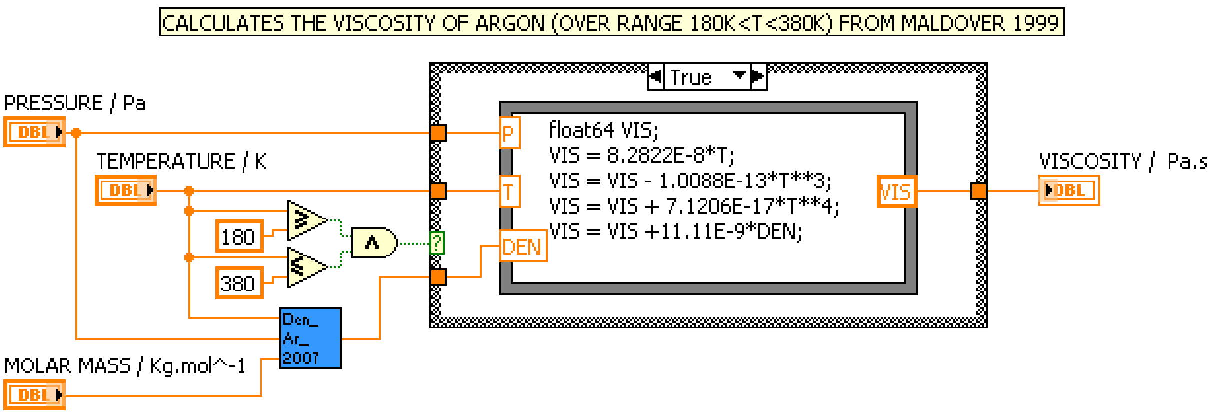

Figure 52 *LabView* code: **VISC_Ar_2007.vi**

19) THERMAL PENETRATION LENGTH: δ_h [m]

The *thermal penetration length* [6] of a gas is given by:

$$\delta_{TH} = \left[\frac{\lambda}{\pi \rho C_P f} \right]^{\frac{1}{2}} \qquad (22)$$

where:

λ is the thermal conductivity.
ρ is the density.
C_p is the heat capacity at constant pressure.
f is the acoustic measurement frequency.

Helium

Figure 53 shows the *thermal penetration length* for helium at 1 atm. for the (0,2) mode and a sphere radius of 50 mm. The *LabView* VI is show in Figure 54.

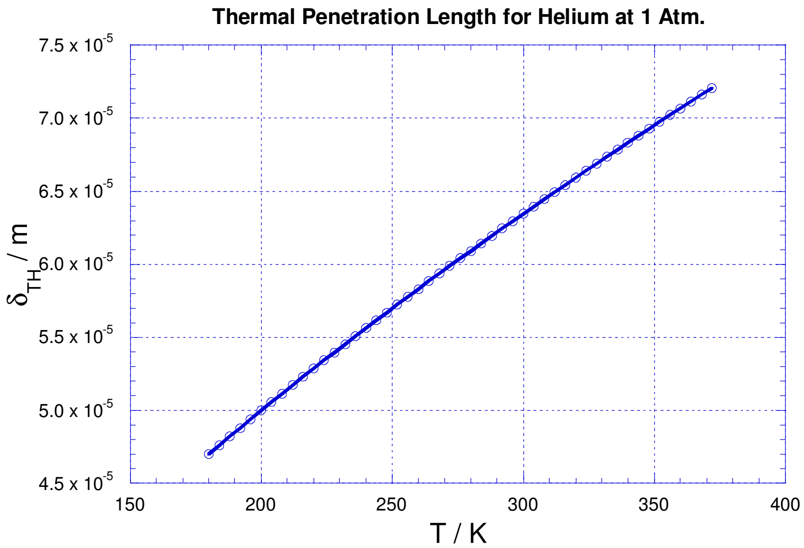

Figure 53 *Thermal penetration length* for helium at 1 atm. (0,2) mode, 50 mm radius sphere.

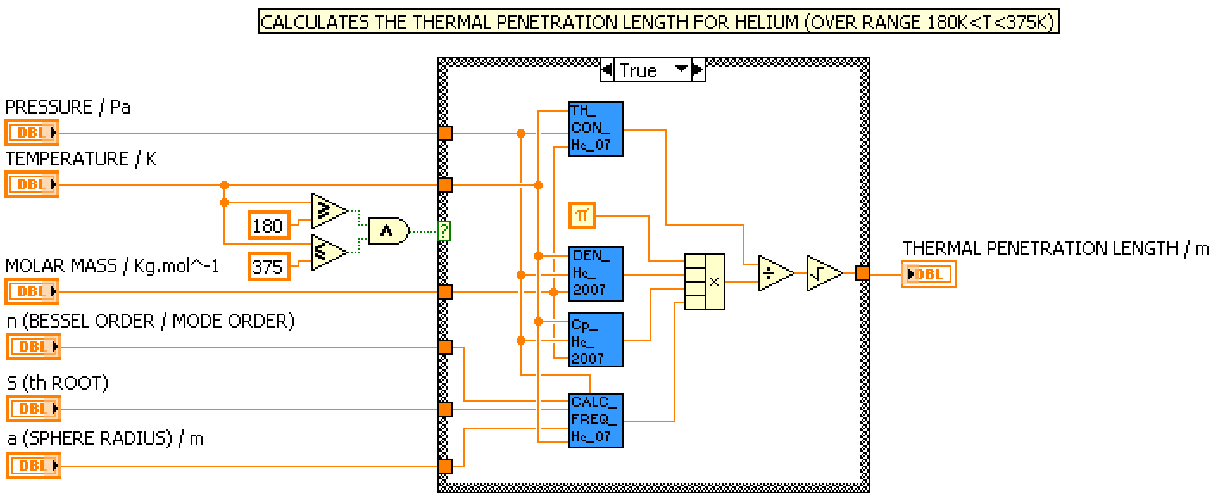

Figure 54 *LabView* code: **TH_PEN_He_2007.vi**

Argon

Figure 55 shows the *thermal penetration length* for argon at 1 atm. for the (0,2) mode and a sphere radius of 50 mm. The *LabView* VI is show in Figure 56.

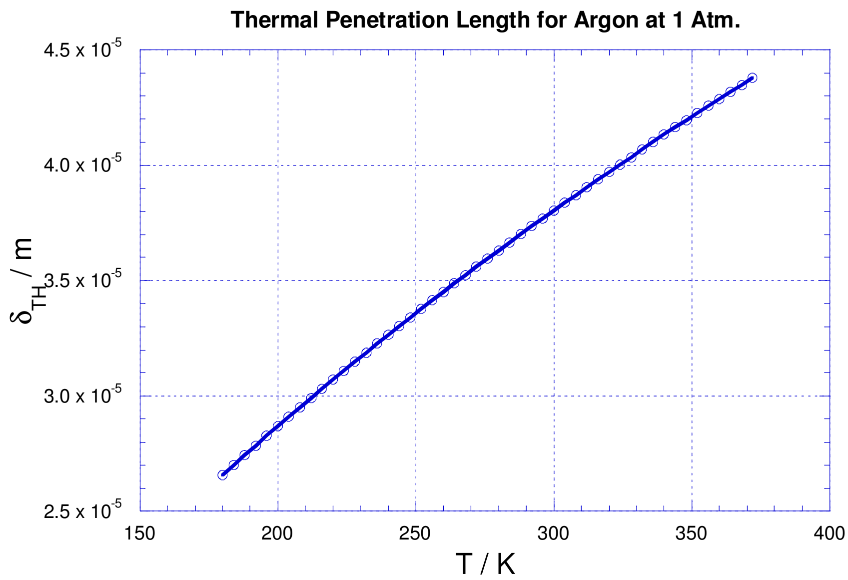

Figure 55 *Thermal penetration length* for argon at 1 atm. (0,2) mode, 50 mm radius sphere.

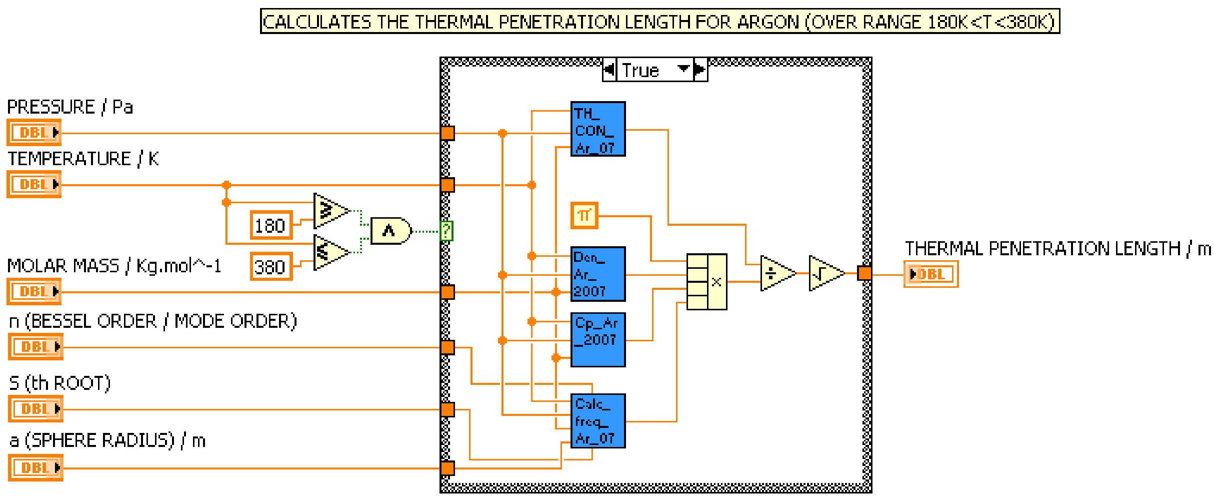

Figure 56 *LabView* code: **TH_PEN_Ar_2007.vi**

20) VISCOUS PENETRATION LENGTH: δ_v [m]

The *viscous penetration length* [6] is given by:

$$\delta_V = \left[\frac{\eta}{\pi\rho f}\right]^{\frac{1}{2}} \tag{23}$$

where:

η is the viscosity.
ρ is the density.
f is the acoustic measurement frequency.

Helium

Figure 57 shows the *viscous penetration length* for helium at 1 atm. for the (0,2) mode and a sphere radius of 50 mm. The *LabView* VI is show in Figure 58.

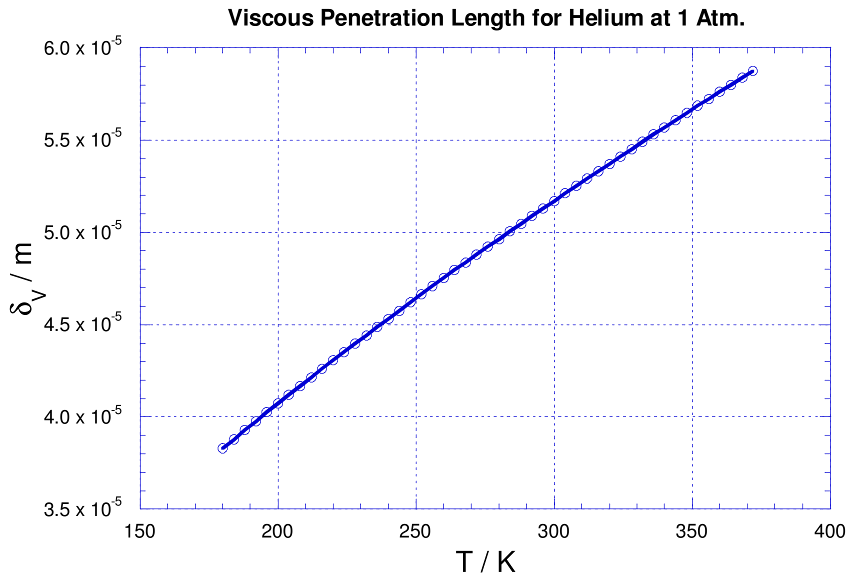

Figure 57 *Viscous penetration length* for helium at 1 atm. (0,2) mode, 50 mm radius sphere.

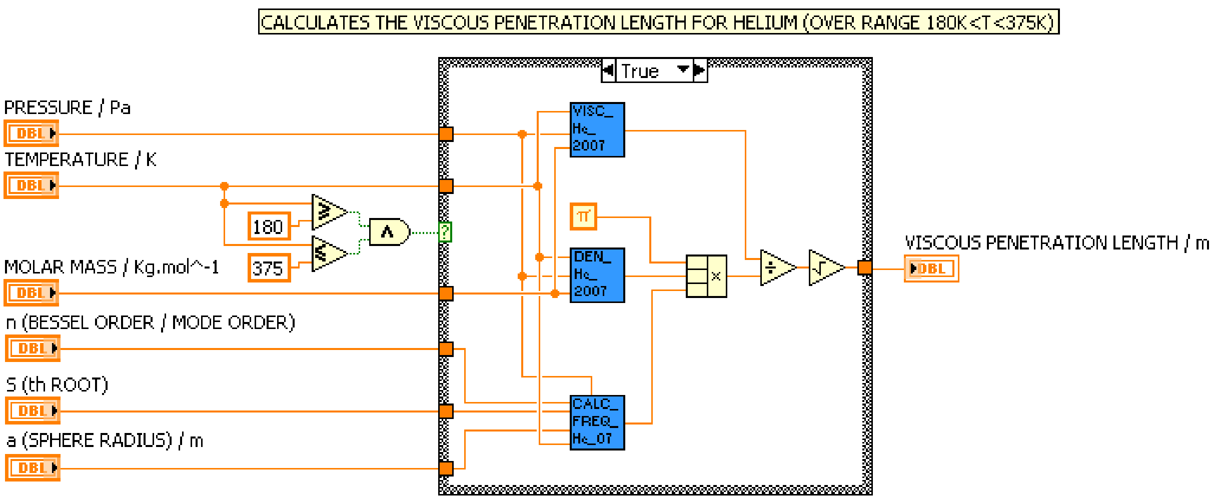

Figure 58 *LabView* code: **VIS_PEN_He_2007.vi**

Argon

Figure 59 shows the *viscous penetration length* for argon at 1 atm. for the (0,2) mode and a sphere radius of 50 mm. The *LabView* VI is show in Figure 60.

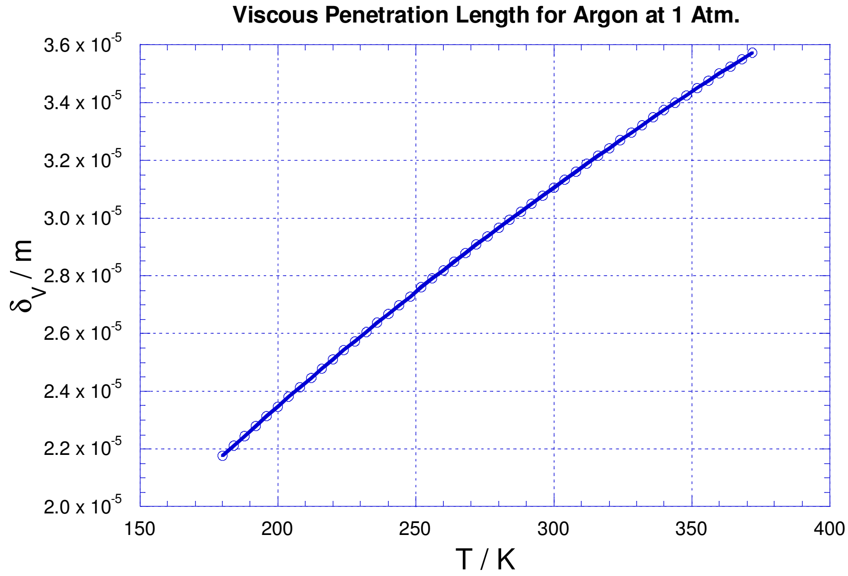

Figure 59 *Viscous penetration length* for argon at 1 atm. (0,2) mode, 50 mm radius sphere.

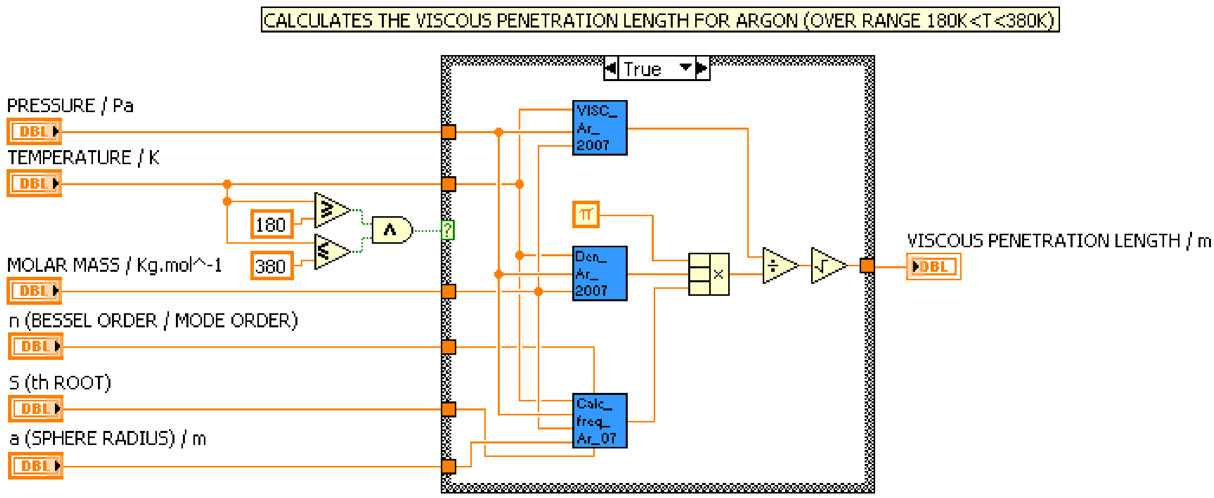

Figure 60 *LabView* code: **VIS_PEN_Ar_2007.vi**

21) THERMAL ACCOMMODATION LENGTH: l_{th} [m]

The *thermal accommodation length* [6] of a gas is given by:

$$l_{th} = \frac{\lambda}{P}\left(\frac{\pi M T}{2R}\right)^{\frac{1}{2}}\left(\frac{2-h}{h}\right)\left(\frac{1}{C_v/R+1/2}\right) \qquad (24)$$

Where h is the thermal accommodation coefficient that can be found experimentally.

Helium

Figure 61 shows the *thermal accommodation length* for helium at 1 atm. for $h = 0.85$. The *LabView* VI is show in Figure 62.

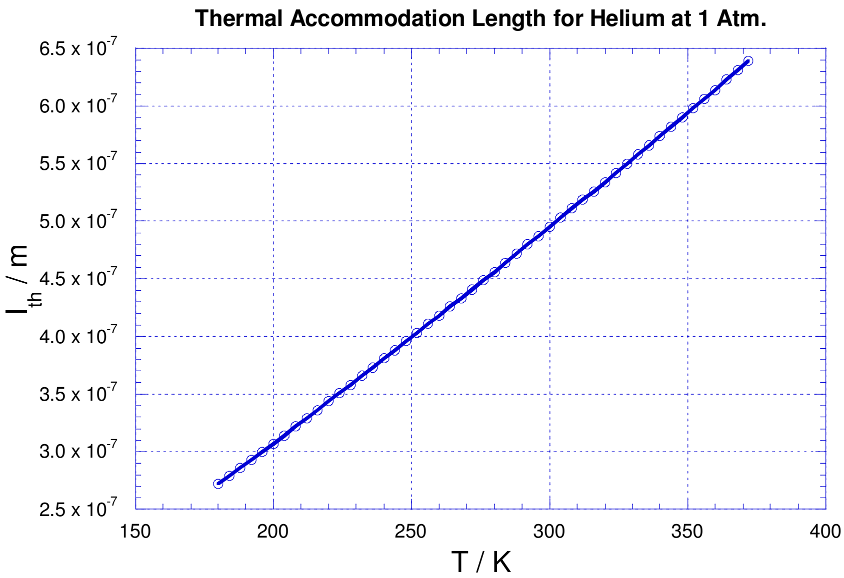

Figure 61 *Thermal accommodation length* for helium at 1 atm. for *h = 0.85*.

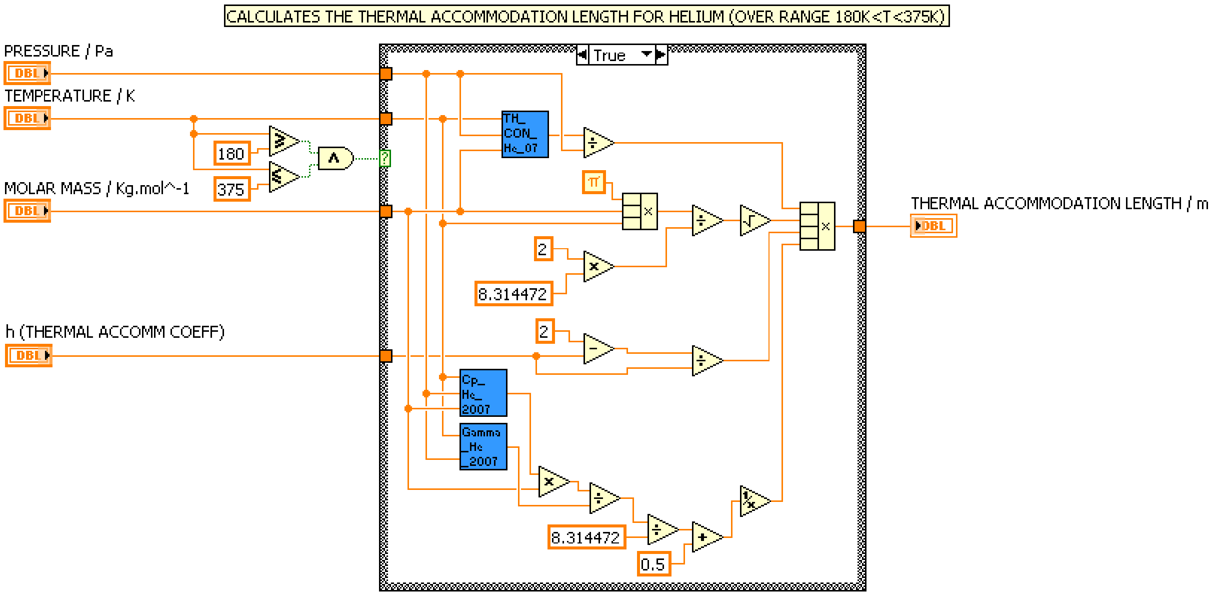

Figure 62 *LabView* code: **TH_ACC_He_2007.vi**

Figure 63 shows the *thermal accommodation length* for argon at 1 atm. for $h = 0.85$. The *LabView* VI is show in Figure 64.

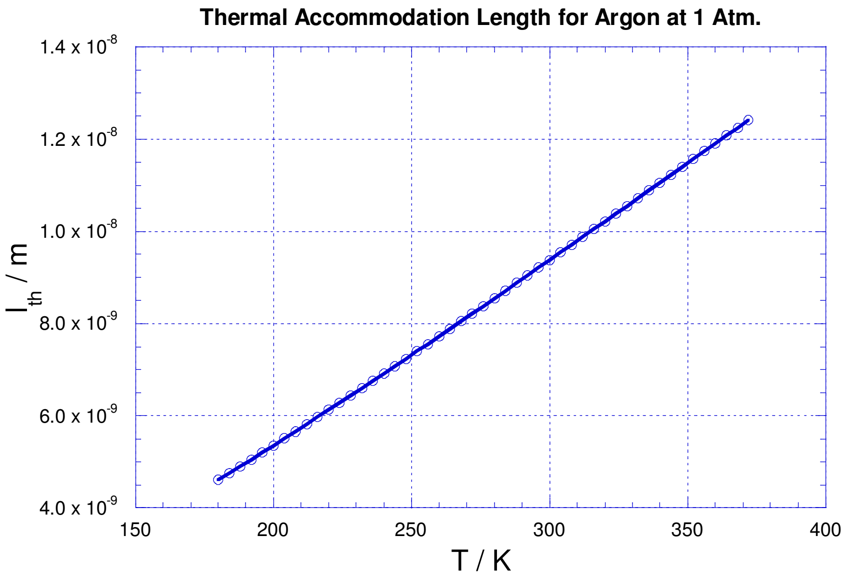

Figure 63 *Thermal accommodation length* for argon at 1 atm. for *h = 0.85*.

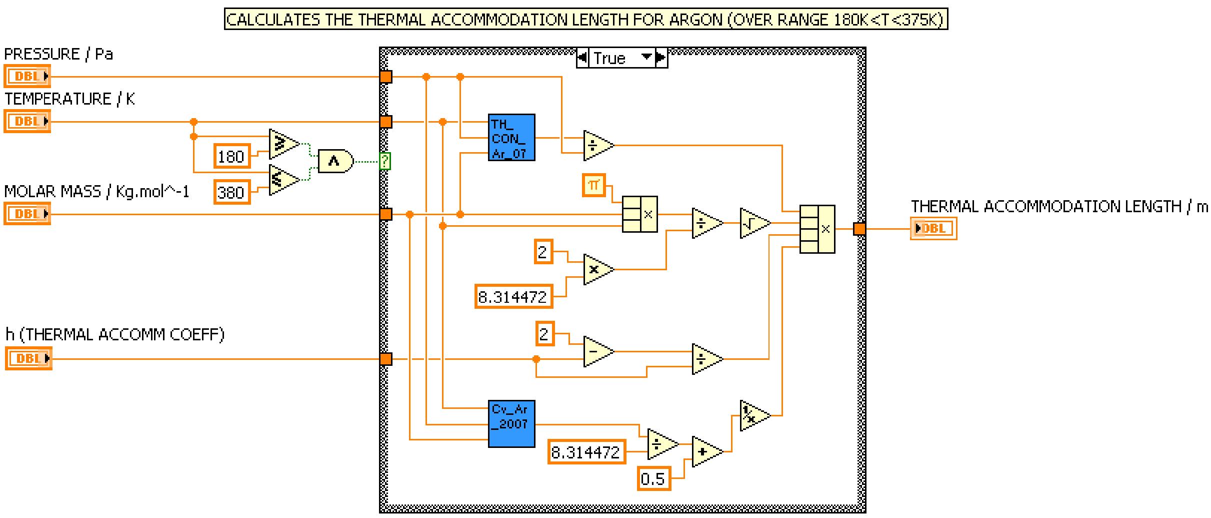

Figure 64 *LabView* code: **TH_ACC_Ar_2007.vi**

22) THERMAL CONDUCTIVITY OF COPPER: λ_{Cu} [$Wm^{-1}K^{-1}$]

The thermal conductivity of copper [10] can be fitted accurately with:

$$\lambda_{Cu} = 373.4253 + 8060.168/T \tag{25}$$

Figure 65 shows the raw data and the fit. Figure 66 shows the *LabView* VI.

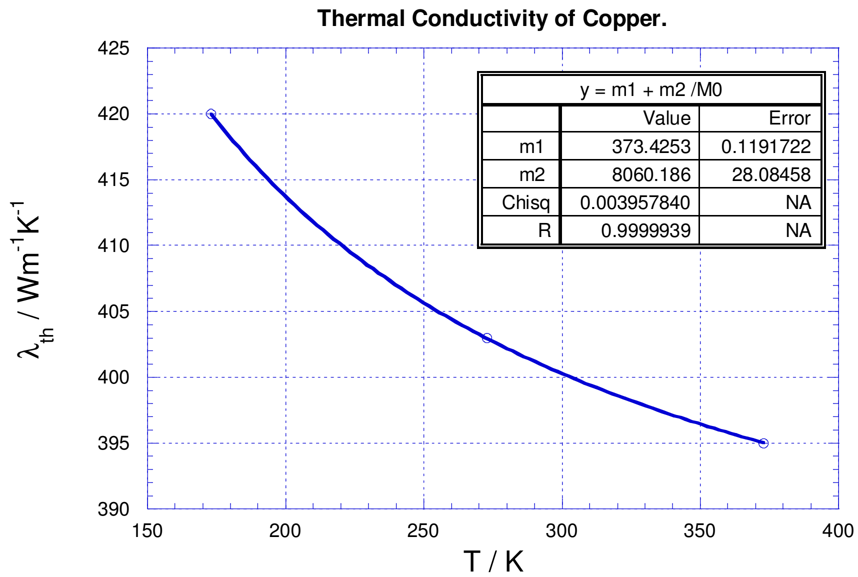

Figure 65 Thermal conductivity of copper.

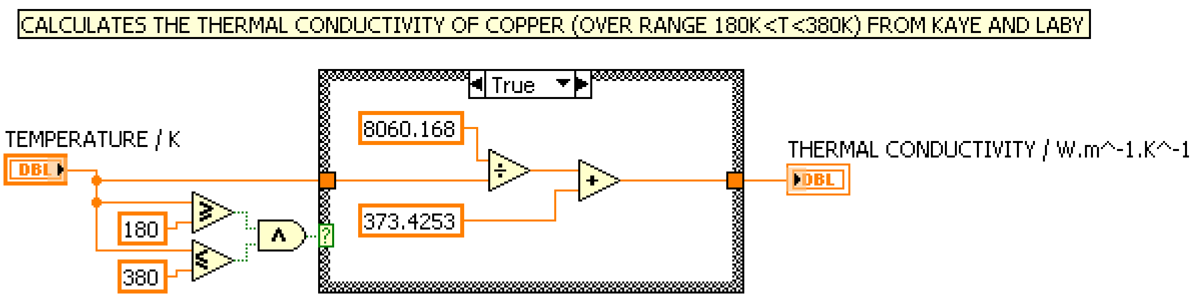

Figure 66 *LabView* code: **TH_CON_Cu_2007.vi**

23) HEAT CAPACITY OF COPPER: C_p [$Jkg^{-1}K^{-1}$]

The heat capacity of copper [10] can be fitted accurately with:

$$C_{p,Cu} = 445.2764\text{-}18048.78/T \tag{26}$$

Figure 67 shows the raw data and the fit. Figure 68 shows the *LabView* VI.

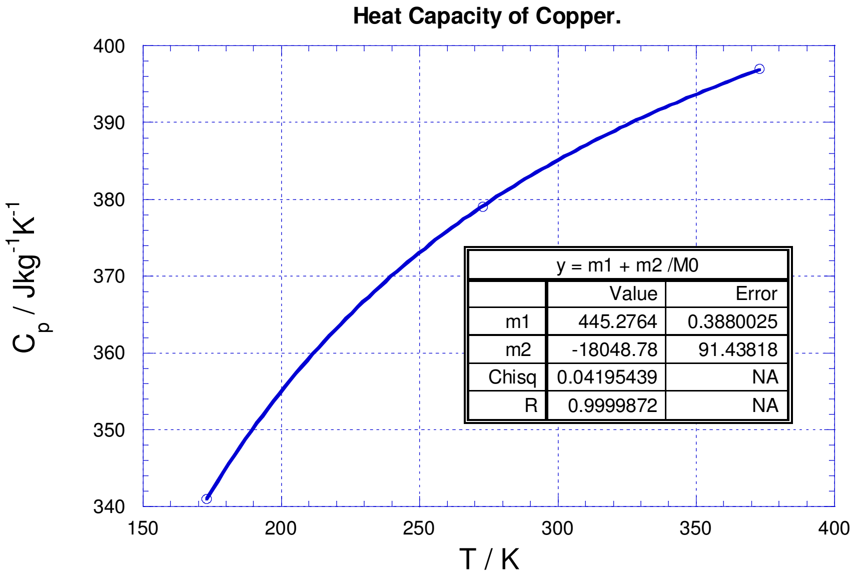

Figure 67 Heat capacity of copper.

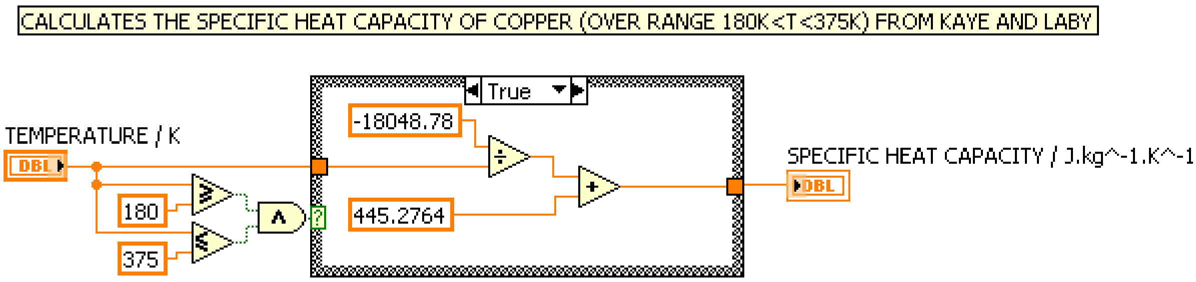

Figure 68 *LabView* code: **Cp_Cu_2007.vi**

24) THERMAL PENETRATION LENGTH FOR COPPER: $\delta_{th,Cu}$ [m]

The *thermal penetration length* for copper [6] is given by:

$$\delta_{th,Cu} = \left[\frac{\lambda_{Cu}}{\pi \rho_{Cu} C_{P,Cu} f}\right]^{\frac{1}{2}} \tag{27}$$

Where ρ_{cu} is the density of copper (8933 kgm^{-3})

Figure 69 shows the thermal penetration length for copper at the (0,2) helium and argon radial mode frequencies (1 atm.). Figures 70 and 71 show the LabView VIs. Note, the VI for helium frequencies is just called **TH_PEN_Cu_2007.VI** , where as the VI for argon frequencies is call **TH_PEN_Cu_Ar_2007.VI** .

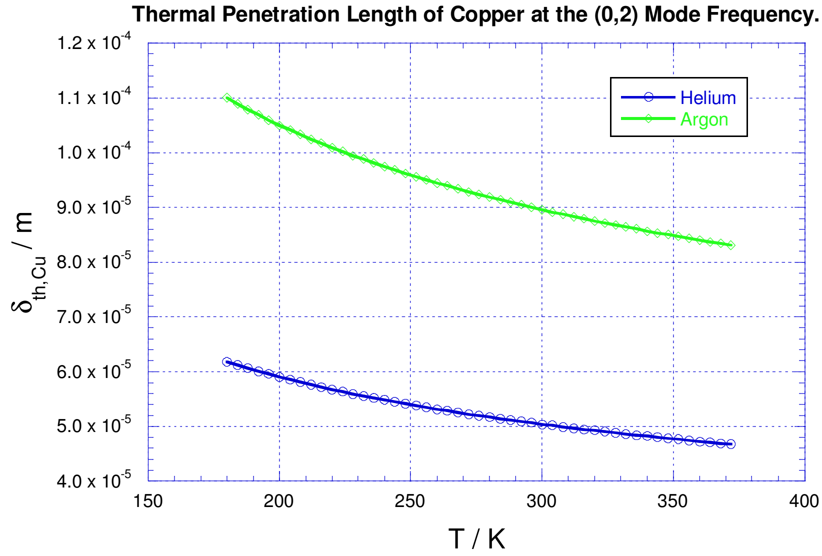

Figure 69 *Thermal penetration length* of copper at the (0,2) helium and argon frequencies.

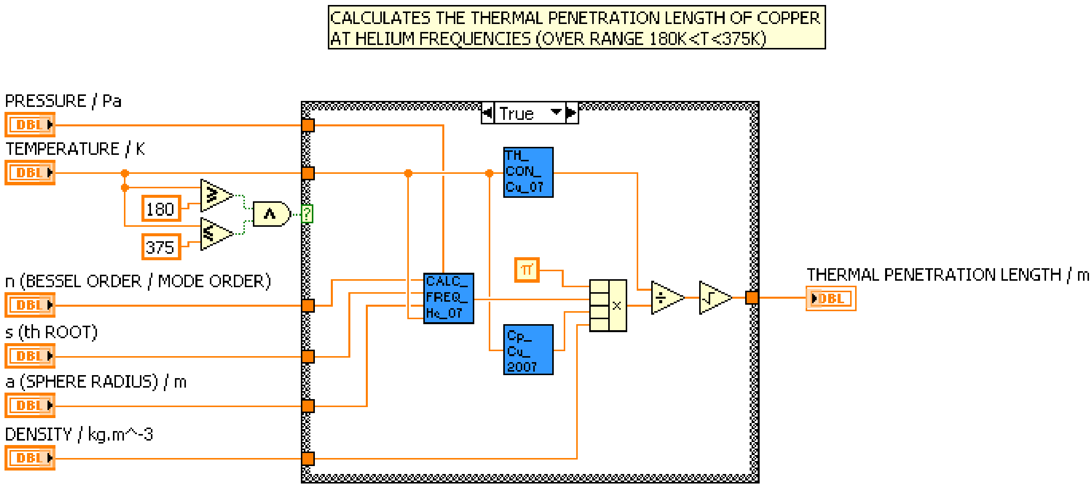

Figure 70 *LabView* code: **TH_PEN_Cu_2007.vi**

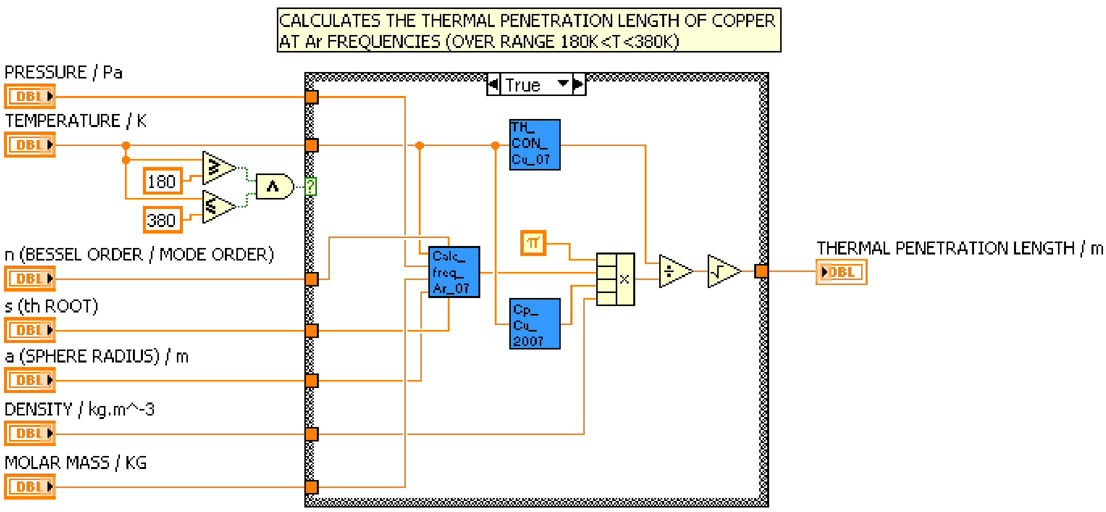

Figure 71 *LabView* code: **TH_PEN_Cu_Ar_2007.vi**

25) THERMAL BOUNDARY LAYER CORRECTION: $\Delta f/f$, g/f

The *thermal boundary layer correction* (TBLC) combines the *thermal penetration length* (δ_{th}), the *thermal accommodation length* (l_{th}) and the *thermal penetration length of the shell* ($\delta_{th,Cu}$) and can be written in terms of the fractional shift in resonance frequency from the ideal frequency ($\Delta f/f$) and the resonance halfwidth (g/f) as [6]:

$$\begin{aligned}\frac{\Delta f}{f} &= \frac{-(\gamma-1)}{2a}\delta_{th}\cdot\frac{1}{1-n(n-1)/Z_{ns}^2} \\ &+\frac{(\gamma-1)}{a}l_{th} \\ &+\frac{(\gamma-1)}{2a}\delta_{th,Cu}\cdot\frac{\lambda_{Gas}}{\lambda_{Shell}}\end{aligned} \tag{28}$$

and

$$\begin{aligned}\frac{g}{f} &= \frac{(\gamma-1)}{2a}\delta_{th}\cdot\frac{1}{1-n(n-1)/Z_{ns}^2} \\ &+\frac{(\gamma-1)}{2a}\delta_{th,Cu}\cdot\frac{\lambda_{Gas}}{\lambda_{Shell}}\end{aligned} \tag{29}$$

Where:

λ_{Gas} is the thermal conductivity of the gas.
λ_{Shell} is the thermal conductivity of the shell.
a is the average radius of the sphere.
δ_{th} is the thermal penetration length (§ 18)
l_{th} is the thermal accommodation length (§ 20)
δ_{v} is the viscous penetration length (§ 19)

Helium

Figure 72 shows the frequency shift and halfwidth of the (0,2) mode due to the *thermal boundary layer* and *bulk dissipation* (§ 26) for helium at a temperature of 273.16 K, sphere radius of 50 mm and *thermal accommodation coefficient* of h = 0.5. The gas thermal penetration is the dominant contribution, with a magnitude of approximately **400 PPM** at 100 kPa.

The second largest contribution to the frequency shift and halfwidth are the *thermal accommodation* and *bulk dissipation* respectively. Figure 73 shows this. At 100 kPa, this amounts to magnitudes of **13.3 PPM** and **14.4 PPM** for the *thermal accommodation* and *bulk dissipation* respectively.

Figure 74 shows the *shell thermal penetration* contribution and it is approximately constant at **0.13 PPM**.

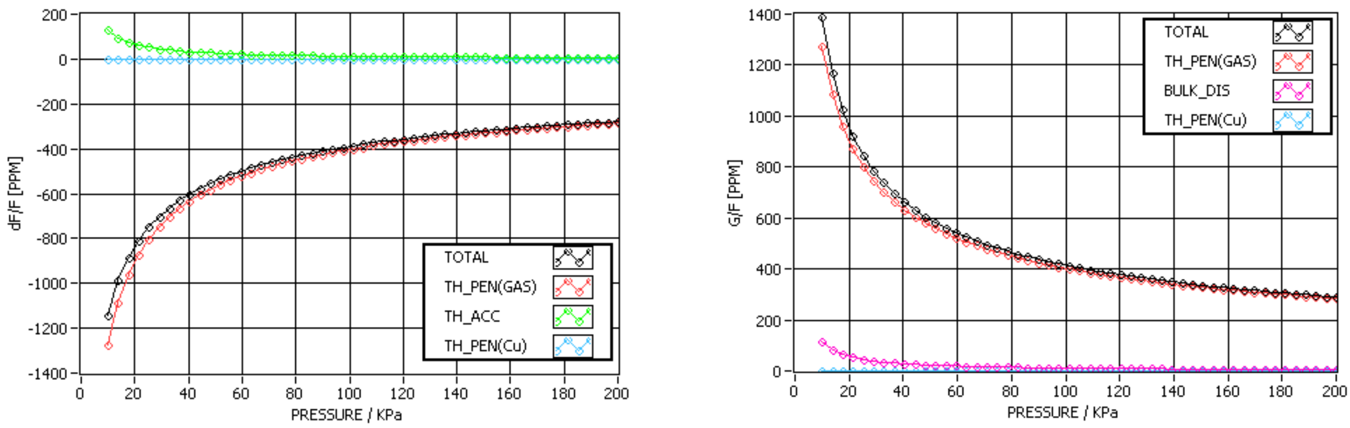

Figure 72 Full scale: frequency shift and halfwidth of the (0,2) mode due to the *thermal boundary layer* and *bulk dissipation*. **Helium**, T = 273.16 K, a = 50 mm, h = 0.5.

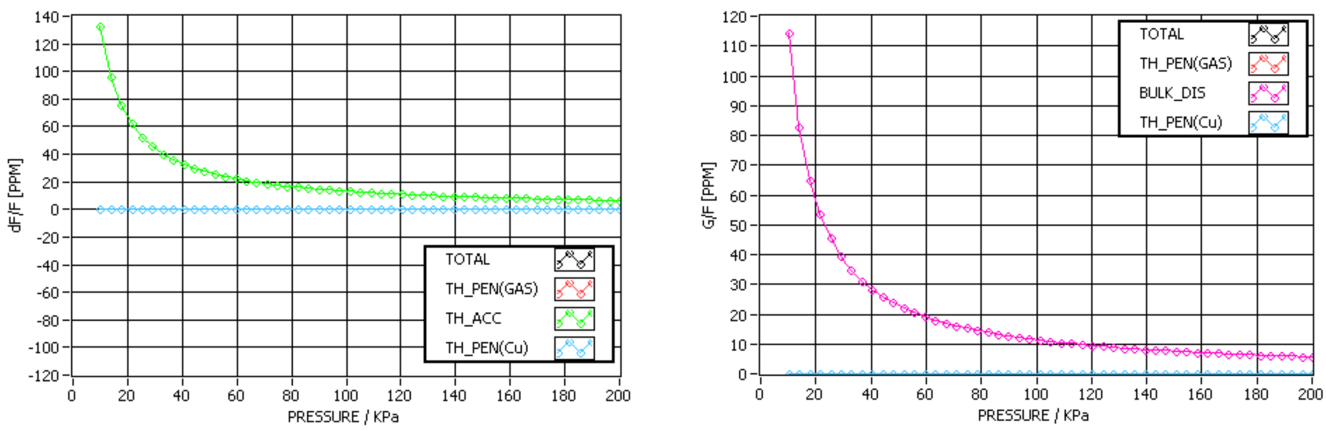

Figure 73 First zoom: Frequency shift of the (0,2) mode due to the *thermal boundary layer* and *bulk dissipation*. **Helium**, T = 273.16 K, a = 50 mm, h = 0.5.

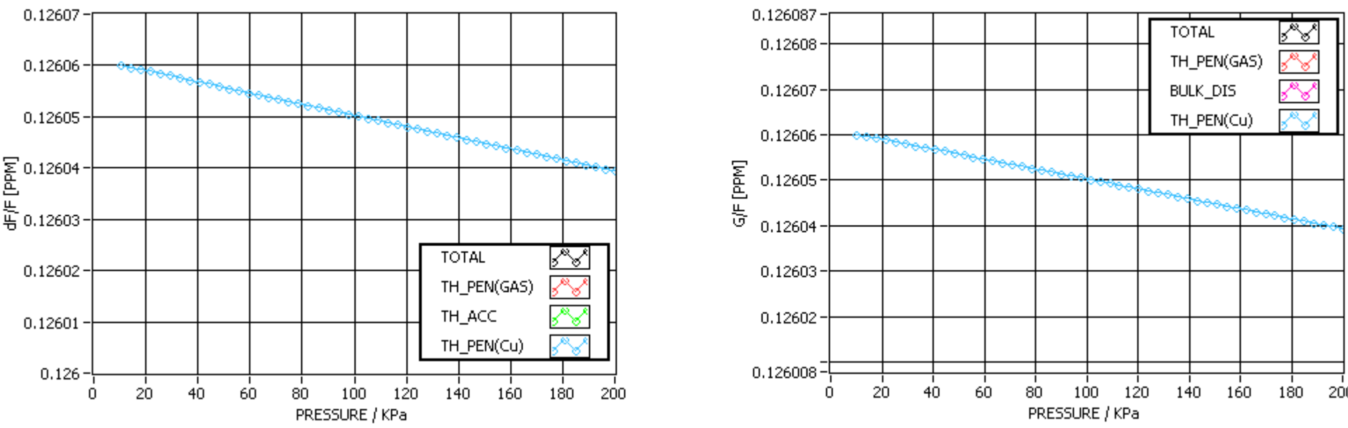

Figure 74 Second zoom: Frequency shift of the (0,2) mode due to the *thermal boundary layer* and *bulk dissipation*. **Helium**, T = 273.16 K, a = 50 mm, h = 0.5.

Argon

Figure 75 shows the frequency shift and halfwidth of the (0,2) mode due to the *thermal boundary layer* and *bulk dissipation* (§26) for helium at a temperature of 273.16 K, sphere radius of 50 mm and *thermal accommodation* coefficient of h = 0.5. The gas *thermal penetration* is the dominant contribution, with a magnitude of approximately **241 PPM** at 100 kPa.

The second largest contribution to the frequency shift and halfwidth are the *thermal accommodation* and *bulk dissipation* respectively. Figure 76 shows this. At 100 kPa, this amounts to magnitudes of **0.25 PPM** and **4.09 PPM** for the *thermal accommodation* and *bulk dissipation* respectively.

Figure 77 shows the *shell thermal penetration* contribution and it is approximately constant at **0.03 PPM** .

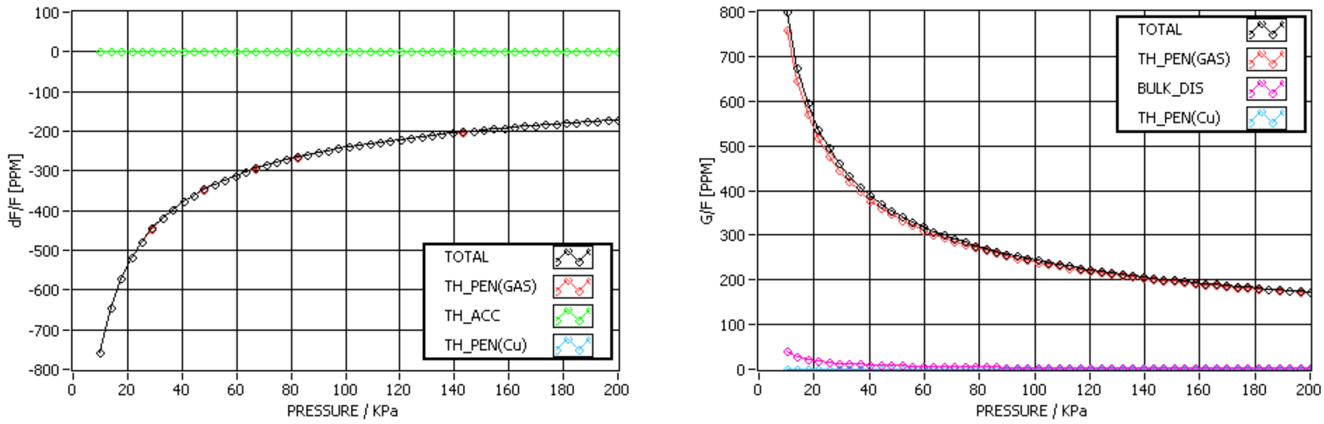

Figure 75 Full scale: frequency shift and halfwidth of the (0,2) mode due to the *thermal boundary layer* and *bulk dissipation*. **Argon**, T = 273.16 K, a = 50 mm, h = 0.5.

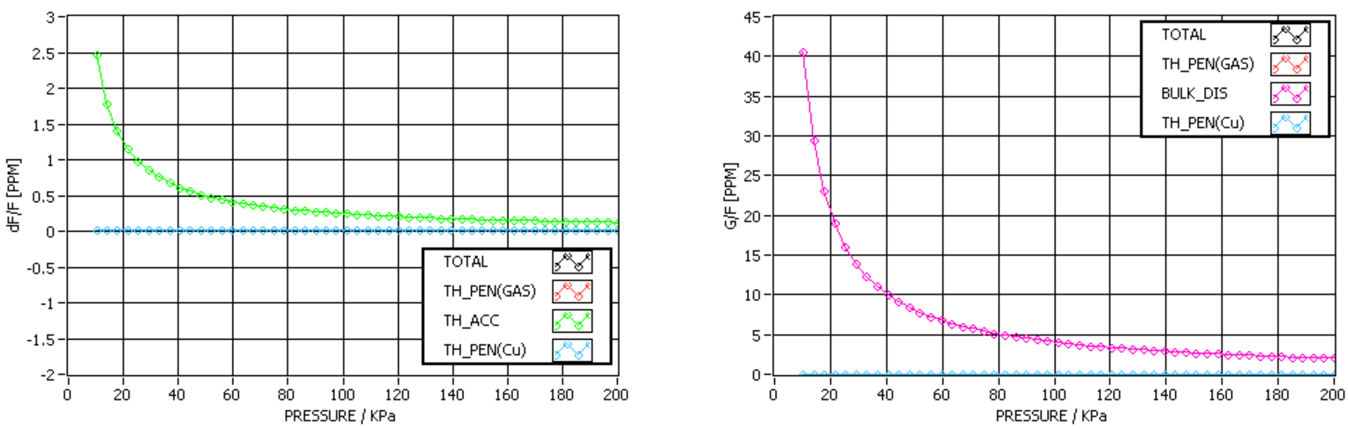

Figure 76 First zoom: Frequency shift of the (0,2) mode due to the *thermal boundary layer* and *bulk dissipation*. **Argon**, T = 273.16 K, a = 50 mm, h = 0.5.

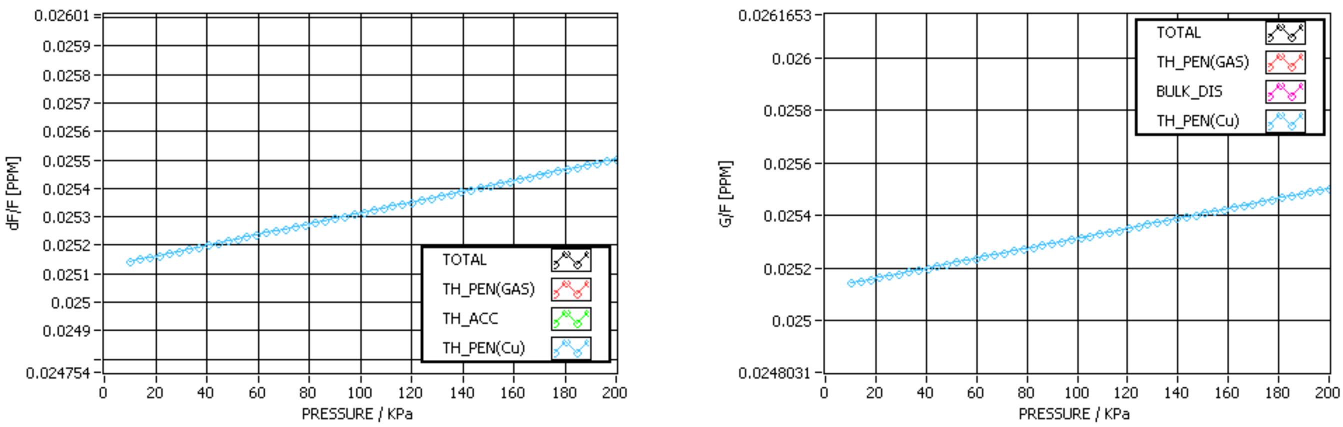

Figure 77 Second zoom: Frequency shift of the (0,2) mode due to the *thermal boundary layer* and *bulk dissipation*. **Argon**, T = 273.16 K, a = 50 mm, h = 0.5.

Table 1 shows a summary of these calculations for Helium and argon at a temperature of 273.16 K and a pressure of 100 kPa for the (0,2) radial mode and a sphere of radius 50 mm and a *thermal accommodation* coefficient of 0.5. It is worthy of note that the magnitudes of all contributions reduce for higher order radial modes and as the pressure increases.

	Gas: Helium		**Gas: Argon**	
Parameter	***ΔF/F* (PPM)**	***G/F* (PPM)**	***ΔF/F* (PPM)**	***G/F* (PPM)**
1. Thermal penetration	-400	400	-241	241
2. Thermal accommodation	13.30	-	0.25	-
3. Thermal penetration (Cu)	0.13	0.13	0.03	0.03
4. Bulk dissipation	-	14.4	-	4.09
TBLC (1+2+3)	-386.57	400.13	-240.72	241.03
Total (4 + 1+2+3)	**-386.75**	**414.53**	**-240.72**	**245.12**

Table 1 Summary of thermal boundary layer and bulk dissipation contributions to the frequency and halfwidth of the **(0,2)** acoustic mode. *a* = 50 mm, *h* = 0.5. *T*=273.16 K, *P*= 100 kPa.

Figures 78 and 79 show the TBLC *LabView* VI's for helium and argon respectively.

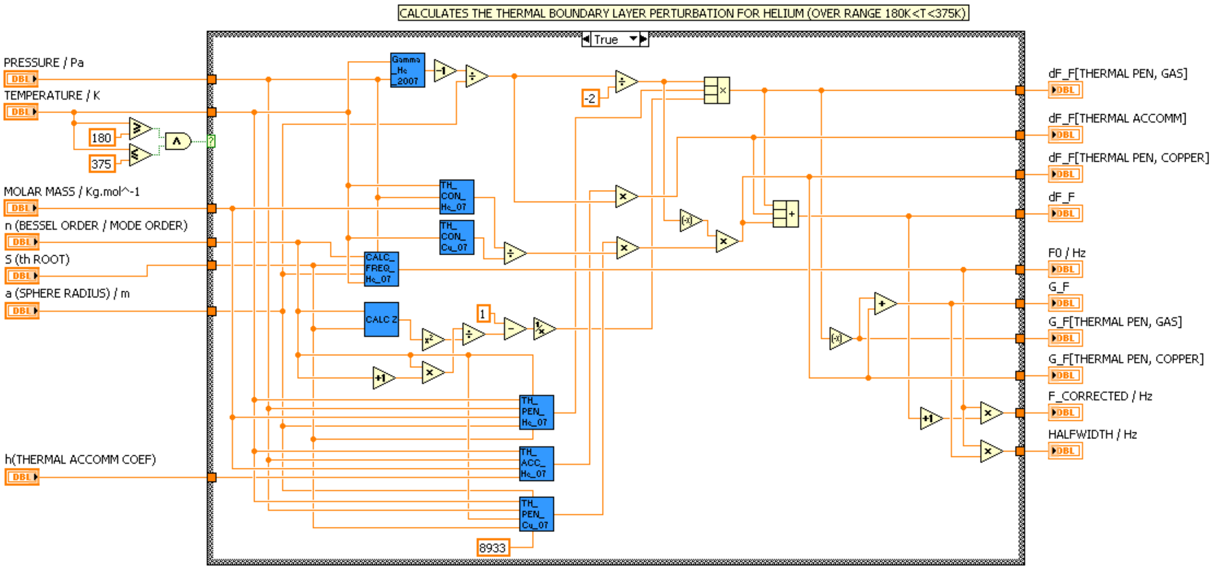

Figure 78 *LabView* code: **TBLC_He_2007.vi**

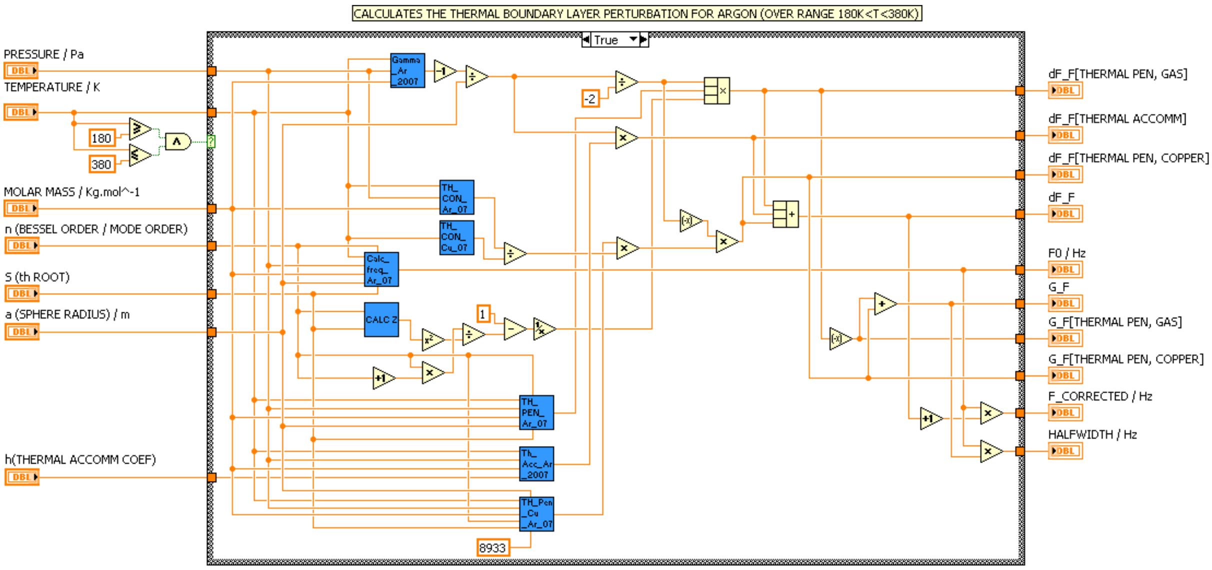

Figure 79 *LabView* code: **TBLC_Ar_2007.vi**

26) VISCOUS BOUNDARY LAYER CORRECTION: $\Delta f/f$, g/f

The *viscous boundary layer* correction is only applicable to non-radial modes (n >0) but is included here for completeness. It is given in terms of the viscous penetration length (δ_v) and can be written in terms of the fractional shift in resonance frequency from the ideal frequency ($\Delta f/f$) and the resonance halfwidth (g/f) as [6]:

$$\frac{\Delta f}{f} = -\frac{\delta_v}{2a}\cdot\frac{n(n+1)}{Z_{ns}^2 - n(n+1)}$$

$$\frac{g}{f} = \frac{\delta_v}{2a}\cdot\frac{n(n+1)}{Z_{ns}^2 - n(n+1)} \qquad (30)$$

Figures 80 and 81 show the *LabView* VI's. Typical values for the VBLC for the (1,3) mode of a 50 mm copper sphere at T = 273.16 K and a pressure of 1 atm. are:

Helium: $(\Delta f/f)_{(1,3)} = -\,(g/f)_{(1,3)} = -8.26$ PPM
Argon: $(\Delta f/f)_{(1,3)} = -\,(g/f)_{(1,3)} = -4.92$ PPM

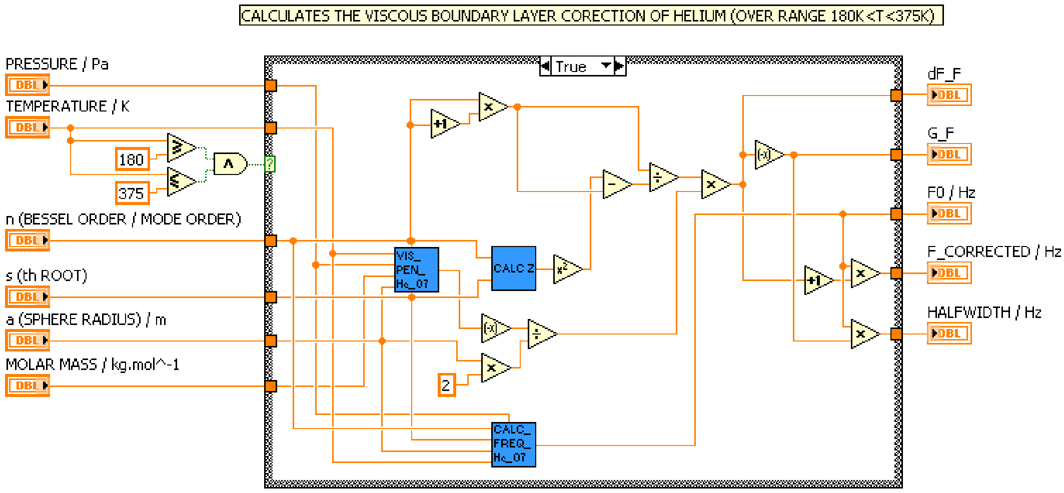

Figure 80 *LabView* code: **VBLC_He_2007.vi**

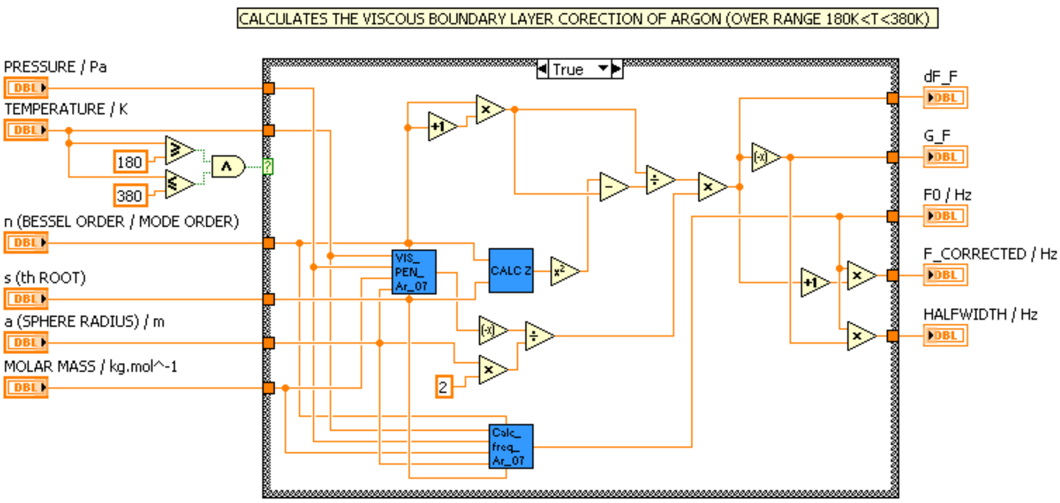

Figure 81 *LabView* code: **VBLC_Ar_2007.vi**

27) BULK DISSIPATION: *g / f*

The *bulk dissipation* correction takes into account the dissipation of the acoustic energy in the bulk of the gas itself. This is observed as an additional contribution to the resonance halfwidth *g* and is given by:

$$\frac{g_b}{f} = f^2 \frac{\pi^2}{u^2}\left[\frac{4}{3}\delta_v^2 + (\gamma - 1)\delta_{th}^2\right] \qquad (31)$$

where:

- δ_v is the *viscous penetration* length (§ 19)
- δ_{th} is the *thermal penetration* length (§ 18)
- u is the speed of sound (§ 1)

The *bulk dissipation* is shown in Figures 72 and 73 for helium and Figures 75 and 76 for argon for the (0,2) radial mode, a sphere radius of 50 mm, a temperature of T = 273.16 K. Figure 82 and 83 show the *LabView* VI's for helium and argon respectively.

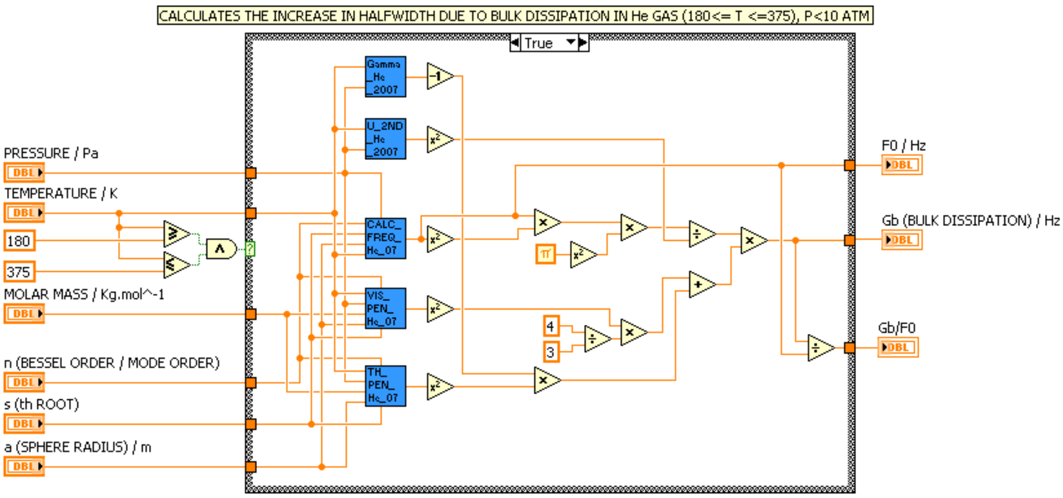

Figure 82 *LabView* code: **BULK_DIS_He_2007.vi**

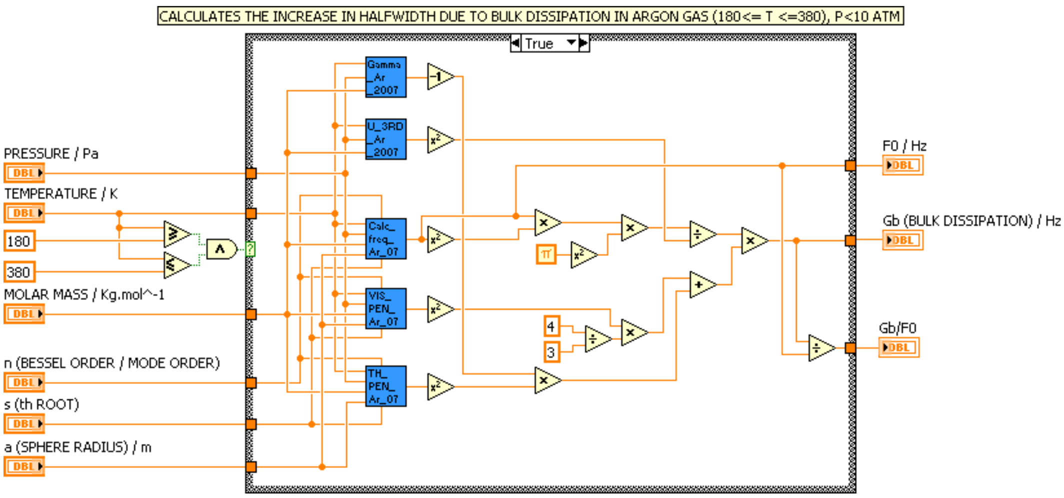

Figure 83 *LabView* code: **BULK_DIS_Ar_2007.vi**

28) SPEED OF SOUND IN COPPER: $U_{L,Cu}$

The longitudinal speed of sound in copper is given by [10]:

$$U_{L,Cu} = \left[\frac{(1-\sigma)}{(1-2\sigma)(1+\sigma)} \cdot \frac{E_{Cu}}{\rho_{Cu}} \right]^{\frac{1}{2}} \tag{32}$$

where:

σ is *Poisson's ratio* = 0.343.
E_{Cu} is *Young's modulus* = 129.8 GPa.
ρ_{Cu} is density = 8933 kg.m^{-3}.

At room temperature, $U_{L,Cu}$ = 4757.9 m.s^{-1}. Figure 84 shows the *LabView* VI.

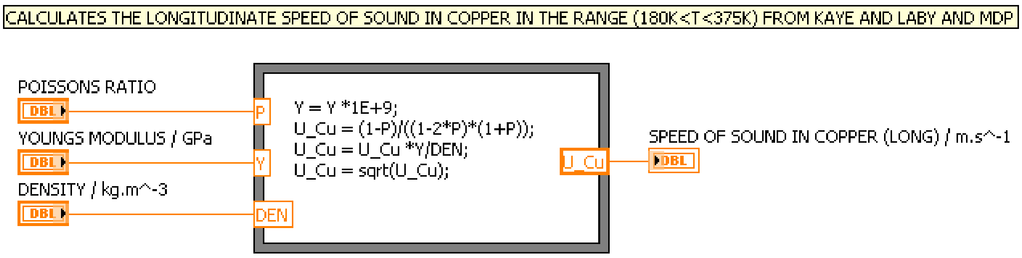

Figure 84 *LabView* code: **U_LONG_Cu_2007.vi**

29) SHELL CORRECTION: $\Delta f / f$

Determines the perturbation to the acoustic <u>radial</u> mode frequency due to shell motion (breathing mode). The shift in resonance frequency is given by [11,12]:

$$\frac{\Delta f}{f} = \frac{\rho_{gas} U_{gas}^2}{\rho_{Cu} U_{L,Cu}^2} \cdot S_0 \tag{33}$$

where:

ρ_{gas} is the density of the gas (helium or argon).
ρ_{Cu} is density of the copper shell.
U_{gas} is the speed of sound in the gas.
$U_{L,Cu}$ is the longitudinal speed of sound in the shell (§ 27).

S_0 is the admittance factor and for the radial modes is given by:

$$S_0 = -q \left[\frac{(1 + AB - qB^2) \cdot TAN(B-A) - (B-A) - qAB^2}{\left[(qA^2 - 1)(qB^2 - 1) + AB\right] \cdot TAN(B-A) - (1 + qAB)(B-A)} \right] \tag{34}$$

with:

$$A = \frac{2\pi fa}{U_{L,Cu}} \qquad B = \frac{2\pi fb}{U_{L,Cu}} \qquad \text{and} \qquad q = \frac{(1-\sigma)}{(2-4\sigma)} \qquad \sigma = \text{poisson's ratio}$$

a and b are the radius of the inner and outer surface of the sphere respectively.

Figure 85 shows the shift in the radial mode frequencies due to shell motion (using Equation 33) for a thin sphere (radius of 50 mm, 5 mm shell thickness) for argon gas at a temperature of 273.16 K.

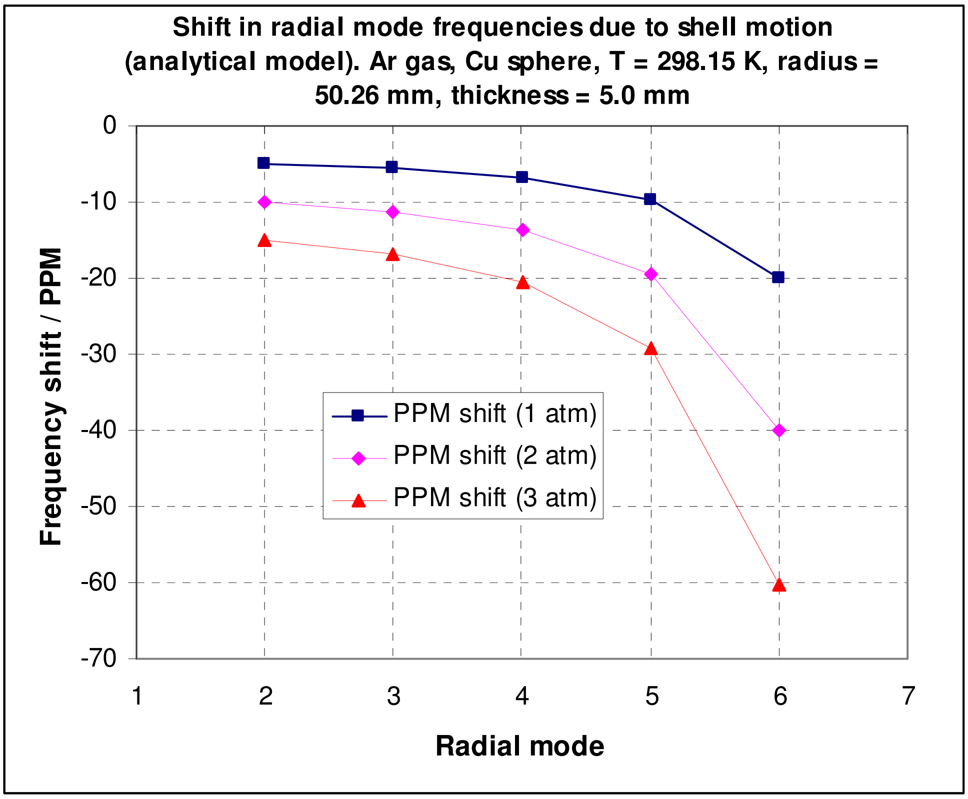

Figure 85 Shift in radial mode frequencies due to shell motion: Argon gas, copper sphere.

Figures 86 and 87 show the *LabView* VI's for Helium and argon gas in a copper sphere respectively.

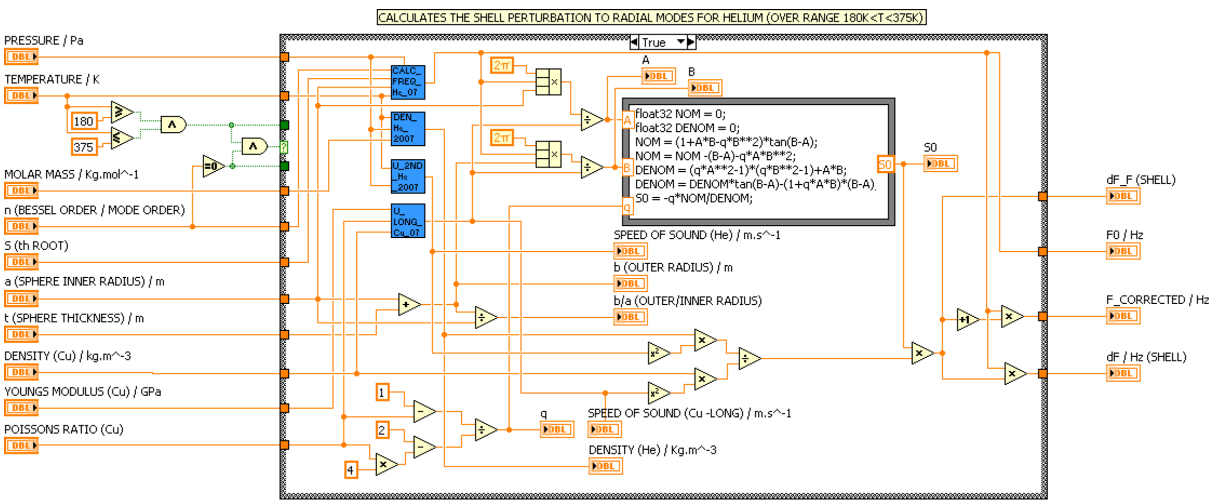

Figure 86 *LabView* code: **SHELL_COR_RAD_MODES_He_2007.vi**

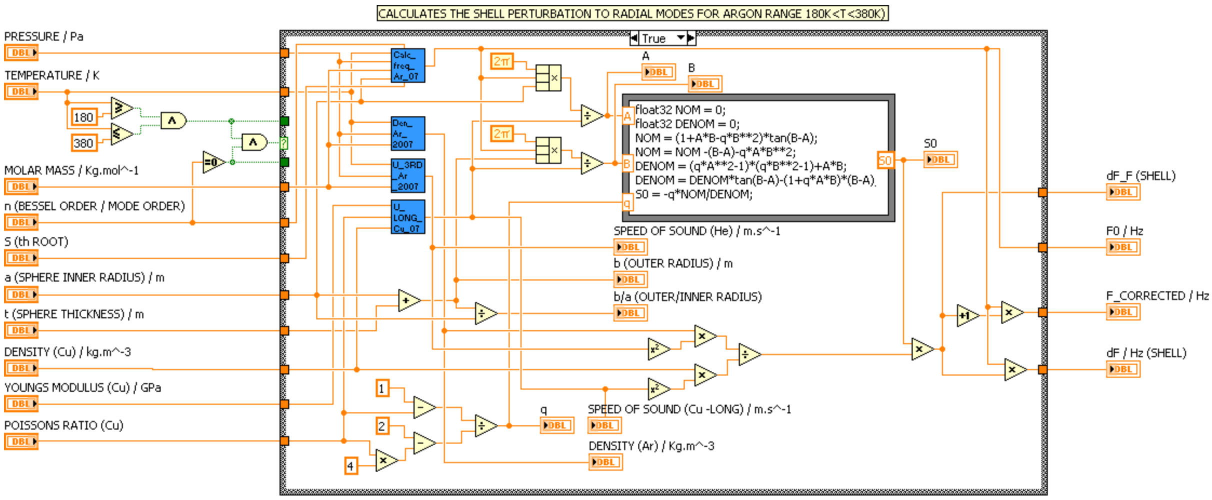

Figure 87 LabView code: **SHELL_COR_RAD_MODES_Ar_2007.vi**

Note: This formalism for the shell correction has since been found not to give the required accuracy. Instead a method based on fitting the raw frequency data and adjusting the position of the breathing mode to make the 2nd acoustic virial coefficient (§7) is used. This is described in §29.

30) SHELL CORRECTION (IMPROVED): $\Delta f / f$

We follow the procedure of *Pitre* [13] in which it is possible to determine the shell correction for each mode and the second acoustic virial coefficient.

We assume the shell perturbation reduces the *speed of sound squared* by:

$$\frac{\Delta c_{shell}^2}{c^2} \approx \frac{2\kappa p}{1-\left(f_{(0,n)} / f_{breath}\right)^2} \tag{35}$$

Where:

- P is the pressure.
- $f_{(0,n)}$ is the nominal frequency of the n^{th} radial acoustic mode.
- f_{breath} is the radially-symmetric resonance frequency of the empty shell (the breathing mode).

and κ is given by:

$$\kappa = \frac{5a}{6t\rho_{shell}\, u_{shell}^2} \tag{36}$$

where:

- a is the sphere's inner radius.
- t is the sphere's thickness.
- ρ_{shell} is the density of the shell (Cu).
- u_{shell}^2 is the longitudinal speed of sound in the shell material (Cu).

The *speed of sound squared* data versus pressure for each isotherm is fitted using:

$$c^2 = A_0 + A_1'P' + A_2'P'^2 + A_{-1}'P'^{-1} \tag{37}$$

where *P'* is the pressure in kPa.

Following [13], we divide both sides of Equation 37 by A_0 and re-cast it in *Pa* units leading to:

$$c^2/A_0 = 1 + A_1P + A_2P^2 + A_{-1}P^{-1} \tag{38}$$

With Equation 38 in this form, the *second acoustic virial coefficient* is given by:

$$\beta_A = RTA_1 \tag{39}$$

As a consequence of Equation 38, this coefficient will have a frequency dependent correction given by:

$$\Delta\beta_A \approx \frac{2\kappa RT}{1-\left(f_{(0,n)}/f_{breath}\right)^2} \tag{40}$$

Where R is the molar gas constant (8.314472) and T is the temperature (273.16 K).

The procedure for determining the shell correction involves adjustment of f_{breath} in Equation 40 until the mode (frequency) dependence of β_A is removed. Figure 88 shows a typical result for the sphere TCU1v3. Without this correction, the value of β_A falls with increasing frequency (mode number) but is relatively constant once the optimum correction has been applied.

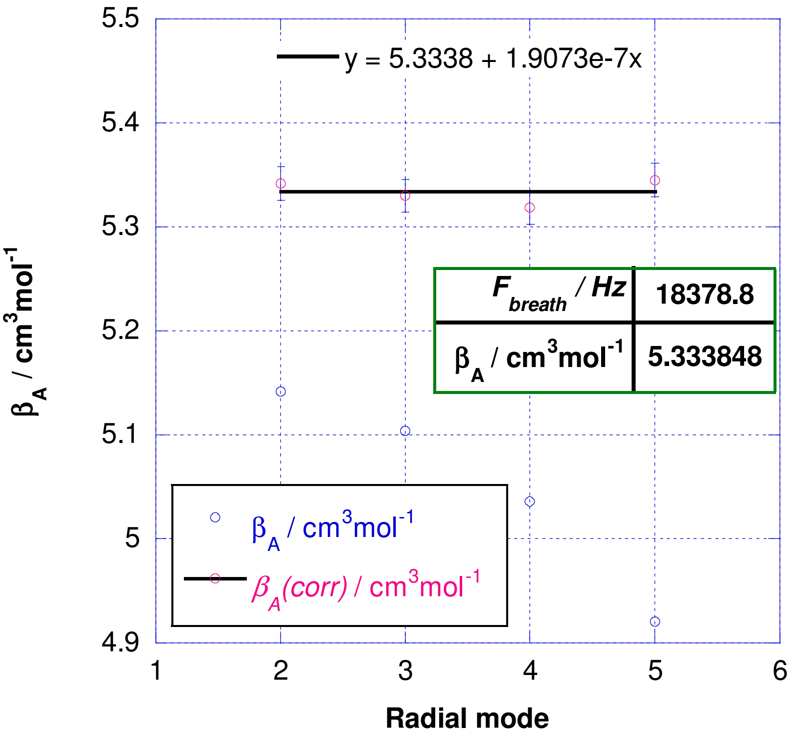

Figure 88 Example of the shell breathing mode correction for sphere TCU1v3.

31) DUCT CORRECTION: $\Delta f/f, g/f$

In order to flow gas into and out of the sphere, ducts of characteristic length and cross-sectional area are used. The method of equivalent 'T' circuits [14] is used to model these perturbations.

The inlet duct normally consists of two cylindrical ducts in series. The first, attached to the sphere, has a length of L_1 and a radius r_1. The second, attached to the first, has a length of L_2 and a radius of r_2. This second duct normally coiled around the middle of the outside of the sphere many times and then passes to the feed-in pipe work of the pressure vessel. The outlet duct consists of a single tube of length L and radius r and vents directly into the pressure vessel. Figures 89 and 90 show the equivalent T circuits for the inlet and outlet ducts respectively:

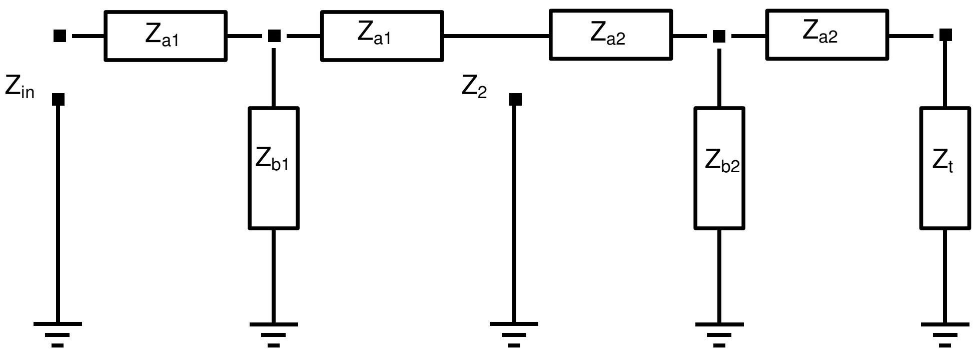

Figure 89 Equivalent T circuit: inlet duct – The input impedance is at the inner wall of the sphere and the terminal impedance (Z_t) is at the entry point of the pressure vessel.

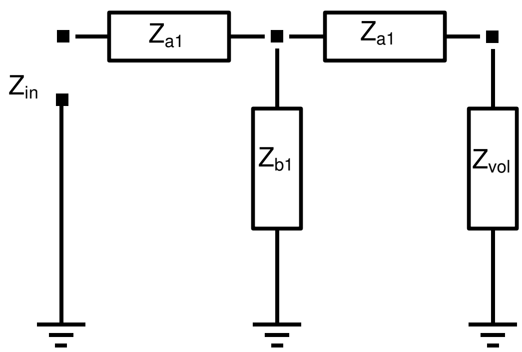

Figure 90 Equivalent T circuit: outlet duct – The input impedance is at the inner wall of the sphere and Z_{vol} is the volume impendence of the pressure vessel.

The input impedance of the inlet duct is given by:

$$Z_{in} = Z_{a1} + \frac{(Z_{a1} + Z_2)Z_{b1}}{(Z_{a1} + Z_2 + Z_{b1})} \tag{41}$$

where:

$$Z_2 = Z_{a2} + \frac{(Z_{a2} + Z_t)Z_{b2}}{(Z_{a2} + Z_{b2} + Z_t)} \tag{42}$$

and Z_t is set to 1E+9 Pa.s.m^{-3} but since the second duct is sufficiently long, changing the value makes little difference.

The input impedance of the outlet duct is given by:

$$Z_{in} = Z_{a1} + \frac{(Z_{a1} + Z_{vol})Z_{b1}}{(Z_{a1} + Z_{b1} + Z_{vol})} \tag{43}$$

With:

$$Z_{vol} = \frac{-i\rho c^2}{\omega V_{vessel}} \tag{44}$$

Where:

ρ is the gas density.
ω is the angular frequency ($2\pi f$).
c is the speed of sound in the gas.

The remaining parameters in the Equations 41 to 43 are defined by the following equations, where the cross-sectional area of the j^{th} duct is $A_j = \pi r_j^2$ and J_v are Bessel functions:

δ_v = viscous penetration length.

δ_t = thermal penetration length.

$$\kappa_v = \frac{1-i}{\delta_v}, \qquad \kappa_t = \frac{1-i}{\delta_t} \tag{45}$$

$$F_{vj} = \frac{2J_1(\kappa_v r_j)}{\kappa_v r_j J_0(\kappa_v r_j)}, \qquad F_{tj} = \frac{2J_1(\kappa_t r_j)}{\kappa_t r_j J_0(\kappa_t r_j)} \tag{46}$$

$$\Gamma_j = i\left(\frac{\omega}{c}\right)\sqrt{\frac{1+(\gamma-1)F_{tj}}{1-F_{vj}}} \tag{47}$$

$$Z_{0j} = \frac{\rho c / A_j}{\sqrt{(1+(\gamma-1)F_{tj})(1-F_{vj})}} \tag{48}$$

$$Z_{aj} = Z_{0j}TANH\left(\frac{\Gamma_j L_j}{2}\right), \qquad Z_{bj} = \frac{Z_{0j}}{SINH(\Gamma_j L_j)} \tag{49}$$

Finally, the perturbation is given by:

$$\frac{\Delta F_n + ig_n}{F_n} = \frac{i\rho c}{4\pi a^2 z_n Z_{in}} \tag{50}$$

where: z_n is the eigenvalue of the nth radial mode, Z_{in} is the input impendence of the duct(s) defined in Equations 41 to 43 and a is the radius of the sphere. Figures 91 and 92 show the input impedance of the inlet and outlet ducts respectively for typical parameters given in Table 2.

Sphere	a = 50 mm
Gas	Argon
T	273.16 K
P	100 kPa
Inlet ducts	L_1 = 100 mm r_1 = 0.254 mm L_2 = 6000 mm r_2 = 0.572 mm
Outlet duct	L = 50 mm r = 0.381 mm

Table 2 typical parameters for the duct correction model.

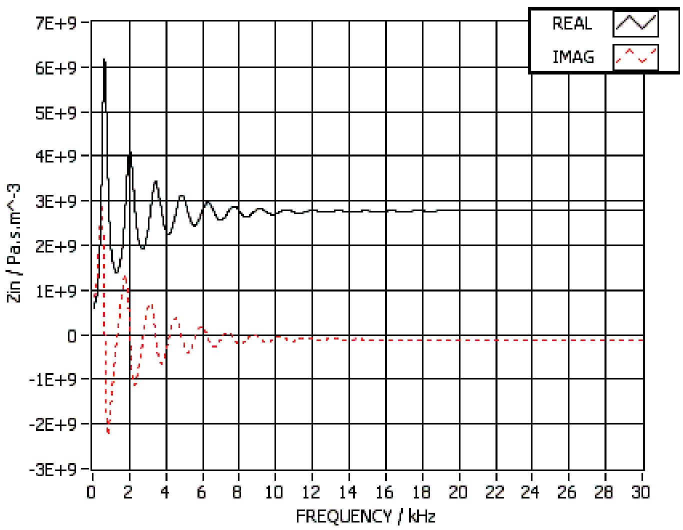

Figure 91 Input impedance of the two-stage inlet duct for the parameters in Table 2.

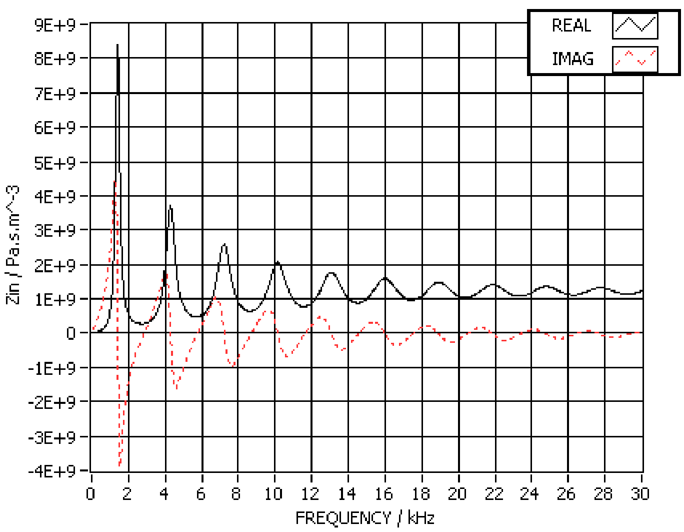

Figure 92 Input impedance of the single stage outlet duct for the parameters in Table 2.

Figures 93 and 94 show the perturbation due to the **inlet** duct on frequency and halfwidth respectively for the parameters given in Table 2.

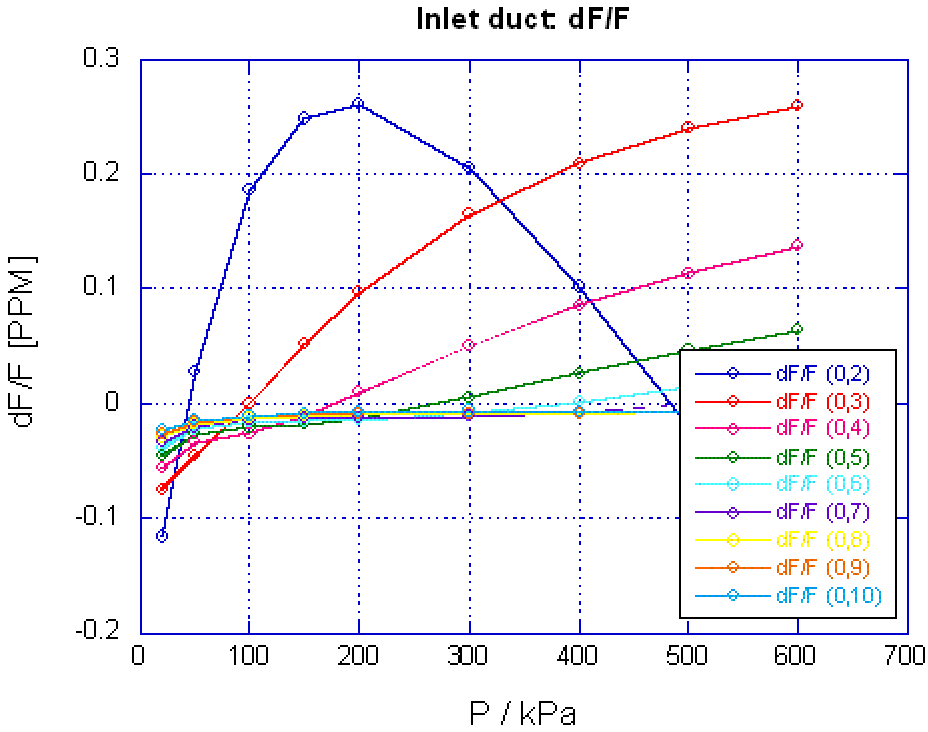

Figure 93 Frequency perturbation: Inlet duct, for the parameters in Table 2.

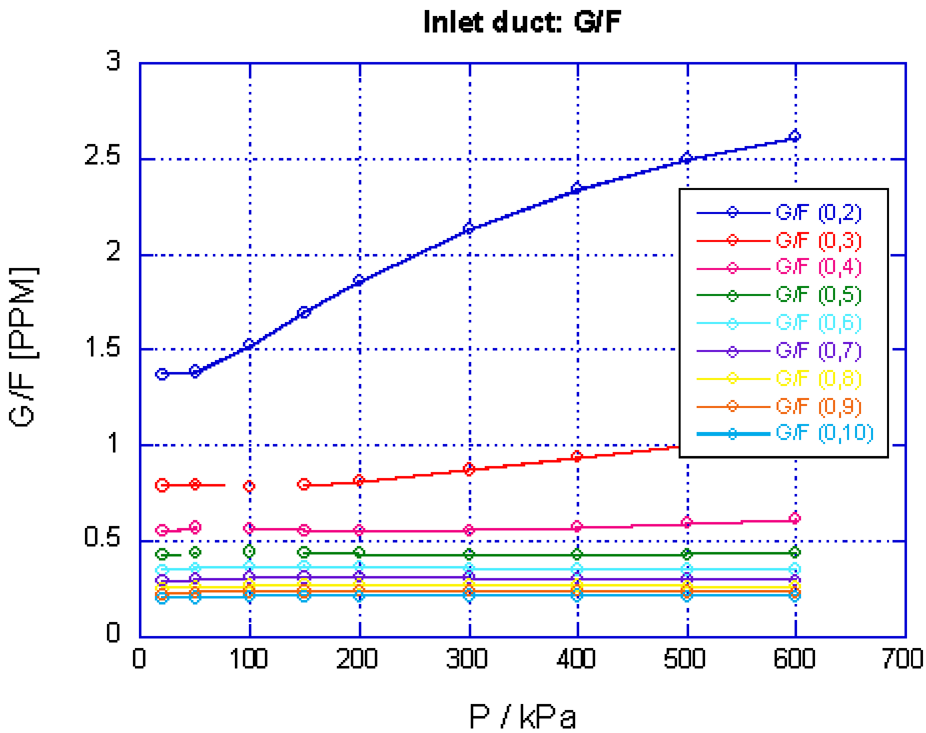

Figure 94 Halfwidth perturbation: Inlet duct, for the parameters in Table 2.

Figures 95 and 96 show the perturbation due to the **outlet** duct on frequency and halfwidth respectively for the parameters given in Table 2.

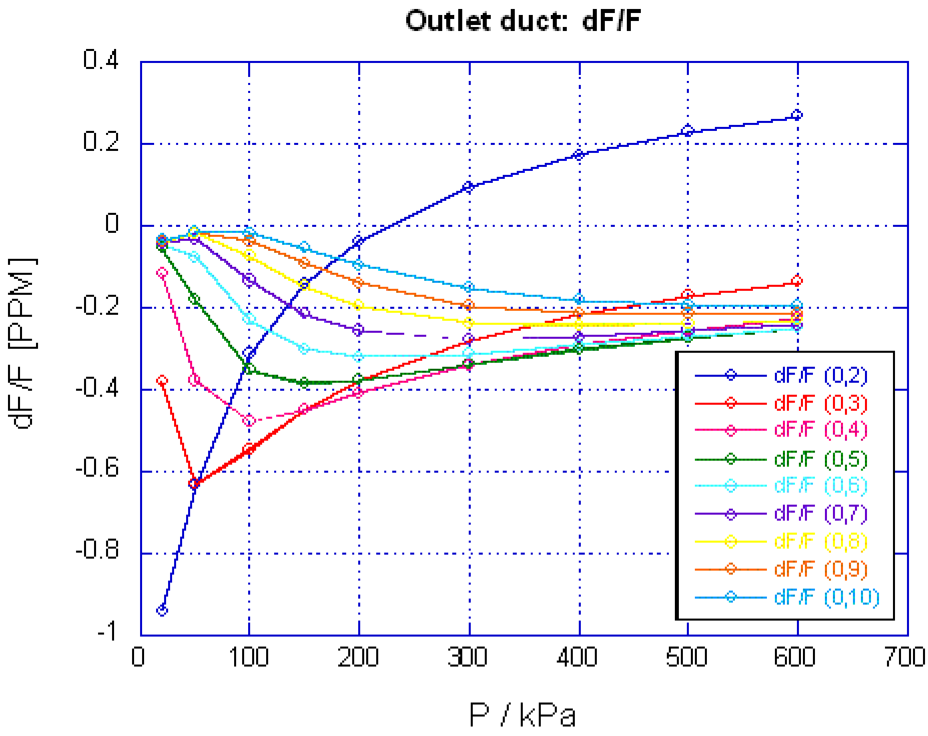

Figure 95 Frequency perturbation: outlet duct, for the parameters in Table 2.

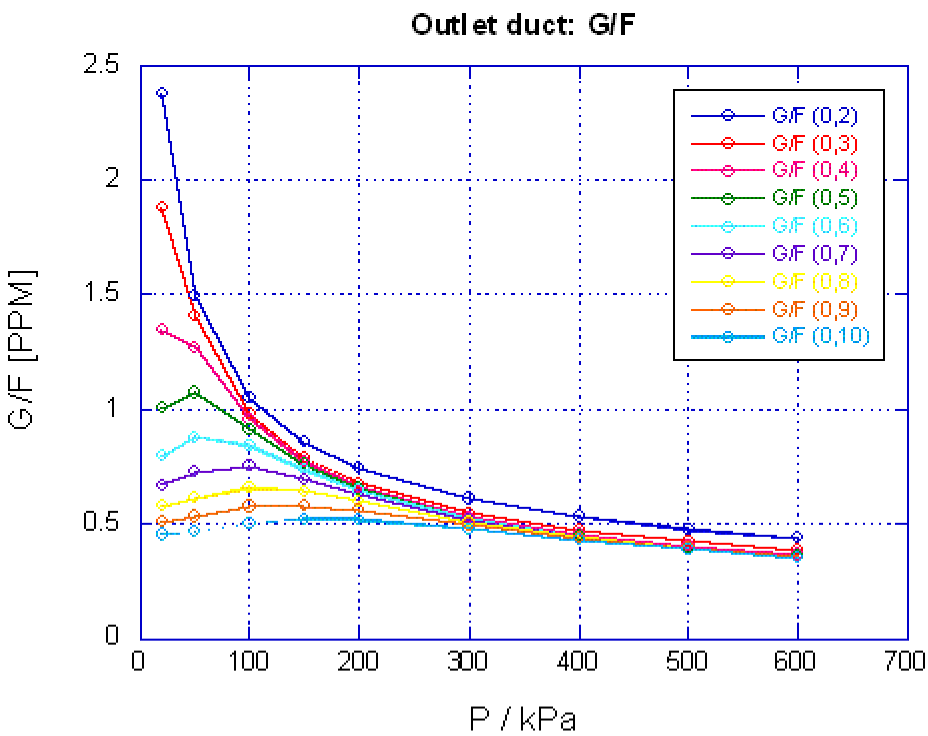

Figure 96 Halfwidth perturbation: outlet duct, for the parameters in Table 2.

Figures 97 and 98 show the combined inlet and outlet duct perturbations for the parameters in Table 2. The (0,2) mode shows the largest variation with pressure:

$$-1.06 \text{ PPM} < dF/F < 0.30 \text{ PPM}$$
$$G/F < 3.75 \text{ PPM}$$

These perturbations must be subtracted from the measured values of F(0,n) and G(0,n).

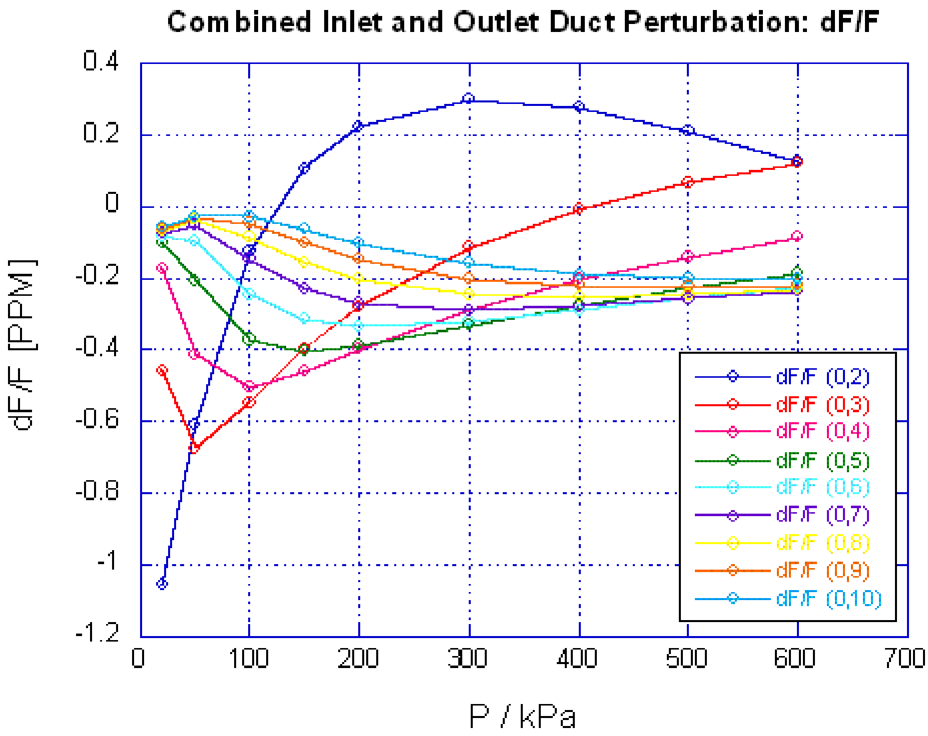

Figure 97 Combined inlet/outlet duct frequency perturbation for the parameters in Table 2.

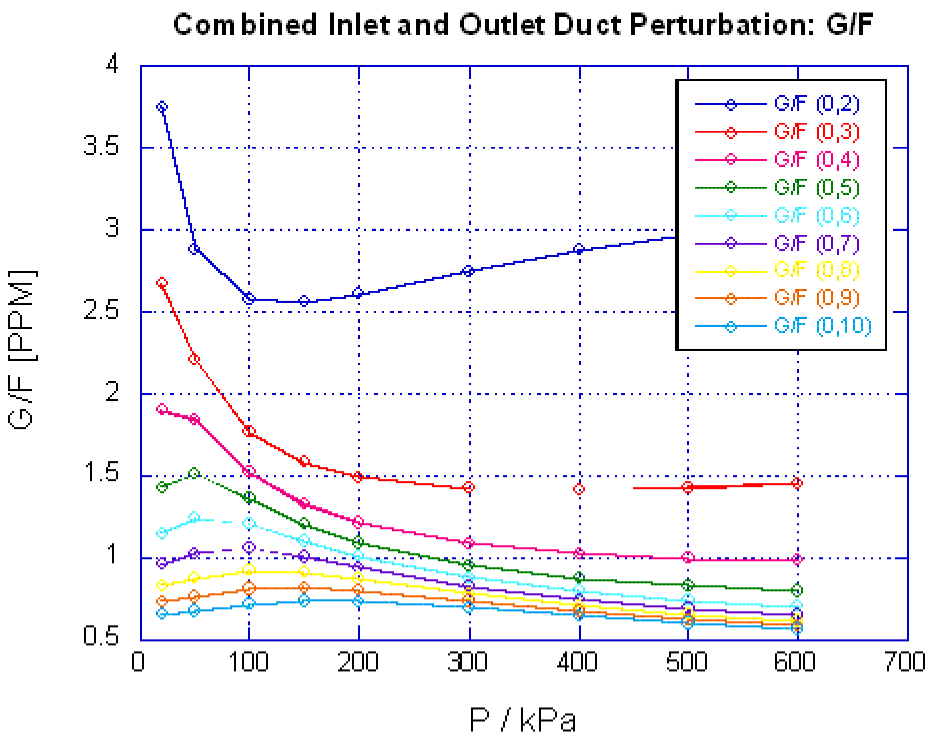

Figure 98 Combined inlet/outlet duct halfwidth perturbation for the parameters in Table 2.

Figure 99 shows the *LabView* VI used to calculate the duct perturbations.

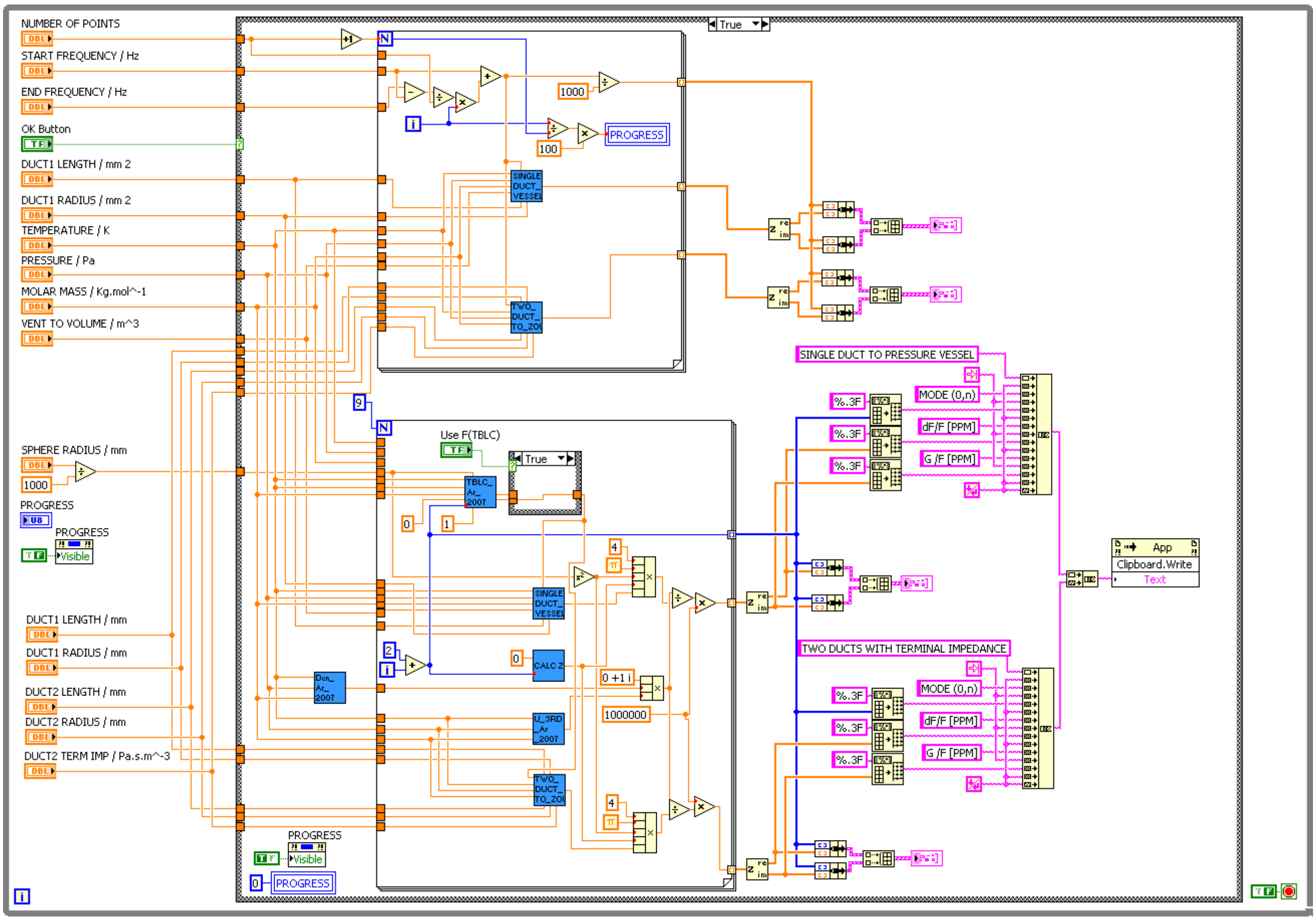

Figure 98 *LabView* code: **DUCT_PERT_FULL.vi**

32) TRANSDUCER CORRECTION: $\Delta f / f$

The frequency shifts to the radial modes induced by the presence of the condenser microphones [6] can be calculated with Equation 51.

$$\frac{\Delta f_{tr}}{f_{0n}} = -\frac{\rho c^2 X_m r_{tr}^2}{2a^3} \tag{51}$$

Where:

- ρ is the gas density.
- c is the speed of sound in gas.
- X_m is the compliance per unit area of the microphone.
- r_{tr} is the radius of the microphone.
- a is the radius of the sphere.

Table 5 shows typical parameter values used in this calculation for ¼ " B&K microphones and a sphere of 50 mm radius and Figure 99 shows the perturbation calculated from Equation 51.

Parameter	
T / K	273.16
a / mm	50.00
r_{tr} / mm	2.50
X_m / mPa^{-1}	1.5E-10

Table 5 parameters values used in determination of the acoustic transducer perturbation.

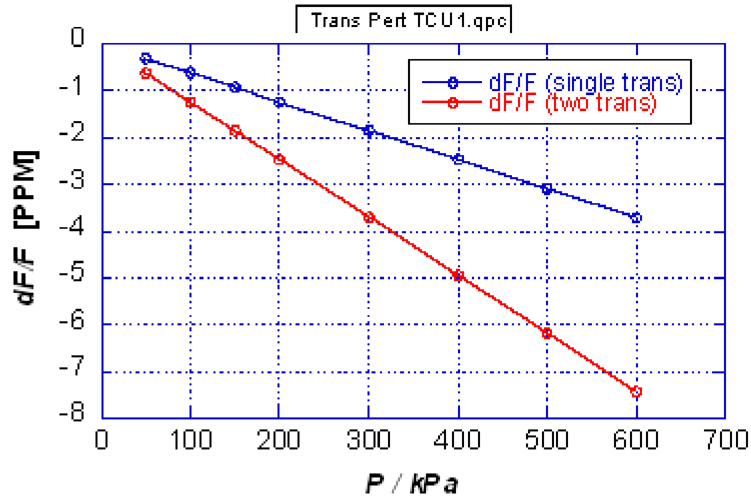

Figure 99 Transducer perturbation: for parameters in Table 5.

Accounting for the two microphones we can express this perturbation as:

***1/P*d_F/F* = -0.0124 PPM / kPa**

These perturbations must be <u>subtracted</u> from the measured values of *F(0,n)*.

Figure 100 shows the *LabView* VI used to calculate the transducer perturbation for a single microphone of given radius and compliance per unit area.

Guianvarc'h has proposed a more accurate model for the transducer perturbation: *Characterisation of condenser microphones under different environmental conditions for accurate speed of sound measurements with acoustic resonators* (CNAM, Feb 09) in which, compared to Figure 99, the frequency shift differs with mode number. Since the perturbation for the lowest four radial modes (0,2) – (0,5) (generally used in the determination of K_b) are still approximately linear in pressure and of similar magnitude, this model has not been exploited at this time.

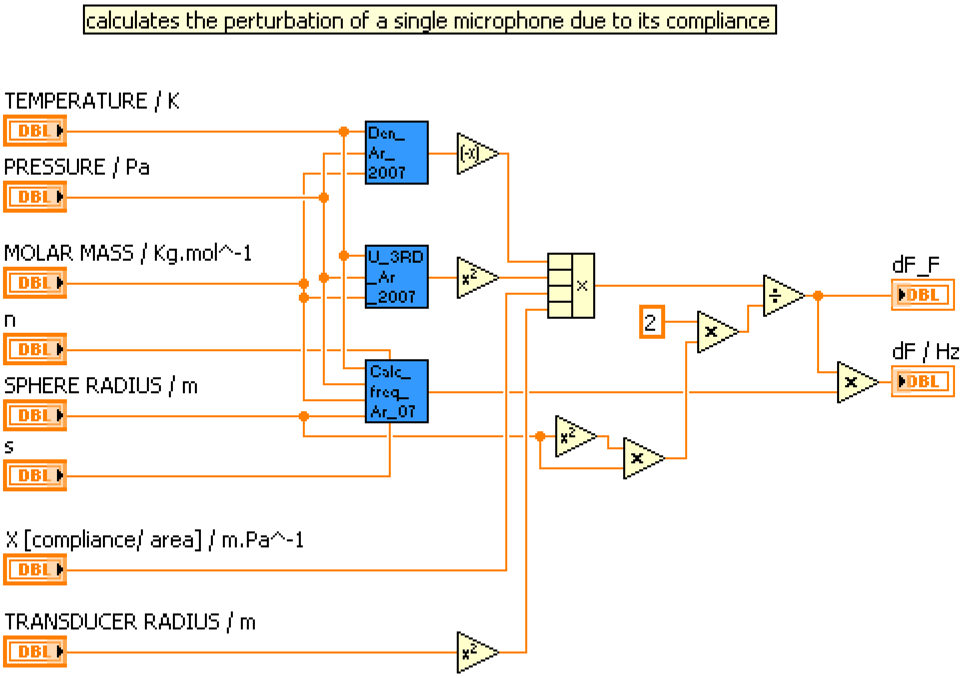

Figure 100 *LabView* code: **TRANSDUCER_PERT_Ar.vi**

33) 2nd ORDER SHAPE CORRECTION: $\Delta f / f$

The second order shape perturbation [15], which accounts for the fact that the sphere is a triaxial ellipsoid, can be calculated using Equation 52, where z_n is the eigenvalue of the n^{th} radial mode and ε_1 and ε_2 are the eccentricities of the sphere calculated from microwave measurements:

$$\frac{dz_n^2}{z_n^2} = \frac{8z_n^2}{135}\left(\varepsilon_1^2 - \varepsilon_1\varepsilon_2 + \varepsilon_2^2\right) \tag{52}$$

To correct the frequency (and not c^2) we must divide this perturbation by two and subtract it from the measurements. Table 6 and Figure 101 show the second order shape perturbation for a typical sphere (TCU1v3) of radius 50.26 mm.

	ε_1	**0.001050**
	ε_2	**0.000801**
Mode	***z(0,n)***	***dF/F* [PPM]**
2	4.493409458	0.539
3	7.725251836	1.593
4	10.904121659	3.174
5	14.066193912	5.282
6	17.220755272	7.917
7	20.371302959	11.079
8	23.519452498	14.768
9	26.666054259	18.984
10	29.811598790	23.727

Table 6 Second order shape perturbation for sphere TCU1v3.

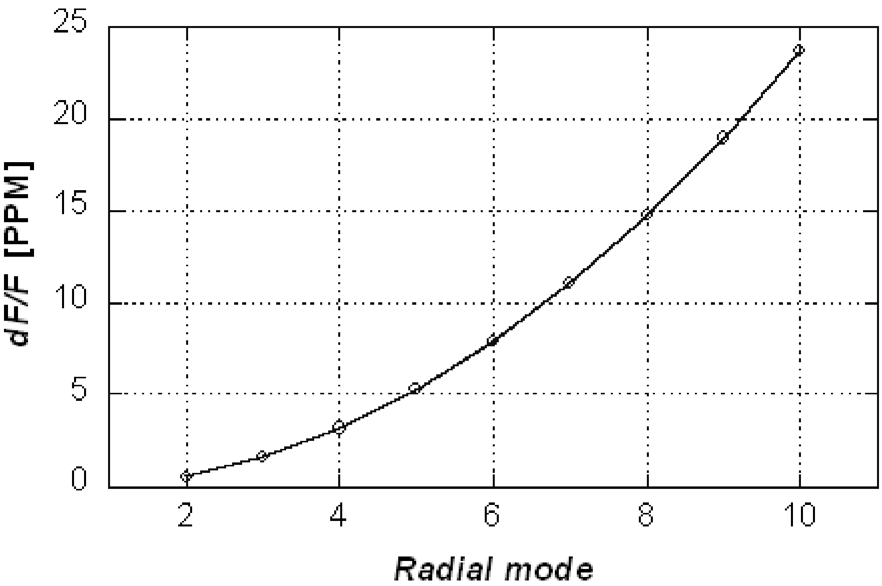

Figure 101 Second order shape perturbation: TCU1v3. ε_1 = 0.001050 and ε_2 = 0.000801.

34) DETERMINATION OF THE SPEED OF SOUND

The resonance frequencies are first corrected to the equivalent values at the temperature of the triple point of water (T_{TPW} = 273.16 K) using the 2nd acoustic virial coefficient (β - given by Equation 5):

$$F_n(T_{TPW}, P) = F_n(T_{meas}, P).\left(\frac{T_{TPW}}{T_{meas}}\right)^{1/2} \frac{\left(1 + \frac{\beta(T_{\mathrm{TPW}})}{RT_{\mathrm{TPW}}} P\right)^{1/2}}{\left(1 + \frac{\beta(T_{\mathrm{meas}})}{RT_{\mathrm{meas}}} P\right)^{1/2}} \quad (53)$$

Where:

T_{meas} is the temperature at the time of measurement.
P is the pressure at the time of measurement.
R is the universal gas constant.
$F_n(T_{meas},P)$ is the resonance frequency at T_{meas} and P.

We then converted to *the speed of sound squared*, c^2, accounting for the fact that the radius of the sphere changes with temperature and pressure:

$$c^2 = \left(\frac{2\pi F_n(T_{TPW}, P)}{z_n}\right)^2 a^2(T, P) \quad (54)$$

Where:

f_n is the frequency of the n^{th} mode.
z_n the corresponding eigenvalue.
a(T,P) is the radius of the sphere at the measurement *T* and *P*.

The temperature and pressure dependence of the radius of a copper sphere is given by:

$$a(T,P) = a_0\left(1 - K_P P + (T - 273.16\ K)K_T\right) \tag{55}$$

Where:

K_P is the fractional isothermal compressibility of copper: **3.024E-12 Pa^{-1}**.
K_T is the fractional thermal expansivity of copper: **16.324E-6 K^{-1}**.
a_0 is the radius of the sphere at T = 273.16 K and P = 0 kPa found from microwave measurements.

At present these two corrections are applied manually – future software will address this.

35) LEAST SQUARES FITTING OF THE INDIVIDUAL MODES

Several *Labview* VI's have been written to perform a least squares fit of the speed of sound squared versus pressure data. They differ in which fitting parameters are free and which are fixed and which parameters are included in the fit.

$$c^2 = A_0 + A_1 P + A_2 P^2 + A_{-1} P^{-1} \tag{56}$$

$$c^2 - A_3^{fixed} P^3 = A_0 + A_1 P + A_2 P^2 + A_{-1} P^{-1} \tag{57}$$

$$c^2 = A_0 + A_1 P + A_2 P^2 + A_{-1} P^{-1} + A_3 P^3 \tag{58}$$

$$c^2 - A_3^{fixed} = A_0 + A_1 P + A_2 P^2 \tag{59}$$

$$c^2 = A_0 + A_1 P + A_2 P^2 + A_3 P^3 \tag{60}$$

Equations 56 and 57 perform fits with no A_3 term and a fixed A_3 term respectively. These are accomplished with the *LabView* VI: **LS_fit_kb_FIRST_PRINCIPLES.vi**

Equation 58 performs a fit in which the A_3 term is a free parameter (it is fitted). This is accomplished with the *LabView* VI: **LS_fit_kb_FIRST_PRINCIPLES with p_3 term.vi**

Equation 59 performs a fit in which the A_3 term is fixed and there is no A_{-1} term. This is accomplished with the *LabView* VI: **LS_fit_kb_FIRST_PRINCIPLES_no_A-1_FIXED_A3.vi**

Equation 60 performs a fit in which the A_3 term is a free parameter (it is fitted) and there is no A-1 term with the *LabView* VI: **LS_fit_kb_FIRST_PRINCIPLES_no_A-1_FREE_A3.vi**

Which fitting routine do we use?

- We no longer use Equation 56 since it has become apparent that an A_3 term should always be used.
- We use Equation 57 to perform preliminary fits with A_3 fixed and equal to 1.45E-9 $m^2s^2kPa^{-3}$ from *Maldover* [6].
- We no longer use Equation 58 since typical datasets don't have enough degrees of freedom to fit both A_3 and A_{-1}.
- We use Equation 59 once we have corrected the data for the true value of the thermal accommodation coefficient and A_{-1} is necessarily equal to zero.
- We would only use Equation 60 if we are confident that we have sufficient data of good quality to estimate a value of A_3 better than that of *Maldover* [6].

The file format for the *LabView* fitting VI's is shown in Table 7. The file should be created in Excel and saved as a '.csv' type file. Things to note:

- Row 1 contains a header describing the measurements
- Row 2 contains the column headings:
  - Column A – P/kPa.
  - Columns B to J – radial mode number (2-10).
  - Column K – absolute uncertainty on the *speed of sound squared* measurement (assumed to vary with pressure only).
- Rows 3 onwards contain the measurements:
  - Column A – the pressures in kPa.
  - Columns B to J – the *speed of sound squared* measurements in m^2s^{-2} units.
  - Any of the data columns can be omitted but must be padded with zeros if there are data columns to the right etc.

	A	B	C	D	E	F	G	H	I	J	K
1	C2 versus P / kPa data TCU1 FIXED Feb 09 Filename: C2_P_TCU1_FIXED.XLS										
2	P / kPa	2	3	4	5	6	7	8	9	10	$U(c^2)$
3	600	94904.92	94904.03	94902.58	94898.99	94859.01	94934.54	94918.28	94917.75	94915.27	0.017633
4	500	94877.39	94876.69	94875.49	94872.55	94838.17	94902.75	94888.72	94888.19	94886	0.018898
5	400	94851.04	94850.52	94849.54	94847.23	94819.28	94871.47	94860.12	94859.76	94857.89	0.02064
6	300	94825.83	94825.44	94824.63	94822.98	94802.11	94841.2	94832.48	94832.36	94830.79	0.02305
7	200	94801.66	94801.44	94800.99	94799.75	94785.64	94811.98	94806.14	94806.12	94804.38	0.027048
8	150	94790.02	94789.89	94789.57	94788.64	94778	94797.58	94793.36	94793.24	94790.4	0.030591
9	100	94778.73	94778.64	94778.44	94777.79	94770.94	94783.96	94780.98	94780.2	94778.86	0.037803
10	50	94767.87	94767.88	94767.93	94767.48	94764.11	94770.68	94769.04	94770.78	94772.2	0.060545
11	600	94904.95	94904.01	94902.56	94898.98	94858.89	94934.3	94918.3	94917.71	94915.24	0.017633
12	500	94877.34	94876.7	94875.55	94872.58	94838.09	94902.68	94888.66	94888.2	94886.01	0.018898
.	.	.	.	.	.	.	.	.	.	.	.
.	.	.	.	.	.	.	.	.	.	.	.
n	P_n	$c_n^2(0,2)$	$c_n^2(0,3)$	$c_n^2(0,4)$	$c_n^2(0,5)$	$c_n^2(0,6)$	$c_n^2(0,7)$	$c_n^2(0,8)$	$c_n^2(0,9)$	$c_n^2(0,10)$	$U_n(c^2)$

Table 7 File format for *LabView* fitting software.

This concludes the document. GJMS Sept 09

36) REFERENCES

1. M. R. Moldover, J. B. Mehl, M. Greenspan, *Gas-filled spherical resonantors: Theory and experiment*, J. Acoust. Soc. Am. **79** (2), 1986.
2. A. J. Zuckerwar, *Handbook of the Speed of Sound in Real Gases*, Volume 1, Academic Press, Elsevier Science.
3. J. J. Hurly, J. B. Mehl, *^{4}He Thermophysical Properties: New Ab Initio Calculations*, J. Res. Natl. Inst. Stand. Technol. **112** (2) 75-94, 2007.
4. REFPROP V8.0 (2008), National Institute of Standards and Technology (NIST).
5. G. Benedetto, R. M. Gavioso, R. Spagnolo, P. Marcarino, *Acoustic Measurements of the Thermodynamic Temperature between the Triple Point of Mercury and 380 K*, Metrologia, **41** 74-98, 2004.
6. M. R. Moldover, J. P. M. Trusler, T. J. Edwards, J. B. Mehl, R. S. Davis, *Measurement of the Universal Gas Constant R using a Spherical Acoustic Resonator*, J. Res. Inst. Stand. Technol. **93** (2) 85-130, 1988.
7. Hirschfelder, Curtiss and Bird, *Molecular Theory of Gases and Liquids*, Wiley (1954).
8. M. R. Moldover, S. J. Boyes, C. W. Meyer, A. R. H. Goodwin, *Thermodynamic Temperatures of the Triple Points of Mercury and Gallium and in the Interval 217 K to 303 K*, J. Res. Natl. Inst. Stand. Technol. **104** 11-31, 1999.
9. L. Pitre, *private communication*, CNAM, Paris, 2008.
10. G. W. C. Kaye, T. H. Laby, *Tables of Physical and Chemical Constants*, 14th Ed. Longman, 1985.
11. J. B. Mehl, *Spherical acoustic resonators: Effects of Shell motion*, J. Acoust. Soc. Am. 78(2) August 1985.
12. C. A. Oxborrow, *The Effects of Geometry on Acoustic and Electromagnetic Resonances in a Spherical Cavity*, Ph.D. Thesis, December 1990.
13. L. Pitre, M. R. Moldover, W. L. Tew, *Acoustic thermometry: new results from 273 K to 77 K and progress towards 4 K*, Metrologia **43** (2006) 142-162.
14. J. B. Mehl, M. R. Moldover, L. Pitre, *Designing quasi-spherical resonators for acoustic thermometry*, Metrologia **41** (2004) 295 – 304.
15. J. B. Mehl, *Acoustic Eigenvalues of a Quasi-spherical Resonator: Second Order Shape Perturbation Theory for Arbitrary Modes*, J. Res. Natl. Inst. Stand. Technol. 122, 163-173 (2007).

37) A PPENDIX – LOCATION OF BACK-UP FILES

Live versions of the complete *LabView* VI set are stored (and updated as required) on two PC's:

PC	Name	Location	Directory
1	Mercury	F5-A6	D: \ Boltzmann constant project \ Experimental \ Acoustics \ SOFTWARE
2	Boltzmann	F5-L7	D:\Kb work Nov 07\Acoustic SW

Periodically and after major updates, the whole software suite is saved to the U drive under:

U\GJMS\Acoustic SW as of dd mmm yy